CHARACTERIZING THE AFGHANISTAN AEROSOL ENVIRONMENT USING SIZE- AND TIME- RESOLVED AEROSOL CHEMICAL COMPOSITION MEASUREMENTS

By

Todd Allen Fortun

RECOMMENDED:

(William Simpson)

Nicole Mölders

Catherine J. Child
Advisory Committee Chair

(William Simpson)
Chair, Department of Chemistry and Biochemistry

APPROVED:

Paul W. Layer
Dean, College of Natural Sciences and Mathematics

Lawrence K Duffy
Dean of the Graduate School

March 5, 2012
Date

CHARACTERIZING THE AFGHANISTAN AEROSOL ENVIRONMENT USING SIZE- AND TIME- RESOLVED AEROSOL CHEMICAL COMPOSITION MEASUREMENTS

A

THESIS

Presented to the Faculty

of the University of Alaska Fairbanks

in Partial Fulfillment of the Requirements

for the Degree of

MASTER OF SCIENCE

By

Todd Allen Fortun, B.S.

Fairbanks, Alaska

May 2012

ABSTRACT

The exposure to aerosols is one danger U.S. soldiers face in Afghanistan that may go unseen. Using the Davis Rotating-drum Universal-size-cut Monitoring (DRUM) cascade impactor, size- and time- resolved aerosol chemical concentrations from Bagram, Afghanistan were collected. These aerosol concentrations were combined with a meteorological analysis and Hybrid Single Particle Lagrangian Integrated Trajectory (HYSPLIT) model meteorological backward trajectories to establish source sectors. These sectors, along with time of year, were then used as a predictive tool for the chemical composition and relative concentration of aerosols in Afghanistan. Principal components analysis (PCA) was used to determined potential source types. PM_{10} and $PM_{2.5}$ were compared to military exposure guidelines and U.S. national ambient air quality standards. Results reveal aerosol concentrations in Afghanistan were at levels for which adverse health effects could be anticipated.

TABLE OF CONTENTS

Page

Signature Page i

Title Page ii

Abstract iii

Table of Contents iv

List of Figures vii

List of Tables xi

List of Abbreviations xii

Acknowledgements xiv

1. Introduction 1

1.1. Definition and formation of aerosols 1

1.2. Thesis goals 1

1.3. Climatology of the Afghanistan region 5

1.3.1. Wind patterns 5

1.3.2. Diurnal cycles 10

1.4. Elemental sources and uses 11

1.5. Aerosol chemistry and seasonality 13

1.5.1. Geological dust 14

1.5.2. Anthropogenic aerosols 18

1.5.2.1. Pakistan 18

Page

1.5.2.2. Kazakhstan, Turkmenistan, and Uzbekistan 20

1.5.3. Biomass burning 22

1.5.4. Aerosols over seas and oceans 22

1.6. Health concerns and standards 23

2. Experimental Methods 29

2.1. Wind roses 29

2.2. DRUM aerosol impactors 30

2.3. HYSPLIT and sector analysis 34

2.4. Principal components analysis 38

2.4.1 PCA procedure 38

2.4.2. Eigenvector loadings 40

2.4.3. PCA on aerosol samples 42

2.5. Chemical mass balance (CMB) model 45

3. Results and Discussion 47

3.1. Wind roses 47

3.2. Elemental concentrations 61

3.2.1. Geological dust 62

3.2.2. Heavy metal events 74

3.3. PM_{10} and $PM_{2.5}$ concentrations and comparison to health safety standards 92

3.4. Sector analysis 98

Page

3.5. PCA 102

3.6. CMB model 109

4. Conclusions 113

5. Future work 115

References 116

LIST OF FIGURES

Page

Chapter 1

Figure 1.1. Location of Afghanistan (in orange) and a map of the surrounding region. The yellow star in Afghanistan denotes the location of Bagram Air Force Base 4

Figure 1.2. Afghanistan cities and topography. Star markers indicate capital cities. Image created via Google Earth (© 2012 Google) in conjunction with U.S. Geological Survey (USGS) topographical map products (USGS, 2012a)..... 9

Figure 1.3. Annual mean major chemical species for (a) TSP, (b) PM_{10}, and (c) $PM_{2.5}$. Concentrations are expressed as mass fractions of oxides, sulfate (in gypsum), chloride (in salt), nitrate, and ammonium (from Engelbrecht et al., 2008) 16

Chapter 2

Figure 2.1. Schematic diagram displaying how higher-momentum, larger particles impact the Mylar™ strip on the edge of a drum while smaller particles are caught in the airstream moving around the drum. The thin black lines with arrows are trajectory paths of each hypothetical particle 32

Figure 2.2. Sector dividing segments radiating outwards from Bagram, Afghanistan. The numbers represent the sector number assigned to each area. Image created via Google Earth (© 2011 Google) 37

Chapter 3

Figure 3.1. Surface wind roses from Kabul, Afghanistan for (a) January to April, (b) May to August, and (c) September to December 2010 49

Figure 3.2. Annual surface wind roses from Kabul, Afghanistan from (a) 00Z, 03Z, 06Z, 09Z, (b) 12Z, 15Z, 18Z, and 21Z 53

Figure 3.3. Surface wind roses from Kandahar, Afghanistan for (a) January to April, (b) May to August, and (c) September to December 2010 56

Figure 3.4. Annual surface wind roses from Kandahar, Afghanistan from (a) 00Z, 03Z, 06Z, 09Z, (b) 12Z, 15Z, 18Z, and 21Z 59

Page

Figure 3.5. Calcium concentrations for Bagram, Afghanistan, from March 17, 2010 to April 6, 2010 63

Figure 3.6. Calcium concentrations for Bagram, Afghanistan, from April 7, 2010 to April 27, 2010 64

Figure 3.7. Calcium concentrations for Bagram, Afghanistan, from April 30, 2010 to May 22, 2010 65

Figure 3.8. Bromine concentrations for Bagram, Afghanistan, from March 17, 2010 to April 6, 2010 67

Figure 3.9. Potassium concentrations for Bagram, Afghanistan, from March 17, 2010 to April 6, 2010 68

Figure 3.10. Backward trajectories for air reaching Bagram, Afghanistan, during a high submicron calcium, bromine, and potassium aerosol event in April 2010 69

Figure 3.11. Zinc concentrations for Bagram, Afghanistan, from February 6, 2010 to February 28, 2010 75

Figure 3.12. Lead concentrations for Bagram, Afghanistan, from February 6, 2010 to February 28, 2010 76

Figure 3.13. Backward trajectories for air reaching Bagram, Afghanistan, during a high lead aerosol event in February 2010 77

Figure 3.14. Backward trajectories for air reaching Bagram, Afghanistan, during a high lead and zinc aerosol event in February 2010 78

Figure 3.15. Sector analysis at Bagram, Afghanistan from February 6, 2010 to February 28, 2010. Note the days of February 6-10 and 22-28 as periods of increased contributions from sector 4 as mentioned in section 3.2.2 79

Figure 3.16. Arsenic concentrations for Bagram, Afghanistan, from February 6, 2010 to February 28, 2010 81

Figure 3.17. Copper concentrations for Bagram, Afghanistan, from March 17, 2010 to April 6, 2010 83

Page

Figure 3.18. Zinc concentrations for Bagram, Afghanistan, from March 17, 2010 to April 6, 2010 84

Figure 3.19. Sector analysis at Bagram, Afghanistan from March 17, 2010 to April 6, 2010. Note the sector percentages from March 23-25 and March 31 to April 2 as described in section 3.2.2 85

Figure 3.20. Backward trajectory for air reaching Bagram, Afghanistan, during a high zinc and copper aerosol event in March 2010 86

Figure 3.21. Chlorine concentrations for Bagram, Afghanistan, from March 17, 2010 to April 6, 2010 87

Figure 3.22. Backward trajectories for air reaching Bagram, Afghanistan, during a high lead, copper, zinc, chlorine, and bromine aerosol event in April 2010 90

Figure 3.23. Zinc to copper elemental ratio (by mass; Zn/Cu) in the 0.34 – 0.56 μm size range for Bagram, Afghanistan, from March 17, 2010 to April 6, 2010. Note the upper boundary was cut off at a mass fraction of 10 in order to better view the low Zn/Cu mass fractions occurring between March 23-25 and March 31 to April 2 91

Figure 3.24. PM_{10} and $PM_{2.5}$ mass concentrations for Bagram, Afghanistan, from February 6, 2010 to February 28, 2010 93

Figure 3.25. PM_{10} and $PM_{2.5}$ mass concentrations for Bagram, Afghanistan, from March 17, 2010 to April 6, 2010 94

Figure 3.26. PM_{10} and $PM_{2.5}$ mass concentrations for Bagram, Afghanistan, from April 7, 2010 to April 27, 2010 95

Figure 3.27. PM_{10} and $PM_{2.5}$ mass concentrations for Bagram, Afghanistan, from April 30, 2010 to May 22, 2010 96

Figure 3.28. Sector analysis at Bagram, Afghanistan from April 7, 2010 to April 27, 2010 100

Figure 3.29. Sector analysis at Bagram, Afghanistan from April 30, 2010 to May 22, 2010 101

Page

Figure 3.30. PCA biplot showing transformed aerosol data and eigenvector loadings. Eigenvector loadings have been extended 30 fold compared to values in Table 3.1 to make them more visible 105

Figure 3.31. PCA biplot showing transformed aerosol data and eigenvector loadings. Eigenvector loadings have been extended 30 fold compared to values in Table 3.2 to make them more visible 106

Figure 3.32. PCA biplot showing transformed aerosol data and eigenvector loadings. Eigenvector loadings have been extended 30 fold compared to values in Table 3.3 to make them more visible 107

Figure 3.33. PCA biplot showing transformed aerosol data and eigenvector loadings. Eigenvector loadings have been extended 30 fold compared to values in Table 3.4 to make them more visible 108

LIST OF TABLES

Page

Chapter 1

Table 1.1. Percentage of dust storms by month from various locations around Afghanistan, Pakistan, and India. Months with the largest frequency of dust storms are shown in bold (from Goudie and Middleton, 2000) 8

Table 1.2. 24-hour particulate matter air MEGs (USAPHC, 2010) 27

Table 1.3. 1-year particulate matter air MEGs (USAPHC, 2010) 28

Chapter 3

Table 3.1. PCA eigenvector loadings for Bagram, Afghanistan. Highlighted in yellow (blue) are negative (positive) significant eigenvector loadings with an absolute value greater than or equal to 0.50/√(Eigenvalue) 70

Table 3.2. PCA eigenvector loadings for Bagram, Afghanistan. Highlighted in yellow (blue) are negative (positive) significant eigenvector loadings with an absolute value greater than or equal to 0.50/√(Eigenvalue) 71

Table 3.3. PCA eigenvector loadings for Bagram, Afghanistan. Highlighted in yellow (blue) are negative (positive) significant eigenvector loadings with an absolute value greater than or equal to 0.50/√(Eigenvalue) 72

Table 3.4. PCA eigenvector loadings for Bagram, Afghanistan. Highlighted in yellow (blue) are negative (positive) significant eigenvector loadings with an absolute value greater than or equal to 0.50/√(Eigenvalue) 73

Table 3.5. CMB model results for Bagram, Afghanistan. Concentration units are in ng m^{-3} 110

LIST OF ABBREVIATIONS

AFB ..... Air Force Base

AGL..... Above Ground Level

ARL..... Army Research Laboratory

CMB ..... Chemical Mass Balance

DRUM..... Davis Rotating-drum Universal-size-cut Monitoring

EPA ..... Environmental Protection Agency

HYSPLIT ..... Hybrid Single Particle Lagrangian Integrated Trajectory

ITCZ..... Inter-Tropical Convergence Zone

MEG..... Military Exposure Guideline

NAAQS..... National Ambient Air Quality Standard

NIST..... National Institute of Standards and Technology

PCA..... Principal Components Analysis

PM..... Particulate Matter

$PM_{2.5}$..... Particulate Matter (<2.5 μm in aerodynamic diameter)

PM_{10} ..... Particulate Matter (<10 μm in aerodynamic diameter)

PMF..... Positive Matrix Factorization

S-XRF ..... Synchrotron X-Ray Fluorescence

TSP..... Total Suspended Particulate

USGS..... United States Geological Survey

USAPHC ..... United States Army Public Health Command

UTC ..... Coordinated Universal Time

WHO ..... World Health Organization

ACKNOWLEDGEMENTS

I would like to give my sincerest thanks to my advisor, Catherine F. Cahill, for this research opportunity, her guidance and support, and being an encouraging friend over the years. I would like to thank Nicole Mölders for her helpfulness as one of my committee members and the large role she played in shaping my college successes and early research career. I would like to thank my other committee member, William R. Simpson, for his valuable insights towards this research and his immense contributions toward my education over the years. I would like to thank Chris Iceman for his computer program contributions and assistance with computer troubleshooting. I would also like to thank Javier Fochesatto for his vital teachings in MATLAB programming. Many thanks go out to all my colleagues and my group members including Mitali Patil, Ashley Wallace, Tara Craft, Sean Egan, Jennifer Chambers, and undergraduate researcher Alesha Castner for stimulating discussions and special thanks to group members: Peter Rinkleff for his teachings in the lab, Taryn Lopez for her early roles in sparking my interests in aerosol research and helping me receive this research opportunity, and Jennifer Bell for critical insights that proved invaluable during the course of researching Middle Eastern aerosols. Finally, a special thanks goes out to my brother Timothy Fortun for his descriptions of Afghanistan while on deployment.

This research was funded by the U.S. Army Research Laboratory through grant numbers W911NF-08-01-0318 and W911NF-09-01-0543.

1. Introduction

1.1. Definition and formation of aerosols

An aerosol is defined as any solid or liquid particle suspended in a gas. Aerosols come in many shapes, sizes, densities, and weights causing difficulties in classifying them. To alleviate this issue, aerosols are classified based on aerodynamic diameter. A particle's aerodynamic diameter is the diameter a particle would have as a perfect sphere with unit density. A particle's aerodynamic diameter will be referred to synonymously as its diameter throughout this thesis.

Particulate matter (PM) is often described in terms of its mass in three different regimes: total suspended particulates (TSP), PM less than 10 μm in diameter (PM_{10}), and PM less than 2.5 μm in diameter ($PM_{2.5}$).

Atmospheric aerosols can be generated in many ways. Loose material on the ground can be mechanically lofted by wind such as occurs with desert dust; aerosols can be emitted directly such as occurs with volcanic ash; particles can be the product of conglomeration of gases undergoing chemical reactions such as occurs with sulfur dioxide to sulfuric acid.

1.2. Thesis goals

The climatology of Afghanistan and central Asia in general plays a vital role in the presence of aerosols spatially and temporally. It affects aerosol

concentrations, compositions, and diurnal and seasonal fluctuations. Little research has been done in Afghanistan itself; therefore, the surrounding regions must be examined to help construct the Afghanistan region's aerosol puzzle.

In addition to discussing the climatology and aerosol characteristics in this region of the world, this thesis will examine past research concerning the health effects of inhaling aerosols and the health safety standards pertaining to aerosols as well as comparing the results to military exposure guidelines (MEGs), National Ambient Air Quality Standards (NAAQS), and World Health Organization (WHO) standards.

This thesis will identify potential sources of aerosols in Afghanistan using a variety of methods including meteorological backward trajectories and principal components analysis (PCA). Regional meteorology has a large influence on these aerosols tending to transport aerosols into Afghanistan from surrounding nations. The surrounding nations in central Asia have numerous air-quality issues including natural dust and heavy metals (see section 1.5). Literature exists documenting these air-quality issues (Shahgedanova and Burt, 1994; Dahl and Kuralbayeva, 2001; Singer et al., 2003; Nabi Bidhendi and Halek, 2007; Schneidemesser et al., 2010), but the literature lacks information concerning air quality in Afghanistan. Therefore, this thesis will help fill the gap where the literature is deficient on the sources and types of aerosols in Afghanistan, especially simultaneous size- and temporally-resolved aerosol characteristics.

The aerosol sampling described in this thesis was conducted at Bagram Air Force Base (AFB) (34.94° N, 69.27° E) in Afghanistan (see Figure 1.1).

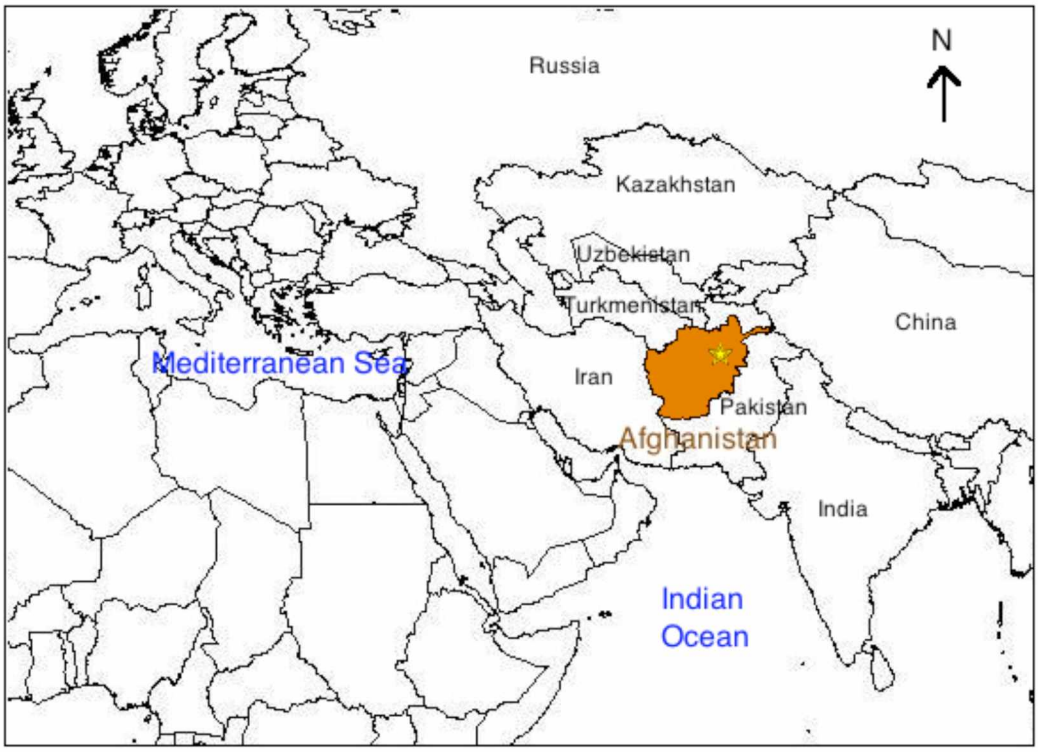

Figure 1.1. Location of Afghanistan (in orange) and a map of the surrounding region. The yellow star in Afghanistan denotes the location of Bagram Air Force Base.

1.3. Climatology of the Afghanistan region

The topography of Afghanistan and the surrounding region and the shifting of the inter-tropical convergence zone (ITCZ) induce distinct regional climatic characteristics. Bagram is located at the northern end of the Kabul Valley and is surrounded on three sides by mountains. Aside from Afghanistan being well removed from the ocean, the mountains along the Afghanistan-Pakistan border significantly reduce the moisture influx into the region. Furthermore, during the Asian monsoon, Afghanistan lies to the north of the ITCZ; therefore, air converges toward the Himalayas from the vast amount of land to the north (Chen et al., 2010a; Wang et al., 2010). These features cause difficulties in producing precipitation, resulting in aerosols to residing in the ambient air for longer periods of time than in wetter areas because the primary aerosol deposition mechanism of washout is turned off (Shrestha et al., 2000). In Kabul, Afghanistan, the months of December through March receive the largest amounts of precipitation with approximately 1 to 3 cm each month while June through October average a few millimeters each month (El Dorado Weather, 2011).

1.3.1. Wind patterns

Surface winds in Afghanistan are high during the summer (average of 3.6 m s^{-1} in Kabul during summer 2010) and low in the winter (average of 2.1 m s^{-1} in

Kabul during winter 2010). Occasionally heavy winds with strong gusts occur. On the larger scale, the upper level westerlies are a dominant wind forcing mechanism (Han et al., 2008). During the winter and into the spring, the westerly sub-tropical jet resides on the southern flank of the Himalaya Mountains. While this jet is present on the southern flank of the Himalayas, the monsoon is inhibited (Schott and McCreary Jr., 2001). With the onset of the warmer months, the ITCZ moves northward. Eventually the sub-tropical jet shifts to the northern flank of the Himalayas allowing the onset of the monsoon in southern Asia and the influx of drier air into central Asia and Afghanistan (Schott and McCreary Jr., 2001; Allen and Armstrong, 2011). Evidence for the regularity of this type of flow pattern can be witnessed in the glacier ice on the Tibetan Plateau. Ice cores show that mineral dust is a major contributor to impurities in the ice found in the northern Tibetan Plateau and that sea salt dominates the impurities in ice found toward the south of the plateau (Cunde et al., 2002).

The general wind patterns of the low to middle troposphere over the Afghanistan region change throughout the year (NOAA CPC, 2011). They can be summarized into four distinct periods. December through March experiences a more westerly/southwesterly flow pattern. April through May, winds are reduced in strength. This is a transition period to the impending monsoon season. From June through September, winds in Afghanistan are strong from the north and northwest, although these tend to reduce in magnitude by August and September. Many have dubbed this time period as the "wind of 120 days". During this time

period, dust storms in Afghanistan are most prevalent (Goudie and Middleton, 2000; see Table 1.1). Finally, October and November experience a post-monsoon transition period back to the more westerly and southwesterly flow. Table 1.1 shows how the shifting of the winds throughout the year cause variations in the frequency of dust storms generated monthly in the different regions of Afghanistan. Mazar-e sharif and Feyzabad, located in northern Afghanistan, see many of their annual dust storms during the months of June through October; Ghazni, located in the Kabul Valley south of Bagram, experiences greater numbers of dust storms April through October; and Bust (also known as Lashkar Gah), located west of Kandahar, can more than double its average monthly dust storm count from less than five to more than ten starting as early as February and lasting through August. These cities, as well as the topography of the Afghanistan, can be seen in Figure 1.2.

Table 1.1. Percentage of dust storms by month from various locations around Afghanistan, Pakistan, and India. Months with the largest frequency of dust storms are shown in bold (from Goudie and Middleton, 2000).

	J	F	M	A	M	J	J	A	S	O	N	D	Av. no. per year
Afghanistan													
Bust	4.7	9.5	10.4	13.7	10.4	8.5	10.4	**14.2**	5.7	4.3	3.3	4.7	30.1
Ghazni	0.0	0.0	2.2	**20.0**	13.3	11.1	13.3	14.8	8.1	10.3	5.2	1.5	19.3
Mazarisharif	0.8	0.8	4.8	4.8	4.0	15.9	15.1	13.5	7.1	**23.0**	8.7	1.6	18.7
Faizabed	0.0	0.0	1.4	7.1	4.3	14.3	20.0	**22.9**	8.6	17.1	4.3	0.0	17.5
Pakistan													
Bannu	0.0	1.2	5.9	4.7	19.6	15.7	**23.5**	15.7	11.8	2.0	0.0	0.0	25.5
Dalbandin	3.5	7.0	14.0	14.0	14.0	14.0	**17.5**	7.0	4.2	2.8	1.0	1.0	28.6
Jacobabed	1.1	0.0	16.3	12.0	18.5	12.0	**21.7**	12.0	4.3	0.0	0.0	2.2	9.2
Panjgur	3.4	17.2	**31.0**	3.4	6.9	17.2	13.8	3.4	0.0	3.4	0.0	0.0	3.6
Peshawar	0	7.4	1.5	3.7	**22.2**	14.8	**22.2**	14.8	12.6	6.7	7.4	0.0	13.5
Quetta	0.0	1.8	7.1	5.4	12.5	17.9	5.4	12.5	**19.6**	16.1	0	1.8	5.6
Rawalpindi	0.0	1.4	4.3	14.2	**21.3**	**21.3**	14.2	9.9	7.1	5.7	0.7	0.0	14.1
India													
Ganganagar	8.9	0.0	11.1	0.0	**33.3**	24.4	13.3	8.9	0.0	0.0	0.0	0.0	17.0
New Delhi	0.0	0.0	10.0	10.0	**40.0**	35.0	3.3	0.0	0.0	1.7	0.0	0.0	8.0
Kanpur	4.4	2.2	8.9	13.3	**44.4**	20.0	0.0	0.0	0.0	4.4	2.0	0.0	5.0
Jamshedpur	0.0	0.0	7.1	23.8	**50.0**	16.7	2.4	0.0	0.0	0.0	0.0	0.0	6.0
Bikaner	1.7	6.7	9.5	11.2	16.8	**27.9**	11.2	7.3	3.4	3.4	0.0	1.1	17.9
Allahabad	0.0	5.9	3.9	13.7	**39.2**	29.4	5.9	0.0	0.0	2.0	0.0	0.0	5.1
$\bar{X}$	1.68	3.59	8.79	10.29	21.81	18.60	12.54	9.23	5.44	6.05	1.72	0.81	–

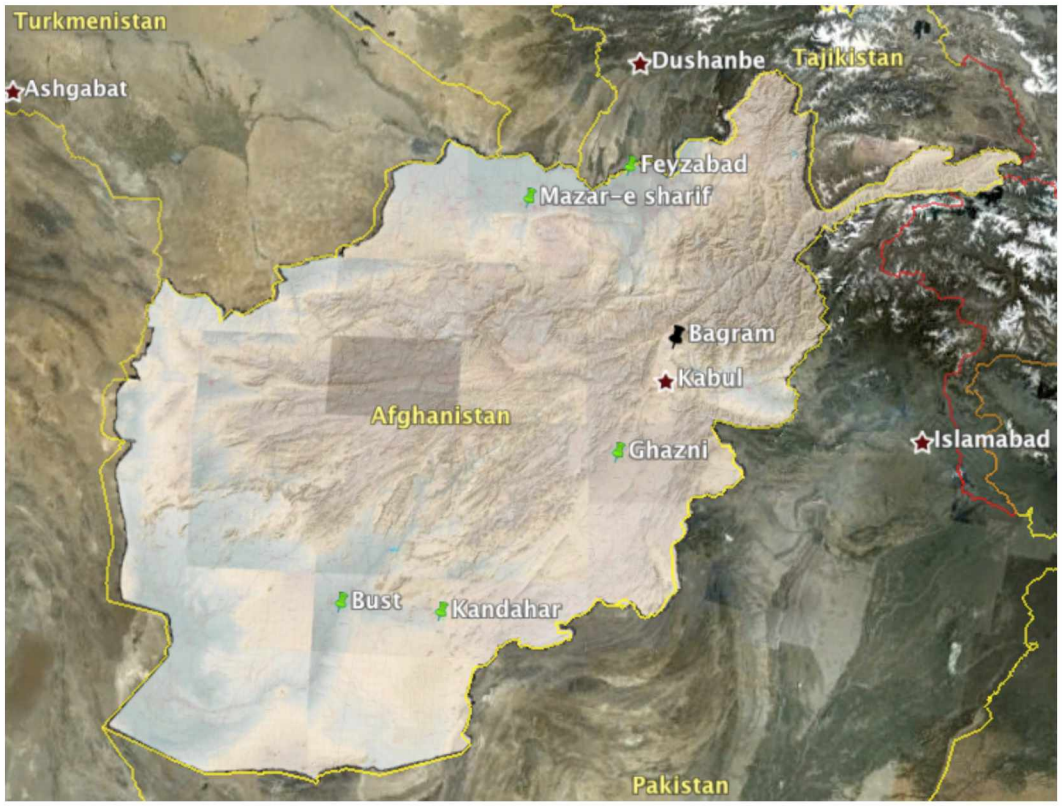

Figure 1.2. Afghanistan cities and topography. Star markers indicate capital cities. Image created via Google Earth (© 2012 Google) in conjunction with U.S. Geological Survey (USGS) topographical map products (USGS, 2012a).

1.3.2. Diurnal cycles

Areas all over the world, especially those with complex terrain, experience diurnal cycles of pollutants and aerosols (Tanner et al., 2005; Vondou et al., 2010; Saide et al., 2011). The same is true in the Himalayas where topographically-influenced diurnal cycles are present. In the northwestern Himalayan region in India, Gajananda et al. (2005) showed that maximum values of Aitken nuclei (i.e. any particle that acts as a condensation nuclei during expansion in an Aitken dust-counter) occur between 11:00 and 14:00 local time. At Manora Peak in the Central Himalayas, Dumka et al. (2010) saw a single defined peak of black carbon in the late afternoons between October and March. In Kathmandu Valley, Nepal, Aryal et al. (2009) found a daily repetitive cycle in the $PM_{2.5}$ data with concentration peaks in the morning and evening periods that diminished during the afternoon and nighttime respectively.

In Kabul, Afghanistan (approximately 40 km south of Bagram), topographically-influenced extreme day and night temperature differences can cause strong nocturnal temperature inversions leading to the build-up of pollutants overnight. Strong diurnal heating leads to some dilution of these pollutants during the day (Engconsult Ltd., 2007).

1.4. Elemental sources and uses

Twenty-seven elements are analyzed in the study described in this thesis. These elements are Al, As, Br, Ca, Cl, Co, Cr, Cu, Fe, Ga, K, Mg, Mn, Mo, Ni, P, Pb, Rb, S, Se, Si, Sr, Ti, V, Y, Zn, and Zr. An understanding of their origins and uses are essential if they are to be sourced back to a specific area. This section will provide a brief, non-exhaustive overview of some of the sources for many of these elements.

Several of the elements are primarily contained in crustal material. These elements include Al, Ca, Cr, Fe, Mg, Mn, Si, and Ti (Emsley, 2002). Many other elements are contained within crustal material, but their anthropogenic uses have a substantial contribution and will be discussed in the following paragraphs.

There are a number of Pb and Zn containing deposits in Pakistan (USGS, 2012b). Lead is used in construction, lead-acid batteries, bullets (this region of the world has been ravaged by war for decades), paints, and gasoline, although many nations have removed lead from petrol products in recent years (Emsley, 2002). Zinc is used as an anticorrosive agent and can contaminate soil during the mining and refining processes (Emsley, 2002). Sulfur dioxide and Cd vapors are produced in large quantities during the smelting of zinc sulfide ores (Emsley, 2002). Zinc is often found alongside Pb and Cu in ores. Copper has a number of industrial applications, including electrical and plumbing equipment (Emsley, 2002). Hundreds of thousands of metric tons of Cu are produced in Kazakhstan,

Uzbekistan, and Iran annually (USGS, 2012d). Molybdenum is a byproduct of Cu and W production and it too has numerous industrial applications such as being used as a lubricant and anti-corrosion additive (Emsley, 2002).

Arsenic is a by-product of Cu and Pb refining (Emsley, 2002). Significant amounts of As result from the burning of fossil fuels. Arsenic, like Pb, is found in bullets. Arsenic is often found naturally with S in mineral compounds as well as volcanic ash (Emsley, 2002).

Gallium is often found in the form GaAs (Emsely, 2002) and Kazakhstan produces an estimated twenty tons of gallium each year (USGS, 2012c). Some refiners collect Ga as a by-product of Zn refining.

Some elements are commonly associated with combustion: K from biomass burning (Cahill et al., 2008), Se and S from coal, and V and Ni from oil combustion (Emsley, 2002). Nickel is found in organisms and often naturally with Fe and S compounds. Significant Ni deposits are found in Russia (Emsley, 2002) and some in the coastal countries of the eastern Mediterranean Sea such as Greece (USGS, 2012c). Sulfur is produced during oil refining, but is also found in salt domes. Some of these salt deposits can be found in Eastern Europe and Western Asia such as in the Caspian Sea region, Arabian Peninsula, and even in Pakistan at the Khewra Salt Mine, the second largest salt mine in the world. These salt deposits, like sea spray from the ocean and seas, contain Cl and Br.

Other elements such as P and Zr are found in the surrounding area of Afghanistan. Significant global P reserves are found in Russia and northern Africa (Emsley, 2002). India is a large producer of Zr (USGS, 2012b).

1.5. Aerosol chemistry and seasonality

Aerosols in Afghanistan and the surrounding region have contributions from both natural and anthropogenic sources (Lella et al., 2006; Engelbrecht et al., 2008; Schneidemesser et al., 2010) and from both local and distant locations (Prospero et al., 2002; Liu et al., 2010). This generates difficulties in establishing source locations. Saharan and Middle Eastern dust, including local dust generated in Afghanistan, vehicle emissions, heavy metals from industrial sources, and controversial burn pits, all contribute aerosols to Afghanistan's ambient air (Engelbrecht et al., 2008). In Bagram, Afghanistan, the three main air pollutant types were found to be geological dust, smoke from burn pits, and heavy metal condensates suspected to be from lead smelting and battery manufacturing facilities (Engelbrecht et al., 2008). However, the "National Defense Authorization Act for Fiscal Year 2010", also known as H.R. 2647 of the 111th Congress, was signed into law by President George W. Bush on October 28, 2009 banning the use of military burning pits in Afghanistan.

1.5.1. Geological dust

As geological dust has been identified as one of the main aerosols affecting Afghanistan, understanding its size distribution, concentration, transport, and composition is crucial to determining exposure levels and health hazards. It has been found that potential sources of aeolian (aeolian processes refer to the wind's ability to shape the Earth's surface through erosion, transport, and deposition) dust are "topographic lows or they are situated in close proximity to mountains and highlands. In mountainous regions (e.g., Afghanistan, Iran, Pakistan, and China), strong dust sources are often found in closed intermountain basins" (Prospero et al., 2002).

In Bagram, it was found that nearly 75% of particulates by mass fall between 2.5 μm and 7.5 μm in aerodynamic diameter and comprises a large portion of the local PM_{10} (Engelbrecht et al., 2008). These particulates are primarily composed of Si, Al, Ca, Mg, and Fe based compounds (Engelbrecht et al., 2008; see Figure 1.3). These facts are indicative of dust sources. In addition, it was determined that a vast majority of the mass in the ultrafine size fraction (< 0.1 μm in aerodynamic diameter) was lead (Engelbrecht et al., 2008). In Lahore, Pakistan, dust sources contribute on average (maximum) 41% (70%) of PM_{10} mass and 14% (29%) of $PM_{2.5}$ mass on a monthly basis while Pb, Zn, and Cd comprised most of the $PM_{2.5}$ mass (Schneidemesser et al., 2010). From these two locations, it can be inferred that the larger-sized aerosols seen in the Kabul Valley and the

eastern plain regions can contribute a significant amount of aerosol mass. Fine-sized heavy metals such as lead also appear to be significant in both locations.

In comparison, it has been found that Saharan aerosols are dominated by mineral dust with an average composition by volume of 64% silicates, 6% quartz, 5% calcium-rich particles, 14% sulfates, 1% hematite, 1% soot, and 9% other carbonaceous material (Kandler et al., 2007).

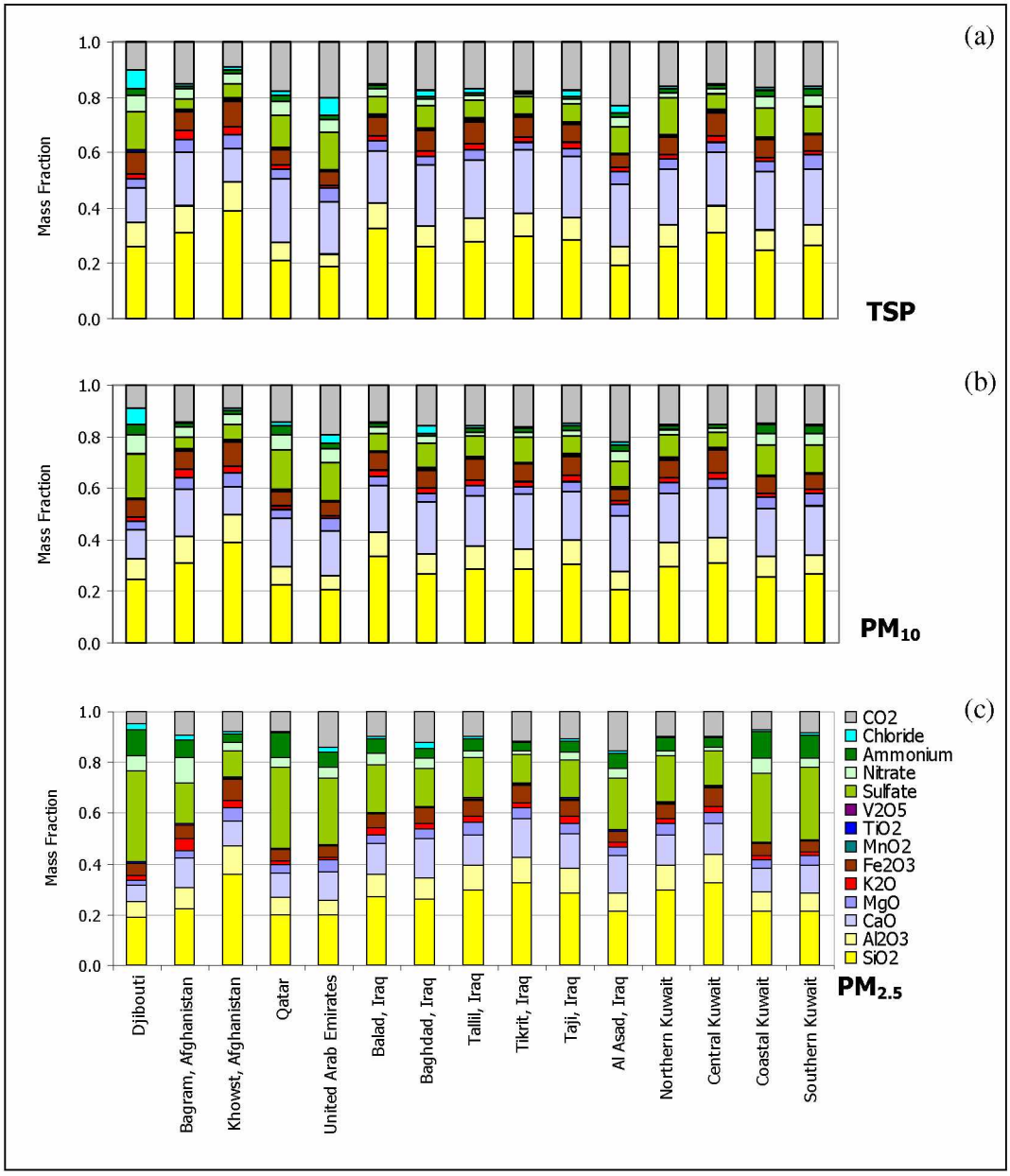

Figure 1.3. Annual mean major chemical species for (a) TSP, (b) PM_{10}, and (c) $PM_{2.5}$. Concentrations are expressed as mass fractions of oxides, sulfate (in gypsum), chloride (in salt), nitrate, and ammonium (from Engelbrecht et al., 2008).

Dust concentrations exhibit seasonal variations. In what has been dubbed "the dust belt," an area extending from the Sahara desert to East Asia, dust activity peaks in the spring (Prospero et al., 2002). Other studies agree with this conclusion: in Lahore, Pakistan, the lowest dust concentrations occur during the monsoon (July through September) and higher concentrations occur during the pre- and post-monsoon seasons (Schneidemesser et al., 2010); at the Arabian Sea, dust at the surface peaks in the winter and spring (Tindale and Pease, 1999); and at a rural mountain site in Nepal, aerosol concentrations were low late in the monsoon season and post-monsoon season, but gradually increased throughout the winter season and into spring (Shrestha et al., 2000). Regions further inland, such as Tehran, Iran, experience higher dust aerosol concentrations in summer (Nabi Bidhendi and Halek, 2007). This behavior is because Tehran does not receive the large influx of precipitation needed to suppress dust aerosol formation. In summary, those areas near the ocean and heavily affected by the precipitation of the summer monsoon see higher dust aerosol concentrations in the pre- and post-monsoon seasons, especially the pre-monsoon season when precipitation has been limited for several months beforehand. Such is the case with India until the summer monsoon rains arrive beginning around June (see Table 1.1). In contrast, those areas further inland and away from the monsoon rains experience higher dust aerosol concentrations during the summer months when the winds arrive at the locations from the north (overland) rather than from the south (over the ocean). However, due to local effects such as topography, aerosols may not follow the

expected seasonal pattern. Local winds (anabatic/katabatic wind, boundary layer turbulence, etc.) can frequently stir up dust even during seasons when the dust concentration is expected to be low, such as was seen at the base of the Rocky Mountains in the United States by Orgill and Sehmel (1976).

Regional winds in the Middle East have the ability to loft dust high into the atmosphere where it can then travel vast distances. Lofting is enhanced by complex terrain (Kim and Stockwell, 2008). When the synoptic conditions are right, dust storms occurring in the Sahara Desert and Middle East can lead to the transport of dust to East Asia (Tanaka et al., 2005). Strong winds associated with cold front passages and deep low-pressure complexes have been known to cause rapid increases in suspended particulate matter resulting in transport of Asian dust from China to the Pacific Ocean (Iino et al., 2004). These Asian dust storms have scattered dust across Asia (Arimoto et al., 2006) and initiated dust transport to the Pacific Ocean (Arimoto et al., 2006), Alaska (Cahill, 2003), and the west coast of the continental United States (Jaffe et al., 2003).

1.5.2. Anthropogenic aerosols

1.5.2.1. Pakistan

In contrast to the dust concentrations that display consistent seasonal fluctuations, heavy metal concentrations in the region are far more variable due to the fact that they have an anthropogenic component; however, some still exhibit

seasonal variations. At Mt. Muztagata in the Eastern Pamirs, just to the east of Afghanistan, Wu et al. (2009) found that As, Bi, Cd, Pb, and Zn have high concentrations during the summer (July to October) and low concentrations during the winter (October to February), a pattern similar to that of crustal aluminum, while Cr, Cu, and Ni display different behavior than crustal aluminum. Mt. Muztagata is distant from anthropogenic sources, thus the presence of anthropogenic pollutants at the site suggests atmospheric transport.

In Lahore, Pakistan, Schneidemesser et al. (2010) found that of the already extremely high aerosol heavy metal concentrations of Pb (4.4 μg m^{-3}), Zn (12 μg m^{-3}), and Cd (0.077 μg m^{-3}), 84% of Pb, 98% of Zn, and 90% of Cd concentrations were less than 2.5 μm in diameter, meaning that these elements were present in the respirable size fraction. Schneidemesser et al. (2010) is consistent with Smith et al. (1996) who found high levels of Pb in the ambient air in Pakistan from leaded gasoline. In addition, Smith et al. (1996) found high ambient levels of Mn, V, As, Cr, and Ni. Faiz et al. (2009) discovered high soil concentrations of Cd, Cu, Ni, Pb, and Zn along the Islamabad Expressway in Pakistan adding evidence that some of the aerosols seen by Smith et al. (1996) and Schneidemesser et al. (2010) are being emitted by motor vehicles.

At a remote site in northern Pakistan, approximately 370 km east of Bagram, Afghanistan, that is distant from urban and industrial sources, Ghauri et al. (2001) found aerosols highly enriched with As, Cd, Cl, Pb, Sb, Se, Tl, and Zn, suggesting anthropogenic contributions to the aerosol load, especially since Cd and

Se are typically associated with coal-burning emissions. Selenium in Pakistan may likely be due to anthropogenic effects, but Se has maritime origins such as dimethyl selenide (Amouroux and Donard, 1996; Amouroux et al., 2001), and could be transported to the region.

Coal burning is also a significant contributor of sulfur in the form of SO_2, which can be oxidized to form SO_4^{2-}. Relatively high concentrations of SO_4^{2-} were found at the same northern Pakistan site with up to about half believed to have been derived from in-cloud SO_2 to SO_4^{2-} conversion of coal burning generated SO_2 (Ghauri et al., 2001).

In general, Pakistan has been suffering from poor air quality across the country for many years. Its poor air quality includes extremely high, annually-averaged levels of PM, SO_2, and Pb amongst other pollutants (Colbeck et al., 2010).

1.5.2.2 Kazakhstan, Turkmenistan, and Uzbekistan

Kazakhstan, Turkmenistan, and Uzbekistan face numerous pollution problems, especially heavy metals such as Cd, Zn, Pb, and Fe (Shahgedanova and Burt, 1994; Farmer and Farmer, 2000; Mukai et al., 2001). These nations, especially Kazakhstan, have large deposits of metals, such as Cu and Mo, available for mining (Chen et al., 2010b). The extraction and use of these natural resources, as well as others such as oil, have led to serious air-quality issues (Dahl and

Kuralbayeva, 2001). In comparison, Afghanistan has numerous deposits of metals, coal, and oil, but they remain relatively underexplored and are not a major economic factor (Kuo, 2007; USGS, 2012b).

As of 2008, the Clearing-House for the Partnership for Clean Fuels and Vehicles stated that Afghanistan and Uzbekistan were two of the few remaining nations that used both leaded and unleaded fuels (Clearing-House, 2011). Afghanistan had plans for phasing out leaded fuels at the time of writing this thesis, but Uzbekistan had not set a date for the phase out of leaded fuels (Clearing-House, 2011).

Further pollution matters in the region, especially in the bordering countries of Kazakhstan and Uzbekistan, arise from the dwindling size of the Aral Sea, and as a result, increased potential to generate aerosols (Singer et al., 2003). Large quantities of salts have deposited out of the Aral Sea brine over the past few decades leading to the formation of gypsum, mirabilite, halite, glauberite, and epsomite (Zavialov and Ni, 2010). These conglomerates can be lofted into the atmosphere by the wind and transported.

Finally, similar to other Middle Eastern countries, dust storms are prevalent in Turkmenistan. Orlovsky et al. (2005) found that dust storms can occur on over 60 days of the year, and in extreme cases, nearly 150 days of the year. Although not a large metal polluter, Turkmenistan has rich deposits of lead, zinc, and copper (Haggett, 2002). Its close proximity to Afghanistan and the prevailing wind

patterns make Turkmenistan a possible source for some of the aerosols in Afghanistan.

1.5.3. Biomass burning

Ions contribute to the composition of aerosols. Cations and anions can bond to form the salts observed in PM. One potential cation is potassium (K^+). High temperature biomass fires emit potassium although the potassium concentrations decrease exponentially for a smoldering fire (Cahill et al., 2008). This behavior makes potassium a good tracer of smoke from biomass burning.

1.5.4. Aerosols over seas and oceans

In February through April of 1999, before the onset of the Indian monsoon, a research vessel collecting aerosols traveled through the Indian Ocean into the Arabian Sea and Bay of Bengal (Ball et al., 2003). It was found that air that had passed over India showed evidence of fossil fuel combustion, biomass burning, and aeolian material while air that had passed over Arabia showed little evidence of biomass burning but had more acidity, mineral dust, and higher nitrate to sulfate ratios compared to the air from India (Ball et al., 2003).

In the Aegean Sea, another research vessel found that sulfur has most of its mass in the submicron size range while crustal elements and Cl are more in the

supermicron size range (Smolik et al., 2003). Additionally, K, V, and Ni exhibited bimodal distributions where higher concentrations in the submicron size range of K resulted from forest fires, and V and Ni resulted from oil combustion (Smolik et al., 2003). Finally, anthropogenic elements Cr, Cu, Pb, and Zn were found in air masses tracing back to the west coast of the Black Sea, northern Greece, and western Turkey (Smolik et al., 2003).

1.6. Health concerns and standards

Air quality affects human health. It can potentially jeopardize the health of soldiers involved in military operations in regions with poor air quality. To understand these effects, the U.S. Army Research Laboratory (ARL) has prioritized the 'Aerosol Characterization for Soldier Health' initiative. This initiative investigates the aerosol species and concentrations to which soldiers in Iraq and Afghanistan have been exposed during the U.S. occupations.

Short- and long-term aerosol exposure, especially to $PM_{2.5}$, can lead to a variety of adverse human health effects including increased morbidity (e.g. asthma, chronic obstructive pulmonary disease, etc.) and premature mortality (Polichetti et al., 2009; EPA, 2011a). Inhaled fine (<2.5 μm in aerodynamic diameter) and ultrafine (<0.1 μm in aerodynamic diameter) particles enter the lungs where they can cause inflammation and other adverse effects within the lungs and can circulate to other organs causing further damage (Kennedy, 2007). Many of these

fine particles are produced by anthropogenic sources predominately through combustion (Kennedy, 2007). However, assessing the extent to which health is affected is challenging (Hall, 1996). An individual's current state of health and activities, the specie exposed to, time of exposure, and intensity of exposure can all influence the impact air quality will have on that individual.

A study by Samet et al. (2000) found that in response to each 10 $\mu g\ m^{-3}$ of PM_{10} measured the day prior, hospitals saw approximately a 0.5% increase in mortality, 1% increase in admissions for cardiovascular diseases, and 2% increase in admissions for pneumonia and chronic obstructive pulmonary disease.

In order to achieve clean air in the United States, the Clean Air Act, amended in 1990 with the Clean Air Act Amendments, mandated the Environmental Protection Agency (EPA) to set National Ambient Air Quality Standards (NAAQS). For PM_{10}, the 24-hour average must not exceed 150 $\mu g\ m^{-3}$; for $PM_{2.5}$, the 24-hour average must remain under 35 $\mu g\ m^{-3}$ and the annual average must be below 15 $\mu g\ m^{-3}$ (EPA, 2011b). Airborne lead concentration standards are determined using a 3-month rolling average standard set at 0.15 $\mu g\ m^{-3}$ and a quarterly average of 1.5 $\mu g\ m^{-3}$ (EPA, 2011b).

The World Health Organization (WHO) guidelines are stricter than the NAAQS. The WHO's 24-hour guideline for PM_{10} is 50 $\mu g\ m^{-3}$ and the annual guideline is 20 $\mu g\ m^{-3}$; the 24-hour guideline for $PM_{2.5}$ is 25 $\mu g\ m^{-3}$ and the annual guideline is 10 $\mu g\ m^{-3}$ (WHO, 2011).

The U.S. military adopts its own standards. Military exposure guidelines (MEGs) are set to protect military personnel. Since the NAAQS are set to protect all age groups across the United States in a wide variety of health conditions, and the MEGs are designed to protect only healthy adults, some MEGs allow higher exposure levels than the NAAQS. Military personnel are assumed to be in better physical condition than the general population and therefore less susceptible to the effects of poorer air quality. Furthermore, some NAAQS, such as lead, are designed to protect children who are more susceptible to lead poisoning (EPA, 2000). However, according to the New York Department of Health, adults exposed to lead are still at risk to neurological, gastrointestinal, and reproductive effects (NY DOH, 2012). The United States Army Public Health Command (USAPHC) has long-term (one-year) MEGs for lead at a concentration of 15 $\mu g\ m^{-3}$ (USAPHC, 2010). USAPHC has PM MEGs as seen in Tables 1.2 and 1.3.

Engelbrecht et al. (2008) conducted aerosol studies using samplers located at 15 U.S. military one of which was Bagram, Afghanistan. Each sampling site had three samplers including one for TSP, PM_{10}, and $PM_{2.5}$. Sample collection occurred on a "1 in 6" day cycle over the course of one year and rotated between three different types of filter media including Teflon® membrane, quartz fiber, and Nuclepore®. This study extends the study by Engelbrecht et al. (2008) by providing both a greater aerosol size breakdown and higher time resolution measurements of the aerosol species, both of which are necessary for accurate pathological analyses. Furthermore, the use of a single sample substrate will

remove one of the potential sources of error mentioned in the study by Engelbrecht et al. (2008).

Table 1.2. 24-hour particulate matter air MEGs (USAPHC, 2010).

Hazard Severity	$PM_{2.5}$	PM_{10}	Description of Military Health and Operational Effects
Critical	500 $\mu g/m^3$	600 $\mu g/m^3$	Above these, most if not all personnel will experience very notable eye, nose, and throat irritation and respiratory effects. Visual acuity is impaired, as is overall aerobic capacity. Some personnel will not be able to perform assigned duties. Some lost-duty days are expected. Those with a history of asthma or cardiopulmonary disease will experience more severe symptoms.** Conditions may also result in adverse, non-health related materiel/logistical impacts.
Marginal	250 $\mu g/m^3$	420 $\mu g/m^3$	Above these, a majority of personnel will experience notable eye, nose, and throat irritation and some respiratory effects. Some lost-duty days are expected. Significant aerobic activity will increase risk. Those with a history of asthma or cardiopulmonary disease are expected to experience increased symptoms.**
Negligible	65 $\mu g/m^3$	250 $\mu g/m^3$	Above these, a few personnel may experience notable mild eye, nose, or throat irritation; most personnel will experience only mild effects. Pre-existing health conditions (e.g., asthma, or cardiopulmonary diseases) may be exacerbated.**

Table 1.3. 1-year particulate matter air MEGs (USAPHC, 2010).

Hazard Severity	$PM_{2.5}$	PM_{10}	Description of Military Health and Operational Effects
Marginal	65 µg/m^3	Not defined	With repeated exposures above this, it is plausible that development of chronic health conditions such as reduced lung function or exacerbated chronic bronchitis, COPD, asthma, atherosclerosis, or other cardiopulmonary diseases could occur in generally healthy troops. Those with a history of asthma or cardiopulmonary disease are considered to be at particular risk. This guideline is an uncertain screening value—it is not a known health effects concentration.
Negligible	15 µg/m^3	Not defined	With repeated exposures above this, it is considered possible that a small percentage of personnel may have increased risk for developing chronic conditions such as reduced lung function or exacerbated chronic bronchitis, COPD, asthma, atherosclerosis, or other cardiopulmonary diseases. Personnel with history of asthma or cardiopulmonary disease are considered to be at particular risk. Exposures below this are not expected to result in development of chronic health conditions in generally healthy troops.

2. Experimental Methods

To fully address the problem of what aerosols soldiers in Afghanistan are breathing and where these aerosols are originating, several pieces of information are needed: size- and time-resolved elemental concentrations, an understanding of the air's "history" as it blows over each site, and correlations between elements to help trace the aerosol's origin. Techniques to gather such information will be discussed in the following sections.

2.1. Wind roses

A wind rose is a circular plot that displays the direction of the wind (angular axis) as a percentage of time that the wind blows from that direction (radial axis). Wind roses allow quick and effective analysis of wind patterns on the local to regional scale.

Hourly METAR wind data was collected from Kabul and Kandahar, Afghanistan, for 2010. Bagram does not have hourly METAR data so Kabul was chosen as a proxy for Bagram because of its relatively close proximity to Bagram (about 40 km south) and availability of data. Likewise, upper air sounding data was gathered from Kabul for the year of 2010.

Using this data, wind roses were constructed for the surface and various upper air pressure levels. Each wind rose was broken down into six curves based

on the percentage of the data that fell into each category. These categories are: total, 0 to 2.49 m s^{-1}, 2.50 to 4.99 m s^{-1}, 5.00 to 7.49 m s^{-1}, 7.50 to 9.99 m s^{-1}, and $\geq$10 m s^{-1}.

2.2. DRUM aerosol impactors

Davis Rotating-drum Universal-size-cut Monitoring (DRUM) aerosol impactors have proven to be effective at collecting aerosols due to their long sampling times and hardiness (Cahill et al., 1985; Raabe et al., 1988; Cahill and Wakabayashi 1993). DRUM aerosol impactors are capable of being placed in remote regions (Cahill, 2003; Cahill et al., 2008). The aerosols collected by the DRUM aerosol impactor are separated by aerodynamic diameter onto separate Mylar™ strips. The rotation rate of the impactor allows continuous measurements of aerosol concentration and composition with study-specific time-resolution to be collected.

The DRUM aerosol impactors operate based on the impaction of particles using momentum. Air is drawn through the sampler at a known, constant, volumetric flow rate of 10 liters per minute. Within the sampler are stages, each containing a single Mylar™-coated metal drum impaction stage. Between each stage is a nozzle that both aims particles directly at the drum and specifies the velocity of the particles based on the area of the nozzle opening. Only particles with a momentum larger than a specific threshold cannot make the turn to avoid

impacting the Mylar™ surface and impact and stick to the surface; the remaining particles move with the airstream around the drum and continue on to the next stage (see Figure 2.1). The nozzle following each stage accelerates the air and allows for a new momentum cut point. The air's velocity increases for each stage for a total of eight stages. The size-fractions contained on stage 1 through 8 were 5 to 10 μm, 2.5 to 5 μm, 1.15 to 2.5 μm, 0.75 to 1.15 μm, 0.56 to 0.75 μm, 0.34 to 0.56 μm, 0.26 to 0.34 μm, and 0.09 to 0.26 μm in aerodynamic diameter, respectively. Thus, larger particles will stick to the drums on the early stages while the smaller particles will stick on later stages. This filters the particles into a small range of sizes at each stage. Meanwhile, the drums slowly turn underneath each nozzle at a rate of 8 mm/day. This rotation allows for the time resolution that generates the DRUM aerosol impactor's uniqueness.

DRUM aerosol impactors do not operate as effectively without a surface coating (Lawson, 1980). Lawson (1980) experimented with different surface coatings on the Mylar™ substrate in cascade impactors. The DRUM aerosol impactor is a form of cascade impactor that has the impaction plate rotate unlike other cascade impactors that have fixed disks, and hence, no time resolution (Lundgren, 1967). Lawson (1980) found that Vaseline and Apiezon L grease worked best and uncoated surfaces have significant losses. In this study, Apiezon L grease coated the Mylar™ strips.

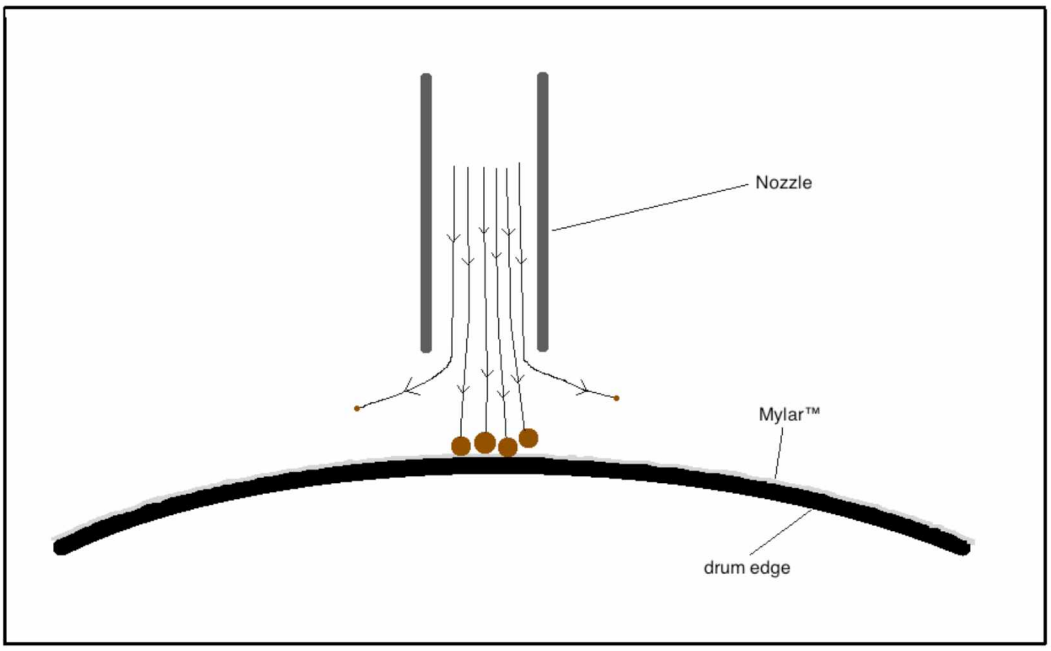

Figure 2.1. Schematic diagram displaying how higher-momentum, larger particles impact the Mylar^{TM} strip on the edge of a drum while smaller particles are caught in the airstream moving around the drum. The thin black lines with arrows are trajectory paths of each hypothetical particle.

To obtain the chemical composition of collected aerosols on the DRUM aerosol impactors, synchrotron x-ray fluorescence (S-XRF) is used (Cahill et al., 1999). The technique is nondestructive and can determine elements ranging from sodium to uranium. S-XRF analysis involves shooting a beam of x-rays at a sample to create vacancies in the inner electron shells of the elements in the sample. Electrons from outer shells fall down to fill the vacant core orbitals, emitting x-rays with energy equal to the difference between the atom's outer and core electron energies, thus conserving energy. Because each element's outer-to-core energy difference is unique, the energy of the emitted (fluorescent) x-ray indicates the identity and amount of each type of element in the sample. After detecting the x-ray energies emitted, the data is plotted upon a spectral graph. The software program WinAxil (Vekemans, et al., 1994) is used to conduct a spectral analysis based upon the statistical significance of peak emissions and thin film, National Institute of Standards and Technology (NIST) traceable standards to determine chemical composition. There were twenty-seven elemental concentrations determined by S-XRF for these samples. These elements are listed in section 1.4.

To achieve total mass loadings during each time period on each drum, a beta-gauge is used. The beta-gauge utilizes radioactive Ni-63 and an electron detector to determine the total mass loading using the Beer's law principal of absorption (Jaklevic et al., 1980). Summing up the total mass loadings on the proper drums results in the PM_{10} and $PM_{2.5}$ concentrations.

2.3. HYSPLIT and sector analysis

The Hybrid Single Particle Lagrangian Integrated Trajectory (HYSPLIT; Draxler and Rolph, 2003; Rolph, 2003) Model is a trajectory model that uses meteorological data to determine backward trajectories. For this thesis, HYSPLIT was initialized with a 25 km ceiling height to ensure that backward trajectories did not exceed the ceiling height boundary. The model simulated 240-hour backward trajectories for Bagram every six hours for the entire year of 2010 for arrival altitudes of 250 m, 2500 m, and 5500 m above ground level. These three altitudes were chosen to profile the atmosphere from near the surface to the middle to upper troposphere.

Four sectors were constructed taking into account the HYSPLIT backward trajectories, annual wind patterns, specific geographical features (such as the Mediterranean Sea, Sahara Desert, and Himalaya Mountains), and political boundaries (such as the borders of Pakistan). The equations for each of the sector separation lines were linear, but because the Earth is spherical, the actual lines curve when viewed on the Earth's surface. These equations for Bagram are:

$$longitude = (-0.2351 \times latitude) + 51.2254$$
$$longitude = (0.1060 \times latitude) + 27.5974$$
$$longitude = (1.2919 \times latitude) - 54.5499$$
$$longitude = (0.7554 \times latitude) - 17.3866$$

where the first equation separates sector 1 and sector 2; the second equation separates sector 2 and sector 3; the third equation separates sector 3 and sector 4;

the fourth equation separates sector 4 and sector 1. Only segments of these lines were used such that each line segment radiates outward from the coordinates of the sampler mentioned in the introduction section. Figure 2.2 displays these sector-dividing segments.

Each of the 240 hours of each individual backward trajectory was then sorted into its corresponding sector using its latitude and longitude. If a point resided on one of the sector separation lines, the point was sorted with the higher number sector, or in the case of the line separating sector 4 and sector 1, the point was placed with sector 1. Based upon the number of points in each sector and the total number of points, the percentage of the time that an air parcel arrives from the individual sector was calculated.

The sector analysis was then formatted in a similar fashion to the aerosol concentration plots generated after the analysis of the DRUM aerosol impactor's aerosol-covered, Mylar^{TM} strips. The percentage of time the trajectories were in each sector was calculated for each six-hour starting time period based on the number of points in each sector from each of the three starting altitude backward trajectories. These percentages were then plotted against time. The overall product displays the percentage of time spent in each sector from the individual backward trajectories versus time. This procedure ultimately allows one to quickly compare aerosol concentrations to the air's history.

A problem with how the sectors were defined is that the prevailing westerlies around Afghanistan's latitude creates a higher bias toward sector 2 and a

lower bias toward sector 4. This problem was taken into account during the analysis of the plot so that small percentages from sector 4 could be considered significant while larger percentages from sector 2 may be less significant. Another possible source of inaccuracy in the determination of the air's history is that the HYSPLIT model is only as good as the input meteorological data used to drive it and that diabatic processes such as latent heat release by cloud condensation and light absorption by gases or particles in the airmass are not well represented. The lack of diabatic processes hinders vertical mixing in the model as compared to reality; therefore three receptor altitudes are used, all aloft, instead of the true receptor altitude at the ground surface. Although these limitations are significant, HYSPLIT backward trajectories with multiple receptor altitudes are an accepted method for determining approximate airmass history.

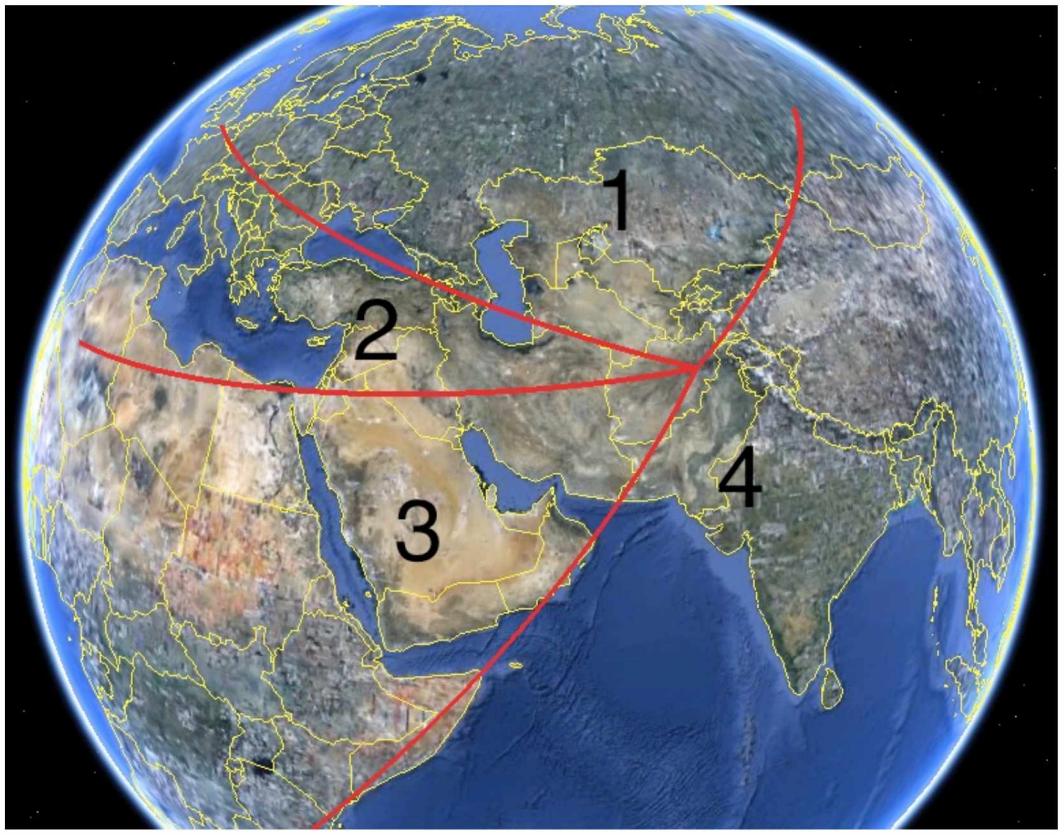

Figure 2.2. Sector dividing segments radiating outwards from Bagram, Afghanistan. The numbers represent the sector number assigned to each area. Image created via Google Earth (© 2011 Google).

2.4. Principal components analysis

PCA is a multivariate statistical ordination technique used to simplify large quantities of data (Pearson, 1901). The underlying principle of PCA is that there is an orthogonal basis of eigenvectors that better describe the variance of the data than do the original axes. PCA utilizes these eigenvectors and their non-negative eigenvalues to transform data to fit axes called 'principal components'. Each subsequent principal component gives a decreasing intensity of the variance within the data.

2.4.1. PCA procedure

This procedure follows that found in Shaw (2003). To begin PCA, each variable in the data is individually normalized to a Z score given by the equation:

$$Z_i = \frac{X_i - \mu}{s}$$

where X_i is the individual observation, μ is the mean, and s is the standard deviation. Next, the Pearson's correlation matrix is determined. The Pearson's product moment correlation coefficients are given by (Shaw, 2003)

$$corr(X,Y) = \frac{\mathrm{cov}(X,Y)}{\sigma_X \sigma_Y}$$

where X and Y represent any two of the variables in question, $cov(X,Y)$ is the covariance of X and Y, and σ is the standard deviation (note that σ=1 after

normalizing the data). After calculating the Pearson's product moment correlation coefficients for all combinations of variables, the next step is to determine the eigenvalues and eigenvectors of this matrix (an explanation of how to find eigenvalues and eigenvectors can be found in Strang (2003)). These values are the eigenvector loadings (i.e. the matrix that contains all the eigenvectors). Finally, to attain the transformed data, axis scores are computed. This computation is done by multiplying the normalized data by the eigenvector associated with the largest eigenvalue for the first principal component axis. The second principal component axis is found by multiplying the normalized data by the eigenvector associated with the second largest eigenvalue and so forth for each subsequent principal component axis. For M number of variables, there will be M eigenvalues and M principal components. Typically many of these principal components will be insignificant as they describe only a very small amount of the variance.

Eigenvalues are used to determine the percentage of variance explained by each principal component axis. The variance percent is given by (Shaw, 2003)

$$V_n = \frac{\lambda_n \times 100}{N}$$

where λ_n is the eigenvalue of the nth axis and N is the number of variables.

Having determined the amount of variance associated with each principal component axis, the next step is discarding axes that are insignificant. After all, the purpose of PCA is to reduce the dimensionality of multivariate data. There are several methods to do this: eliminate all principal components that have

eigenvalues below a threshold value (this value has often been taken as unity), use as many principal component axes as necessary to reach a threshold cumulative variance percentage, or use the broken-stick model. The broken-stick model (Mac Arthur, 1957) is named as such because it determines the expected value if one were to break a stick into pieces where each piece is smaller than the previous piece. The mathematical formula for this method is (Mac Arthur, 1957)

$$B(p,k) = \frac{1}{p}\sum_{j=k}^{p}\frac{1}{j}$$

where p is the number of variables in the PCA and B is the expected value of the k^{th} largest segment. An axis is considered to be significant if the variance explained by the k^{th} axis is larger than $B(p,k)$ and random noise if less than $B(p,k)$. Another method is a graphical method. More details about this method can be found in Jolliffe (2002).

To eliminate principal component axes deemed random noise in this study, the broken-stick model will be utilized.

2.4.2. Eigenvector loadings

Eigenvector loadings are important in determining the meaning of each axis. The higher the magnitude of the loading, the more influence it has on that particular axis. Positive loadings mean that the loading from the particular variable is positively correlated to the axis and vice-versa for negative loadings. However, a

PCA axis can be arbitrarily multiplied by a scalar and still retain its uniqueness. A negative scalar would cause the signs of all the eigenvector loadings associated with that axis to be flipped.

While the eigenvector loading values are one concern, how variables compare to other variables is another. Loadings of variables that are of the same sign are correlated with each other and anti-correlated with variables that have opposite sign loadings.

To establish what eigenvector loading values are significant upon a principal component axis, past studies have used various methods such as establishing a threshold value (Pio et al., 1989; Viana et al., 2006) and/or using a Varimax rotation on the eigenvector loadings matrix (Thurston and Spengler, 1985; Viana et al., 2006). Another method, used in studies such as Cianfrani et al. (2006), will be used in this study. It uses the equation (Afifi et al., 2004)

$$LT = \frac{0.50}{\sqrt{Eigenvalue}}$$

where LT is the loading threshold value. This equation arises due to variables loading significantly on a principal component when the correlation is greater than 0.50.

2.4.3. PCA on aerosol samples

PCA is an effective way to help source the elements in aerosol samples (Smeyers-Verbeke et al., 1984; Viana et al., 2006; Chan and Mozurkewich, 2007). If elements arrive at the DRUM aerosol impactor from the same source, they should have specific elemental ratios to one another compared to elements from a different source with different elemental ratios. These elemental fractions will remain relatively constant for a specific source. Therefore, the concentrations should change proportionally if more or less material arrives from that specific source. In other words, elements are highly correlated with one another from a single source. If the source changes, then the elemental ratios will most likely also change. Therefore, if aerosols arrive from multiple sources simultaneously, the correlation will likely change. PCA uses the eigenvector loadings as a way to show correlations among elements.

To begin the PCA on the aerosol samples from Afghanistan, the data was organized for PCA in such fashion that each column contained a selected element. There were 22 of the 27 measured elements selected for PCA. The analysis procedure excluded Mo, Rb, Sr, Y, and Zr, because of their near-detection limit concentrations. The analysis procedure would then place the DRUM data for the element in the column. For example, if stage 1 and stage 2 were selected for PCA and both contained 350 rows of data, then lines 1-350 for each selected element would be stage 1 data and lines 351-700 would be stage 2 data. This process

continued for each stage. The data then underwent the processes described in section 2.4.1 to calculate the necessary values.

Past studies showed that when using PCA on atmospheric constituent data, component axes are interpreted as source types (Smeyers-Verbeke et al., 1984; Thurston and Spengler, 1985; Viana et al., 2006). The source type can be determined by analyzing the size-fraction and element loadings found in the eigenvector-loading matrix. For example, a combustion source is more likely to be visible in the smaller size fractions. By using the loading factors, source profiles from the data can be constructed and compared to previously determined source profiles such as those seen on the EPA's website (EPA, 2011c). However, it may be that an element is found in multiple sources and comprises of a significant amount of the mass in each of those sources. PCA would show this as a low amount of the variance explained by that element (a small loading value in the eigenvector) despite the source profile(s) showing significant contribution by that element. This situation can be made more problematic due to some elements (especially those associated with dust) having elevated concentrations nearly all the time. The opposite is also true in the case of a low concentration element being significant to a single source. PCA would show the eigenvector loading value to be relatively high despite the element being relatively insignificant in terms of mass. Therefore PCA source profiles are more about the element's uniqueness to the source and ample quantities of the element present such that it is analytically

significant rather than mass explained. These scenarios indicate why it is important to look for the presence of unique elements within the source profiles.

PCA source profiles based on elemental loadings were determined for all size ranges simultaneously. The PCA could have been divided up into coarse and fine fractions, but because many actual source profiles only account for either PM_{10} or $PM_{2.5}$ (in contrast to $PM_{2.5-10}$ that would be needed for the coarse size range), and $PM_{2.5}$ source profiles provide reasonable representations of the other fractions (Labban et al., 2004), all drum stages were considered at once.

As previously mentioned, the eigenvalue associated with each principal component is used to give the amount of variance within the data explained by that particular principal component. Thus, when each principal component is associated with a source type, the amount of variance that source type contributes to the overall dataset can be determined.

To show both the PCA transformed data and the eigenvector loadings, biplots can be constructed. Thus biplots allow one to easily observe how variables correspond with the data. For this study, the transformed aerosol data and the eigenvector loadings for each element were plotted on the same diagram for each sample period.

2.5. Chemical mass balance (CMB) model

Upon determining sources from PCA, the chemical source profiles associated with each were used in the EPA-CMB8.2 model (EPA, 2004; Coulter and Scalco, 2005). Chemical mass balance models attempt to calculate the measured mass concentration by fitting mass fractions and contributions from individual sources. If all sources are accounted for, the calculated mass concentration should theoretically match the measured mass concentration.

The overall governing equation for the EPA-CMB8.2 model is (EPA, 2004; Coulter and Scalco, 2005)

$$C_i = \sum_{j=1}^{p} a_{ij} S_j, i = 1, n$$

where C_i is the ambient concentration of specie i, a_{ij} is the fractional concentration of specie i in the emissions from source j, S_j is the total mass concentration contributed by source j, p is the number of sources, and n is the number of species for $n \geq p$. Both C_i and a_{ij} are known and the S_j are found by a least squares solution to the system of equations generated by the user's selection of samples and source profiles.

The output of the CMB model included the estimated total mass concentration, source contributions to the overall mass, and elemental masses. The results of the CMB model were used to determine the approximate source contribution percentages of Afghanistan's significant aerosol sources.

Attempts were made to relate sources to the individual 1.5-hour samples, but likely due to the high resolution and the possibility of sources altering throughout the day, these attempts failed. Therefore, to better relate the PCA sources with source profiles in the CMB model, elemental concentrations were averaged over all drums stages and the entire sampling period. The total concentrations used in the model input file were the sum of each of the sample periods' all-size-fraction averaged mass concentrations. These averages were used rather than the total mass loading measurements from the beta-gauge because the total mass concentration calculated by the model is the sum of these 27 elements, and if all 27 elemental concentrations were perfectly matched by the model, the measured and calculated masses should be equal. Furthermore, the beta-gauge data includes of all oxygen, carbon species, etc. that were not measured via S-XRF nor found in the source profiles, thus using the beta-gauge total mass concentrations to apportion the sources is not feasible.

3. Results and Discussion

It is important to note here that unless otherwise stated, all times for the remainder of this thesis are in coordinated universal time (UTC).

Many synoptic weather events will be discussed in this section, but the associated weather charts are not shown within this thesis. The reader is directed to the U.S. National Climate Data Center world weather map archive to view these maps (NCDC, 2012).

3.1. Wind roses

The wind direction over Kabul (due to lack of wind data from Bagram) and Kandahar (Kandahar is examined to help analyze the air flow in the Kabul Valley) vary by the time of the year. In addition, diurnal cycles are witnessed. Both are significantly influenced by topography.

Surface winds in Kabul averaged about 2.1 m s^{-1} in the winter and about 3.6 m s^{-1} in the summer of 2010. Figure 3.1 shows the wind in Kabul is generally from the northwest throughout the year. During the summer Indian monsoon months (June through September), there is a significant amount of wind coming from the southeast (Figure 3.1). Winds tend to arrive from the southeast rather than the south because Kabul resides in the northern portion of the Kabul Valley, on the west side near the mountains, and has mountains immediately on its southern

flank. This wind pattern adds evidence that during the summer months, air has more tendency to flow up the Kabul Valley into Kabul and Bagram compared with the winter months.

a)

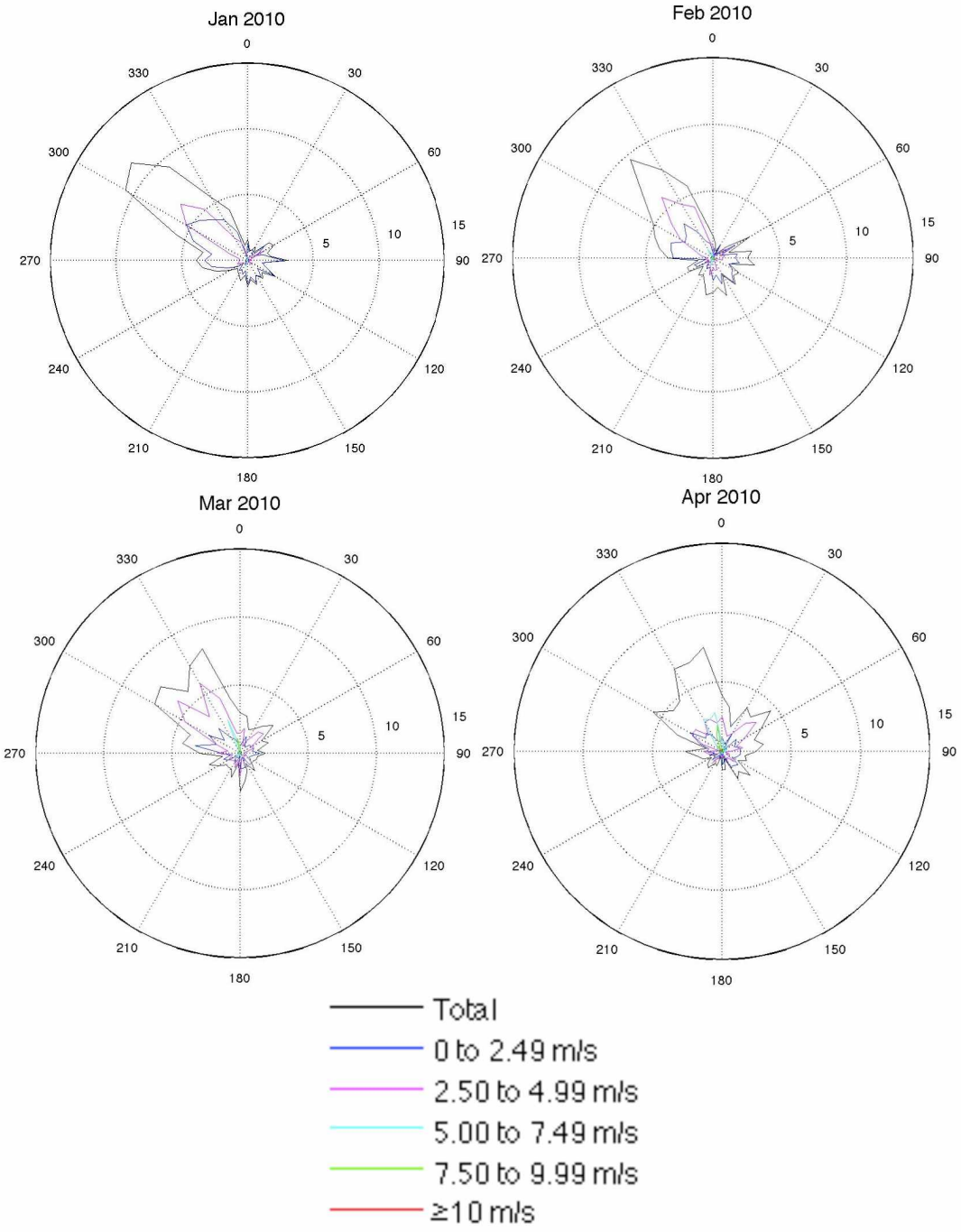

Figure 3.1. Surface wind roses from Kabul, Afghanistan for (a) January to April, (b) May to August, and (c) September to December 2010.

b)

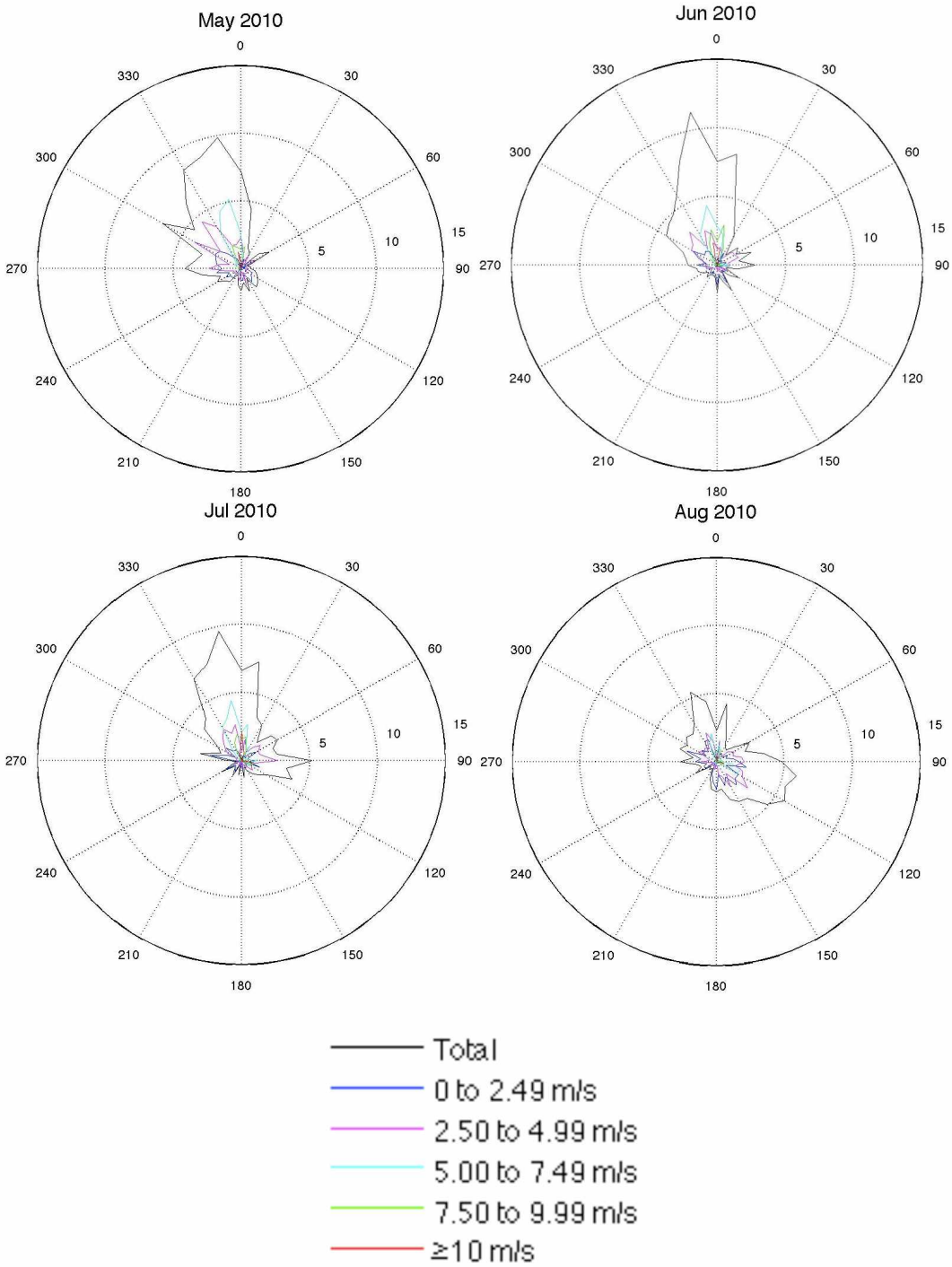

Figure 3.1. Continued.

c)

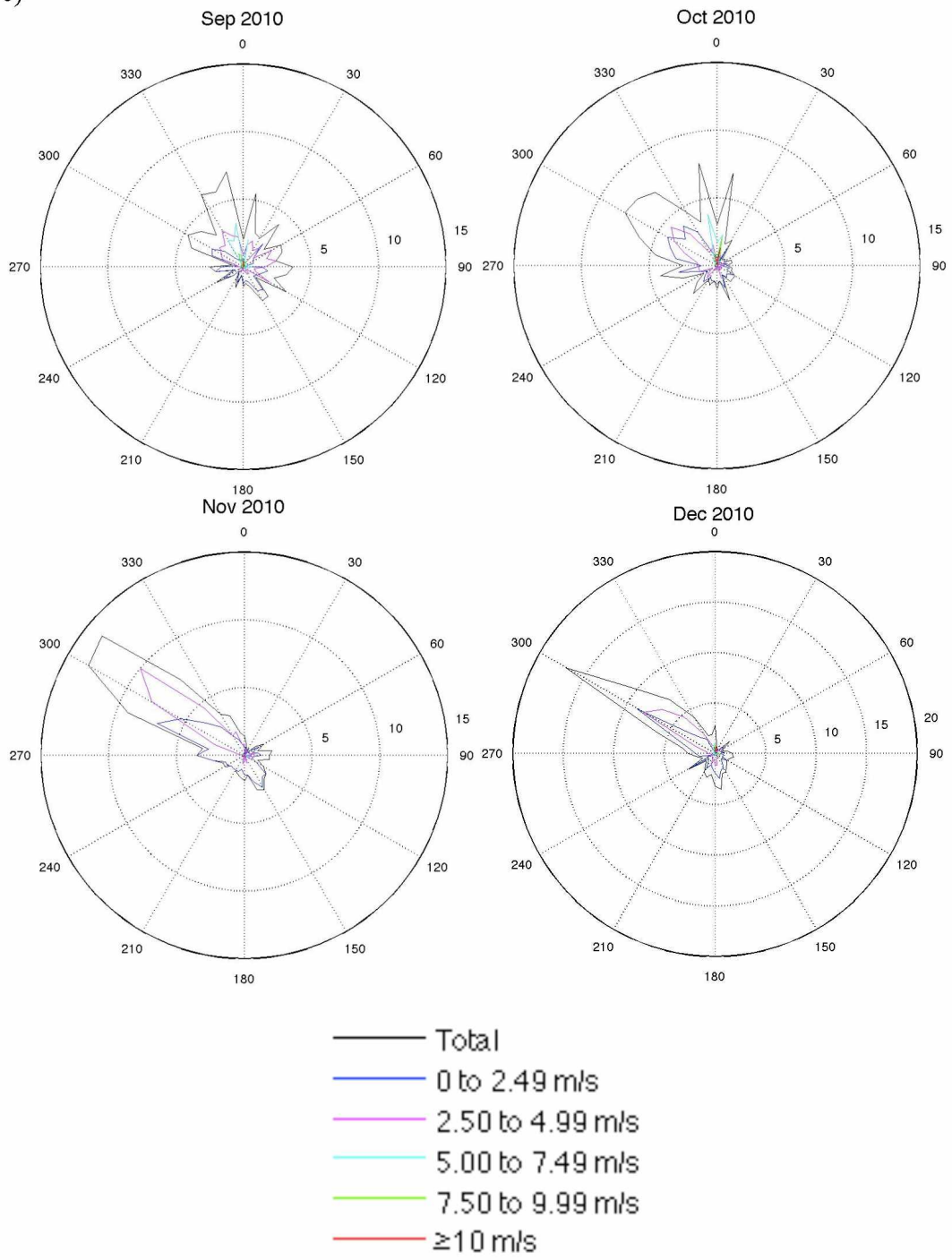

Figure 3.1. Continued.

Also seen in Kabul's summer wind roses (Figure 3.1) is a northerly component. The large-scale convergence of air toward the ITCZ during the Indian monsoon causes transport of air from the north into Afghanistan. The poor air quality mentioned in section 1.5.2.2 in countries north of Afghanistan will have higher tendency to be transported into Afghanistan during the summer months because the air comes from the north more frequently. Additionally, higher wind speeds during the summer will result in greater amounts of aerosol lofting and, therefore, increased aerosol transport.

Kabul has a diurnal cycle. At 03 UTC (local time 0730), the wind flow is essentially completely from the northwest (Figure 3.2). Mountains reside to the northwest of Kabul so this can be taken as the drainage of air down the Kabul Valley with replacement of air coming down or through the mountains to the northwest. As the day goes on, more southerly and southeasterly components are observed (Figure 3.2). The air can be visualized as ascending the Kabul Valley from the south due to the strong surface heating and elevation effects.

a)

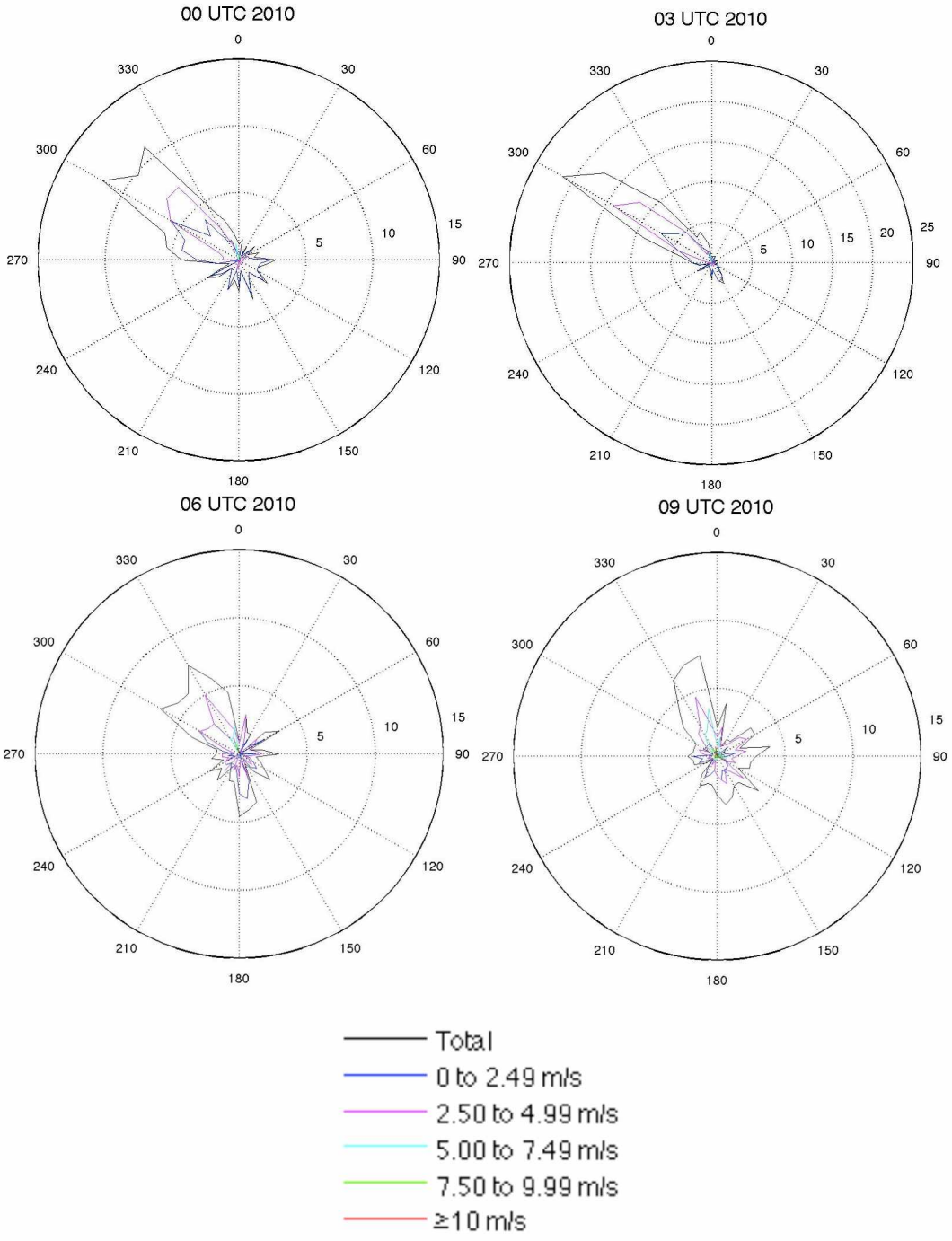

Figure 3.2. Annual surface wind roses from Kabul, Afghanistan from (a) 00 UTC, 03 UTC, 06 UTC, 09 UTC, (b) 12 UTC, 15 UTC, 18 UTC, and 21 UTC.

b)

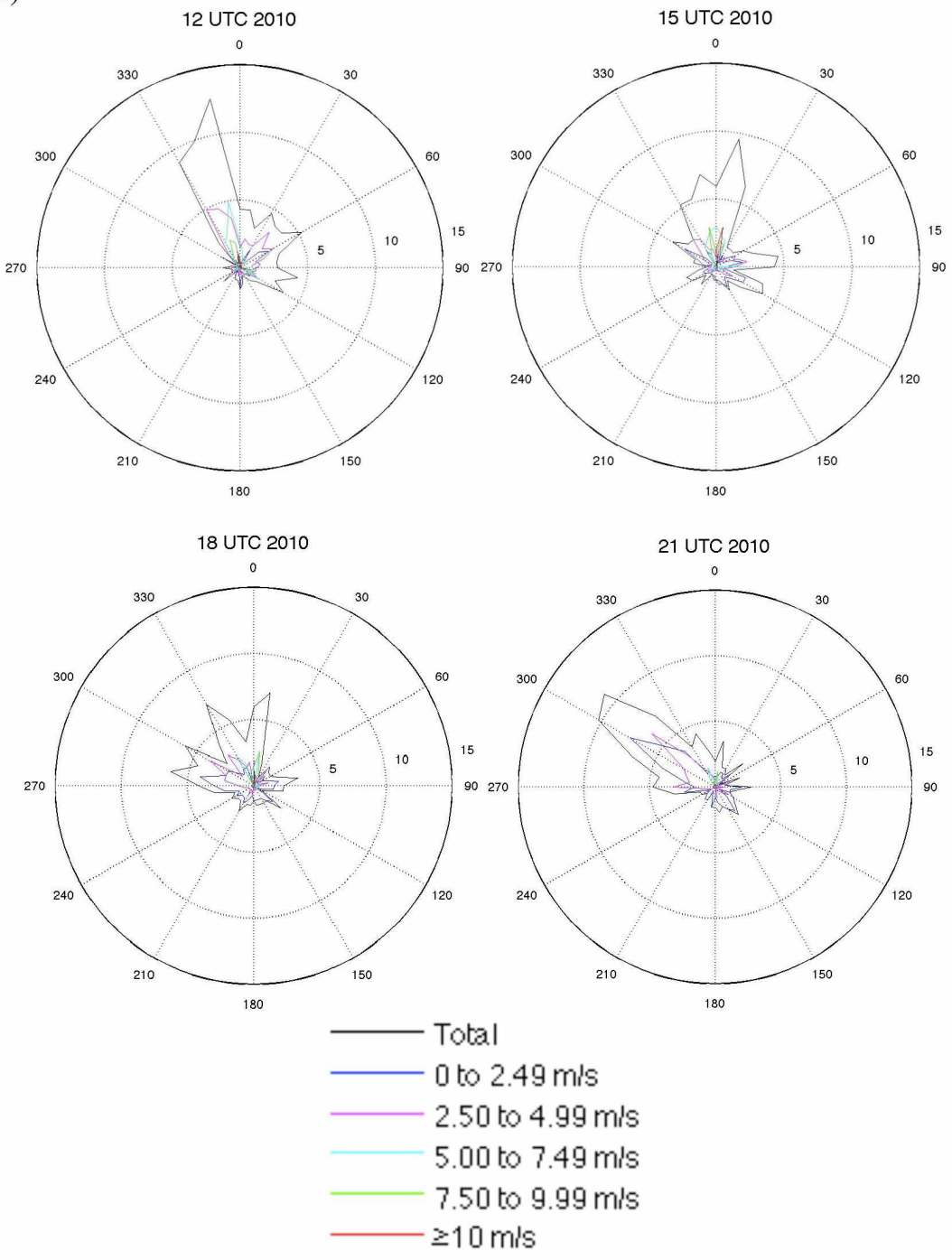

Figure 3.2. Continued.

In Kandahar, surface winds averaged about 2.7 m s^{-1} in the winter and 3.0 m s^{-1} in the summer of 2010. Wind patterns in Kandahar are much more defined than in Kabul, but the same pattern of air flowing up and down the Kabul Valley appears. During the winter months, the surface winds are generally from the northeast (Figure 3.3). This pattern follows what was seen in Kabul in that during the winter months, air generally flows down the Kabul Valley. As the summer Indian monsoon strikes, the surface airflow is shifted to a more westerly flow (Figure 3.3). This flow pattern follows what was seen in Kabul in that the air generally flows up the Kabul Valley during the summer months.

The diurnal cycle in Kandahar is easily visible. During the early hours of the day, the wind comes down the Kabul Valley from the northeast (Figure 3.4). As the day progresses, the wind shifts to westerly flow going toward the Kabul Valley (Figure 3.4).

These diurnal cycles can cause aerosols to be recycled into the ambient air each day at each location until they are either removed by deposition or blown away. This diurnal effect will be seen in the elemental concentration graphs and will be discussed in section 3.2.

In terms of wind intensities, both locations see higher wind speeds in the summer months and afternoons/evenings than in winter and night/mornings. The strong convergence of air toward the ITCZ creates the stronger wind speeds during the summer, and daily solar heating leads to convection and higher wind speeds during the afternoons and evenings.

a)

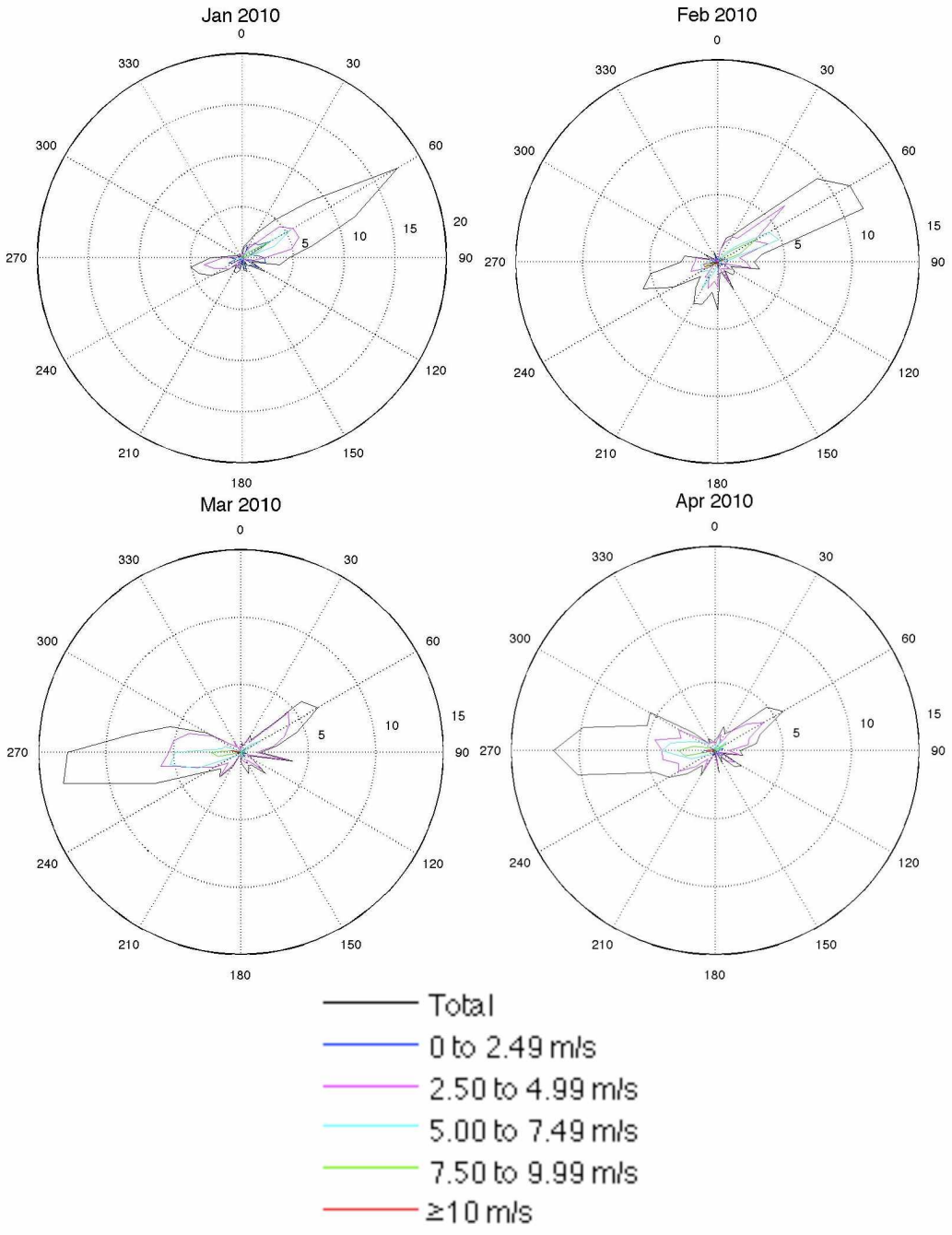

Figure 3.3. Surface wind roses from Kandahar, Afghanistan for (a) January to April, (b) May to August, and (c) September to December 2010.

b)

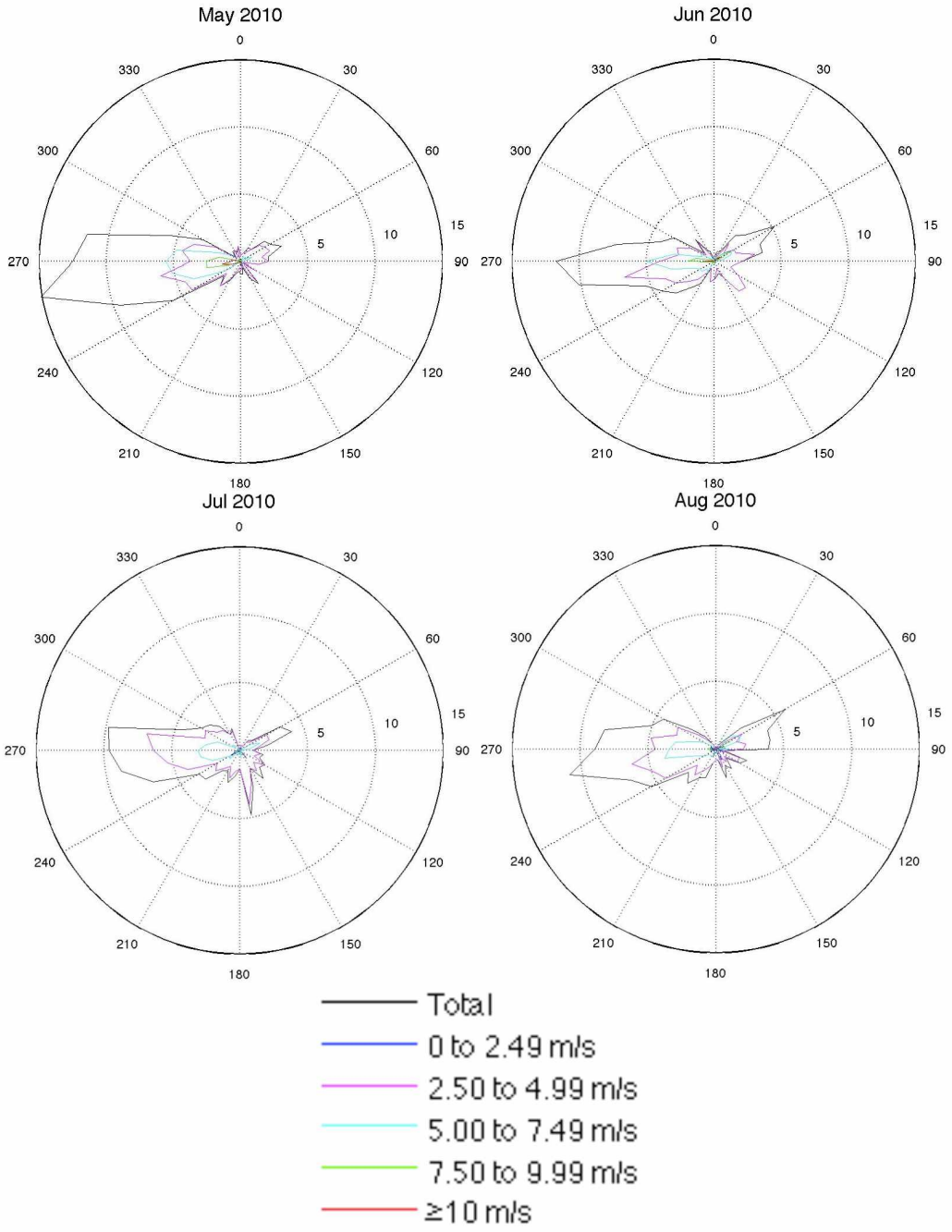

Figure 3.3. Continued.

c)

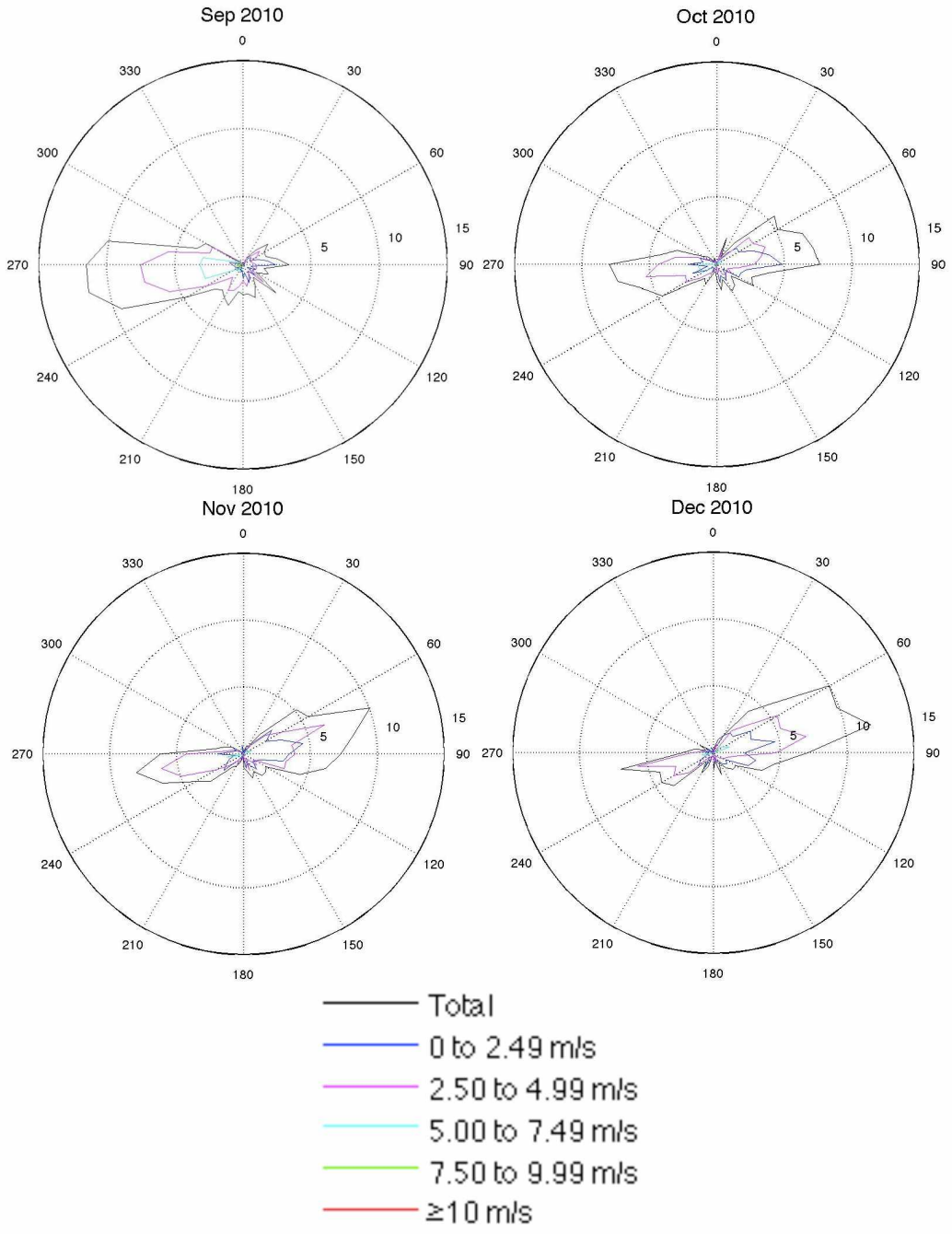

Figure 3.3. Continued.

a)

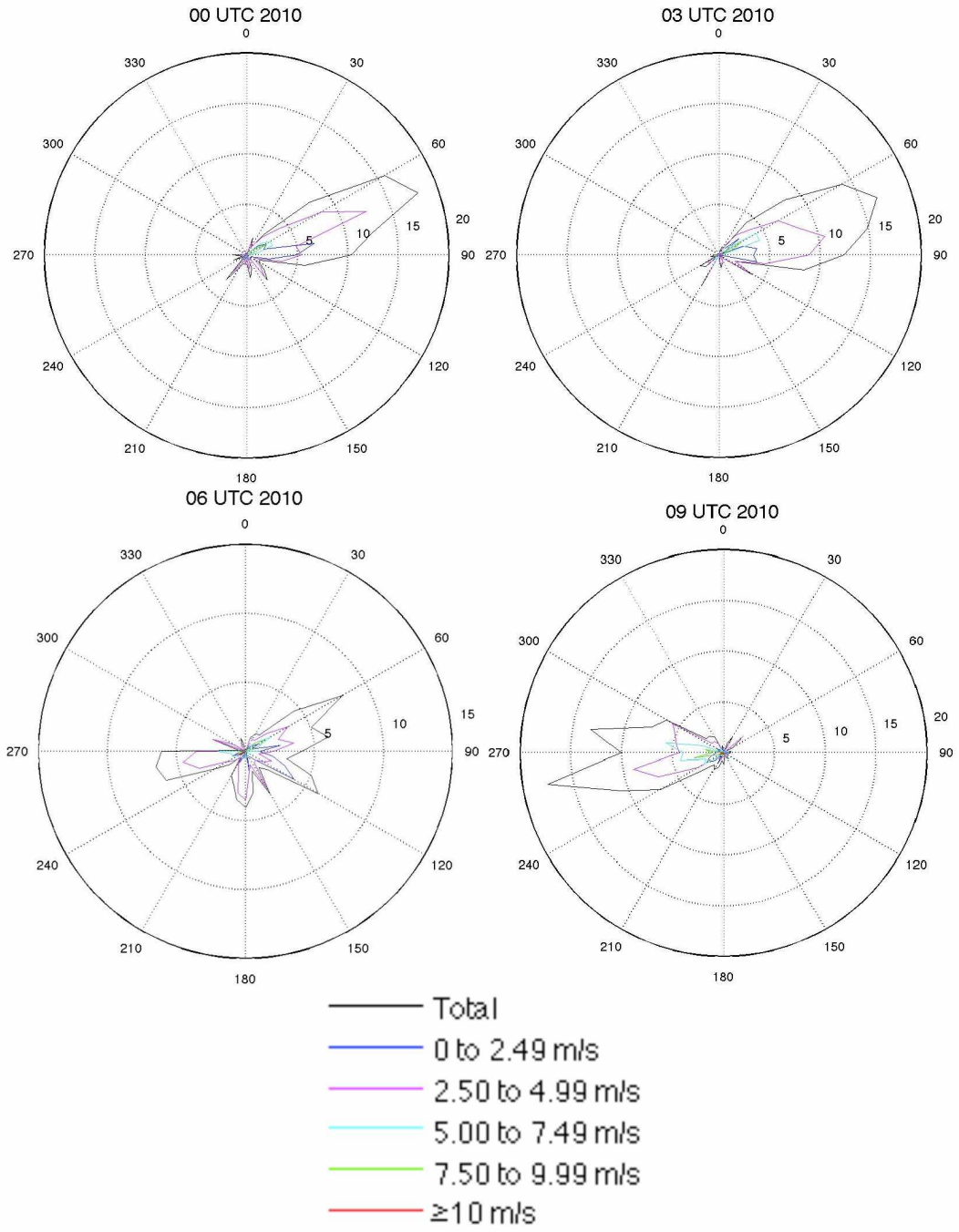

Figure 3.4. Annual surface wind roses from Kandahar, Afghanistan from (a) 00 UTC, 03 UTC, 06 UTC, 09 UTC, (b) 12 UTC, 15 UTC, 18 UTC, and 21 UTC.

b)

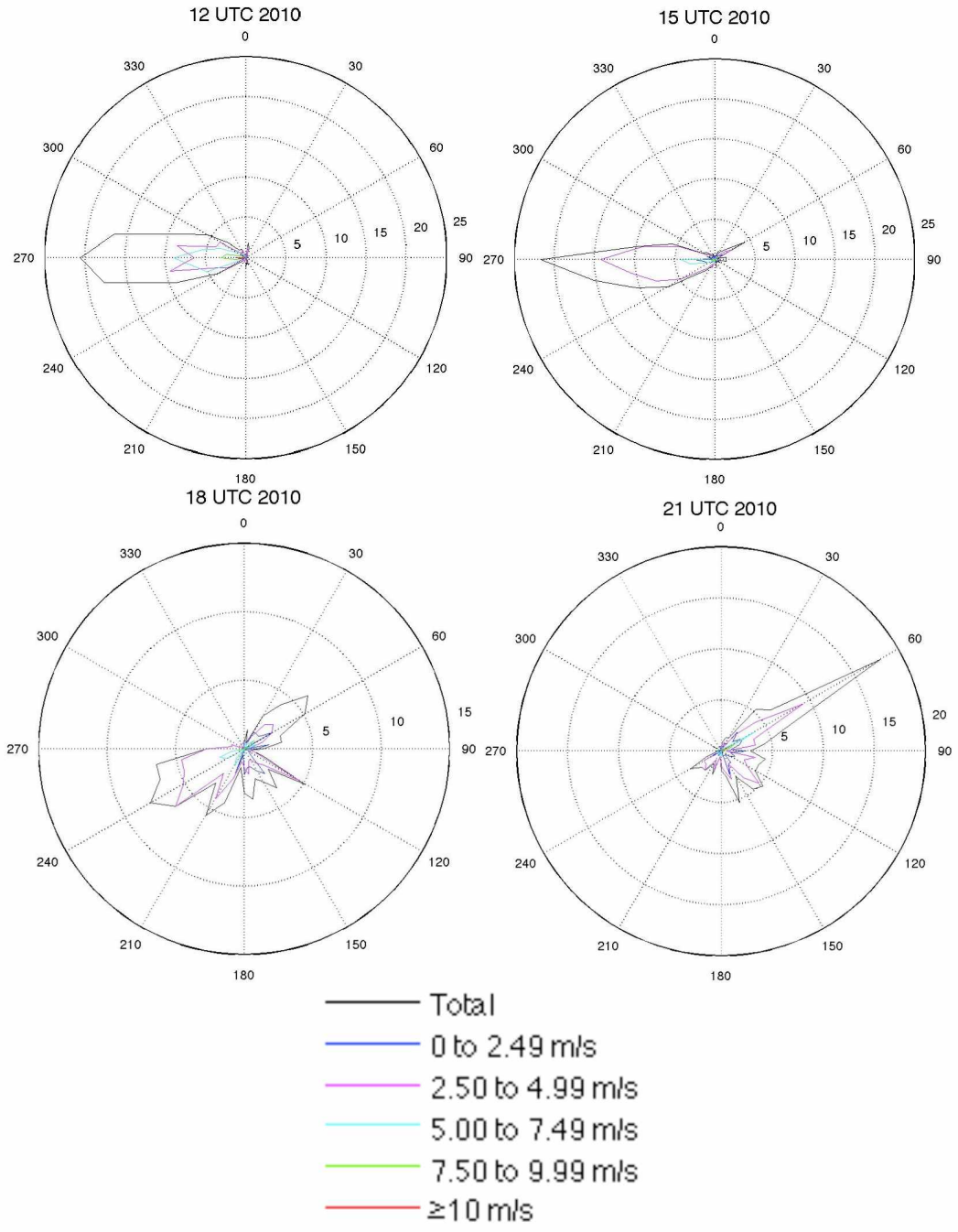

Figure 3.4. Continued.

3.2. Elemental concentrations

Equipment complications and human installation errors resulted in the loss of a significant amount of data in 2010 and 2011. The available results from the Afghanistan DRUM sampler at Bagram AFB are presented here. The results are not nearly as extensive as desired, but do present some patterns that can be generalized for time periods of lost data.

In the events that will be discussed in sections 3.2.1 and 3.2.2, an upper air trough pattern (associated with lift due to positive vorticity advection) coupled with a surface-based low-pressure system was present at a potential aerosol source likely causing the lofting of aerosol particles due to the stronger winds and uplift associated with each meteorological pattern. This reasoning is consistent with strong synoptic low-pressure systems being responsible for the significant aerosol lofting found in Iino et al. (2004). During the monsoon season, winds are stronger and more persistent, likely resulting in a larger number of aerosol lofting events as seen in the percentage of dust storms in Afghanistan in Table 1.1.

A common feature that arises in many of the concentration plots is a diurnal cycle. Once elements are injected into the ambient air they tend to have daily concentration peaks that gradually decrease in magnitude over the course of the next few days, unless there is further injection of aerosols. In the latter case, daily concentration peaks may actually increase in the days that follow an initial aerosol injection. Overall, aerosols can essentially be recycled for days after being injected into the local ambient air.

3.2.1. Geological dust

Another common feature that arises in a number of the elemental concentrations vs. time plots is the gradual reduction in concentration as the monsoon season approaches. This behavior is easily seen among the geological dust elements such as Ca between the months of March and May (see Figures 3.5-3.7). Climatically speaking, the lower-tropospheric wind, and therefore the ability of aerosols to undergo saltation or suspension, is reduced and then increases as the pre-monsoon winter transitions into the summer monsoon. In 2010, the average 700 hPa wind speed at Kabul was about 5.9 m s^{-1} in February, 4.3 m s^{-1} in March, 3.2 m s^{-1} in April, and 4.3 m s^{-1} in May.

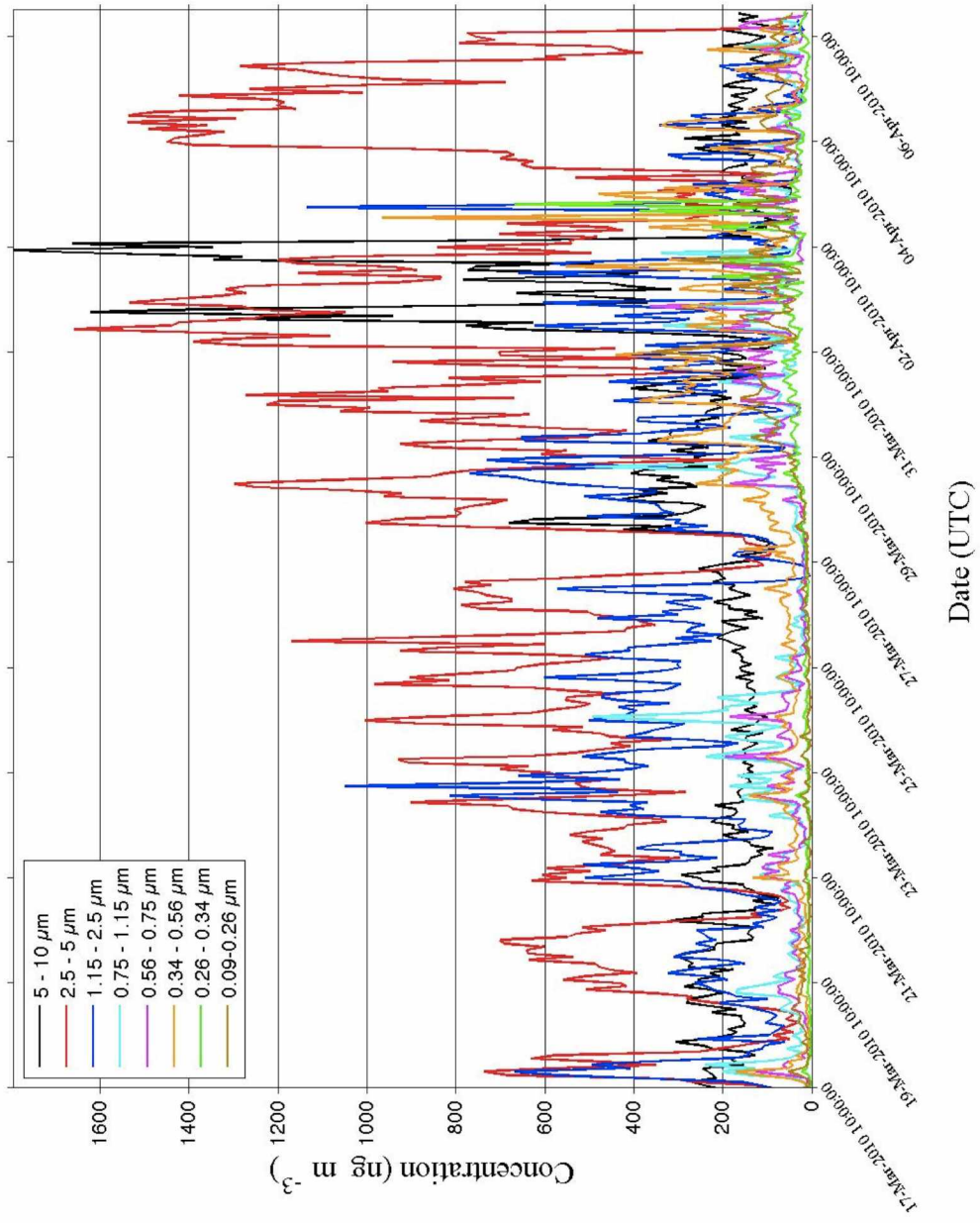

Figure 3.5. Calcium concentrations for Bagram, Afghanistan, from March 17, 2010 to April 6, 2010.

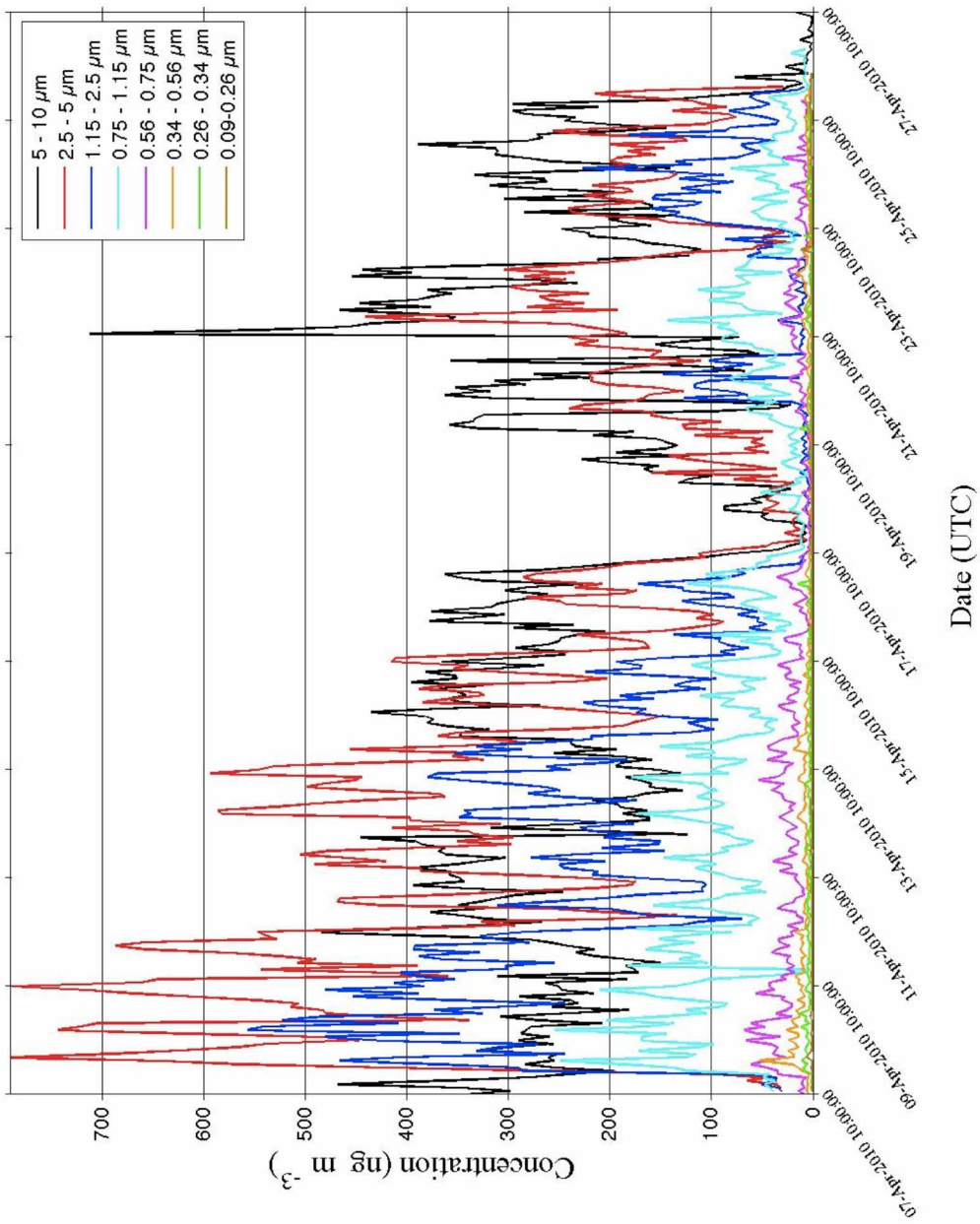

Figure 3.6. Calcium concentrations for Bagram, Afghanistan, from April 7, 2010 to April 27, 2010.

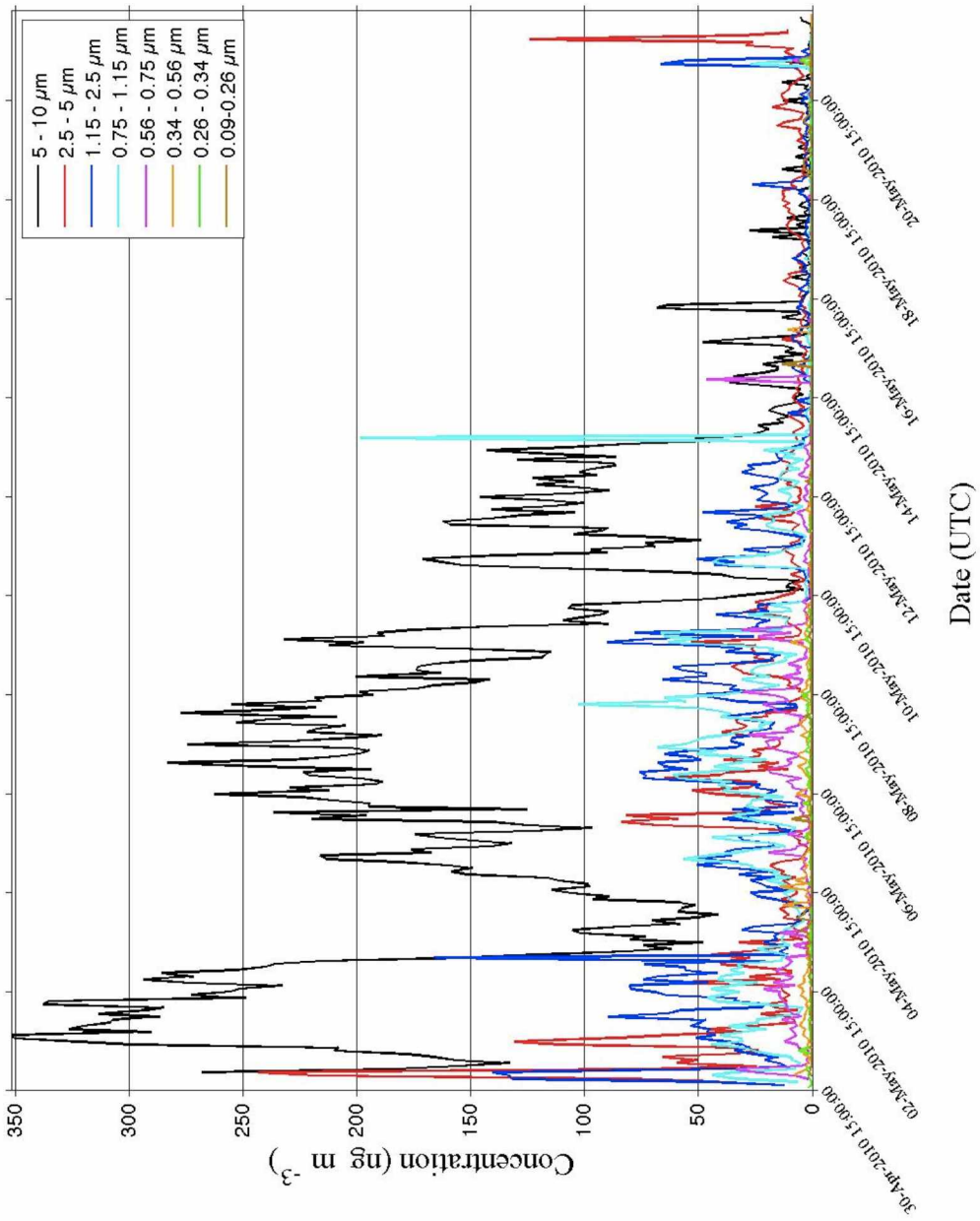

Figure 3.7. Calcium concentrations for Bagram, Afghanistan, from April 30, 2010 to May 22, 2010.

Geological dust elements (Al, Ca, Co, Cr, Fe, Mg, Mn, Si, Ti), generally speaking, have high concentrations (in the hundreds of ng m^{-3}) and the larger-sized dust particles dominate the elemental mass. Furthermore, the smaller the particle size, the less dust mass is observed (Figures 3.5-3.7). This finding is what would be expected of localized geological dust aerosols. Occasionally the submicron sized particles spike in concentration and can compose of a significant portion of the mass. These events are likely due to the transport of particles from other regions and not a localized source. An example of this can be seen in the Ca concentration around April 3, 2010 (Figure 3.5). Expanding on this example, submicron concentrations of Br and K spike at the same time as the Ca concentrations (Figures 3.8-3.9). Backward trajectories show the air has history near the Dead Sea (Figure 3.10) where large concentrations of Br and K can be found (Garcia-Veigas et al., 2009).

Unlike anthropogenic and heavy metal elements, dust aerosols are difficult to trace back to a specific source because aerosols from local and distance sources can be present, a large portion of the Middle East is covered by desert, and concentrations are elevated most of the time. As expected, PCA analysis shows dust elements highly correlated with each other during all sample periods within the first principal component axis and account for the greatest amount of the variance within the data (Tables 3.1-3.4).

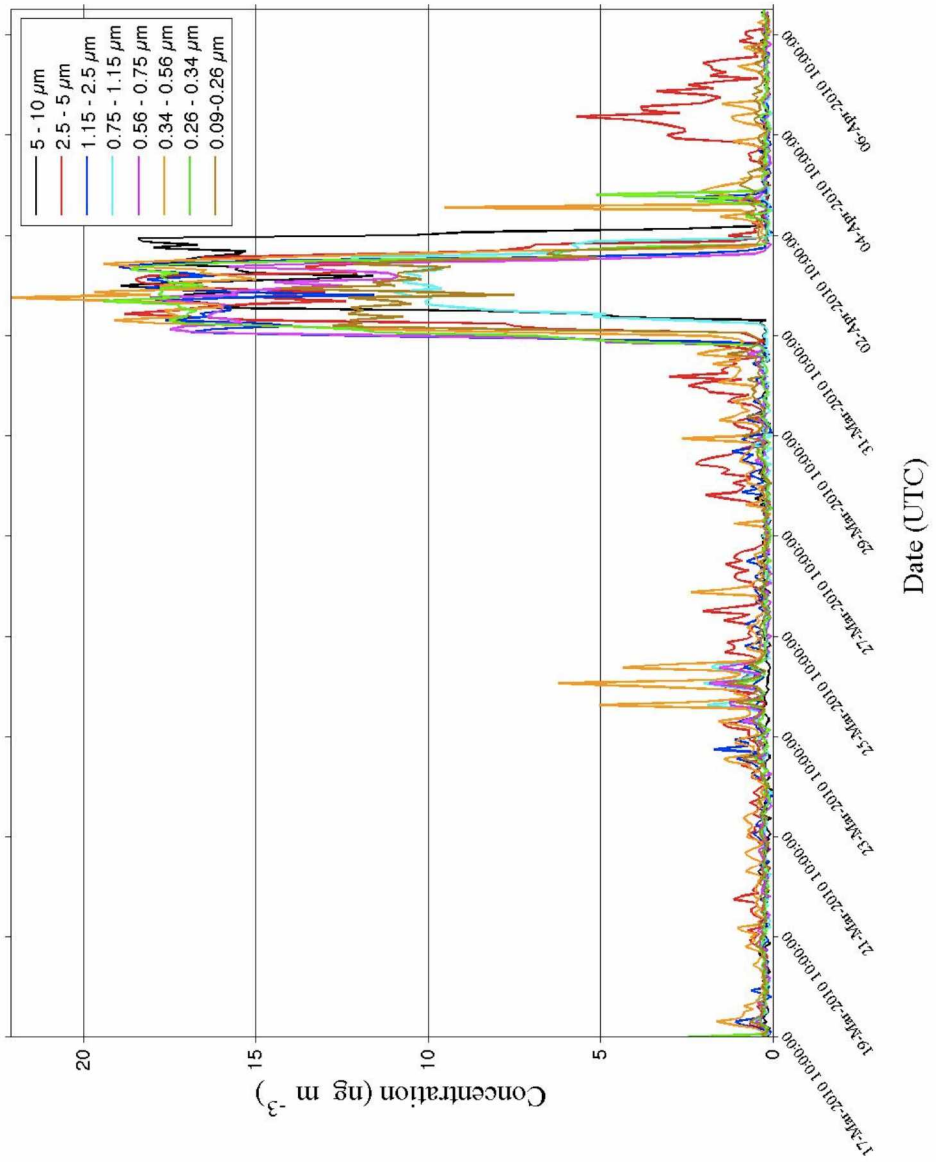

Figure 3.8. Bromine concentrations for Bagram, Afghanistan, from March 17, 2010 to April 6, 2010.

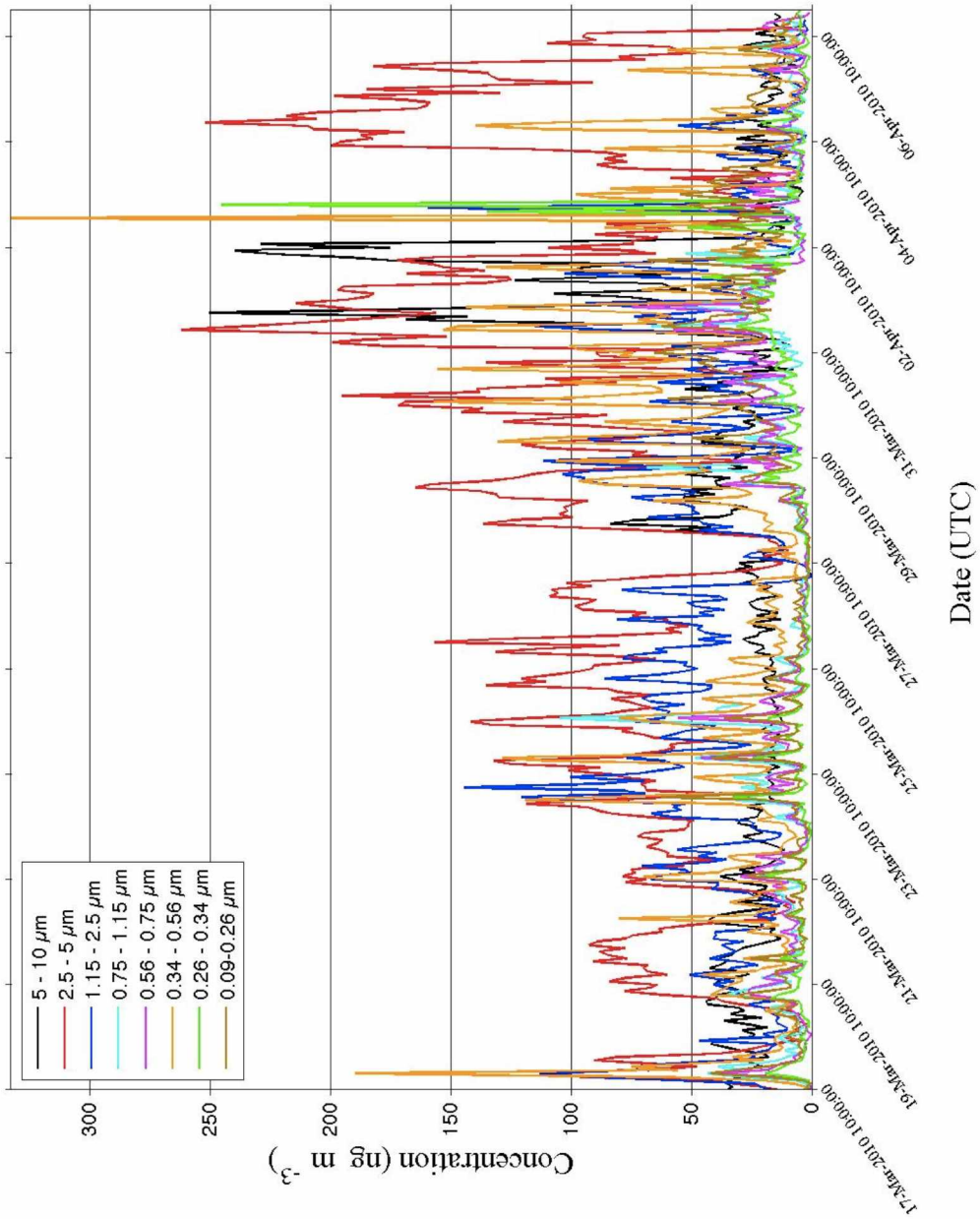

Figure 3.9. Potassium concentrations for Bagram, Afghanistan, from March 17, 2010 to April 6, 2010.

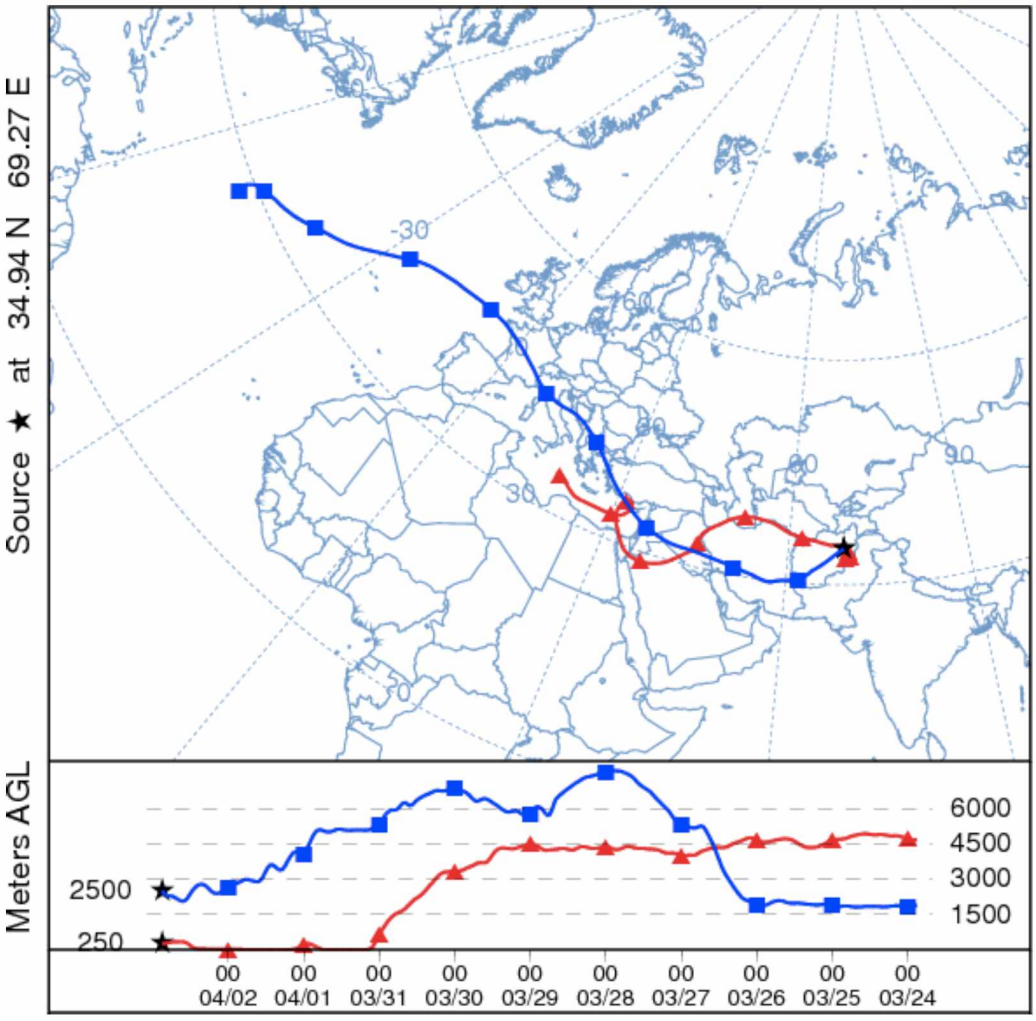

Figure 3.10. Backward trajectories for air reaching Bagram, Afghanistan, during a high submicron calcium, bromine, and potassium aerosol event in April 2010.

Table 3.1. PCA eigenvector loadings for Bagram, Afghanistan. Highlighted in yellow (blue) are negative (positive) significant eigenvector loadings with an absolute value greater than or equal to $0.50/\sqrt{Eigenvalue}$.

02/06/2010 - 02/28/2010

	Principal Component		
	1	**2**	**3**
Al	-0.2804	-0.076	-0.0165
As	0.0483	0.466	0.0977
Br	-0.1548	0.4111	0.1731
Ca	-0.2835	-0.0568	0.0221
Cl	-0.199	0.2099	-0.156
Co	-0.2728	-0.0344	0.1756
Cr	-0.1823	-0.0701	-0.437
Cu	-0.0019	0.3126	-0.1692
Fe	-0.2842	-0.048	-0.0028
Ga	-0.2482	-0.017	0.3418
K	-0.2705	0.1423	0.0255
Mg	-0.2657	-0.0465	0.0558
Mn	-0.2817	-0.0273	-0.0616
Ni	0.0401	0.0746	0.0881
P	-0.2345	-0.1052	0.1577
Pb	-0.2604	0.02	0.273
S	-0.0112	0.4689	0.0127
Se	0.1688	0.1517	0.3591
Si	-0.2793	-0.082	-0.033
Ti	-0.2204	-0.0557	-0.0565
V	-0.0835	0.0462	-0.5182
Zn	-0.1242	0.3992	-0.2266
Eigenvalue	12.1373	2.9476	1.5033
Variance %	55.1695	13.3981	6.833
Cum. Var. %	55.1695	68.5676	75.4006
Potential Source	Crustal	Metal Proc.	

Table 3.2. PCA eigenvector loadings for Bagram, Afghanistan. Highlighted in yellow (blue) are negative (positive) significant eigenvector loadings with an absolute value greater than or equal to $0.50/\sqrt{Eigenvalue}$.

03/17/2010 - 04/06/2010

	Principal Component		
	1	**2**	**3**
Al	-0.2869	0.055	0.0053
As	0.0728	-0.3285	0.0147
Br	-0.0974	-0.4177	0.2656
Ca	-0.29	0.0404	0.0474
Cl	-0.0864	-0.43	0.2423
Co	-0.2753	0.008	0.1621
Cr	-0.1178	-0.0211	-0.2894
Cu	-0.0018	-0.3382	-0.173
Fe	-0.2921	0.0195	0.0334
Ga	-0.2599	0.0172	0.2243
K	-0.2828	-0.0758	-0.0602
Mg	-0.2703	0.0503	0.0674
Mn	-0.2867	-0.0084	-0.0607
Ni	-0.0074	-0.2609	0.1564
P	-0.2544	0.105	-0.1232
Pb	-0.2583	-0.0133	0.16
S	-0.0662	-0.294	-0.4428
Se	0.1334	-0.3202	0.3158
Si	-0.2858	0.0606	0.0013
Ti	-0.2848	0.0375	0.0206
V	-0.0593	-0.0598	-0.3808
Zn	-0.1167	-0.3567	-0.3981
Eigenvalue	11.5586	3.0132	1.8943
Variance %	52.5393	13.6965	8.6106
Cum. Var. %	52.5393	66.2358	74.8464
Potential Source	Crustal	Marine/ Metal Proc.	

Table 3.3. PCA eigenvector loadings for Bagram, Afghanistan. Highlighted in yellow (blue) are negative (positive) significant eigenvector loadings with an absolute value greater than or equal to $0.50/\sqrt{Eigenvalue}$.

04/07/2010 - 04/26/2010

	Principal Component		
	1	**2**	**3**
Al	-0.2863	-0.0004	0.0386
As	0.099	-0.2339	-0.3185
Br	0.0262	-0.4636	0.2007
Ca	-0.2894	-0.0039	0.0264
Cl	0.0285	-0.4613	0.2182
Co	-0.275	-0.0873	0.0818
Cr	-0.1573	-0.0451	-0.0204
Cu	0.015	-0.2307	-0.4898
Fe	-0.2904	-0.0128	-0.0059
Ga	-0.25	-0.1092	0.1215
K	-0.2841	-0.1008	-0.0031
Mg	-0.2707	-0.0244	0.0799
Mn	-0.2822	-0.0094	-0.028
Ni	0.0469	-0.3936	0.2459
P	-0.2573	0.1253	0.029
Pb	-0.2542	-0.0613	0.0328
S	-0.0458	-0.3572	-0.311
Se	0.1528	-0.337	0.1734
Si	-0.2835	-0.0114	0.0407
Ti	-0.2687	-0.012	0.0273
V	-0.1281	0.0051	-0.1668
Zn	-0.12	-0.126	-0.5658
Eigenvalue	11.588	3.9306	1.56
Variance %	52.6726	17.8663	7.0909
Cum. Var. %	52.6726	70.5389	77.6298
Potential Source	Crustal	Marine/ Metal Proc.	

Table 3.4. PCA eigenvector loadings for Bagram, Afghanistan. Highlighted in yellow (blue) are negative (positive) significant eigenvector loadings with an absolute value greater than or equal to $0.50/\sqrt{Eigenvalue}$.

04/30/2010 - 05/22/2010

	Principal Component		
	1	**2**	**3**
Al	-0.2901	0.0404	-0.0059
As	0.0493	-0.4895	-0.1439
Br	-0.1174	-0.2905	0.035
Ca	-0.2894	0.0394	-0.0043
Cl	0.0062	-0.1831	0.0916
Co	-0.2782	0.023	0.016
Cr	-0.0366	-0.0453	0.6648
Cu	0.0429	-0.3672	0.1318
Fe	-0.2894	0.0311	0.0046
Ga	-0.2698	0.0176	0.0029
K	-0.2889	0.009	-0.0061
Mg	-0.2765	0.0344	-0.0158
Mn	-0.2719	0.0339	-0.0118
Ni	0.0257	-0.0489	0.7014
P	-0.2692	0.0689	0.0194
Pb	-0.2642	0.0069	0.0083
S	-0.1458	-0.4347	-0.1039
Se	0.1587	-0.2646	-0.0741
Si	-0.2622	-0.0892	-0.0307
Ti	-0.2554	0.0629	-0.004
V	-0.0649	-0.0159	-0.0013
Zn	-0.1317	-0.4689	-0.0032
Eigenvalue	11.5206	1.5905	1.2503
Variance %	52.3666	7.2295	5.6833
Cum. Var. %	52.3666	59.5961	65.2794
Potential Source	Crustal		

3.2.2. Heavy metal events

Engelbrecht et al. (2008) found relatively high trace metal concentrations of Zn, Cd, and Pb in Bagram. As mentioned in sections 1.5.1 and 1.5.2, high concentrations of these elements have been observed in Pakistan. Backward trajectory and concentration analyses in this thesis reveal that indeed a significant fraction of Bagram's Zn and Pb (Cd concentrations were not determined) concentrations originate in Pakistan. But as stated in section 1.5.2.2, these heavy metal elements have also been observed in the nations to the northwest of Afghanistan.

Two very similar high Pb and Zn events are seen in the data from February 6 to February 10, 2010 and February 22 to February 28, 2010 (Figures 3.11-3.12). Starting backward trajectories from Bagram at 250 m and 2500 m above ground level (AGL) during these time periods show air history in Pakistan (see Figures 3.13-3.14). Furthermore, sector analysis reveals large percentages of backward trajectory time in sector 4 (Figure 3.15). Elevation differences between Pakistan (low elevation) and Afghanistan (higher elevation) could be responsible for air not being able to pass over the mountains effectively until a lifting mechanism forces it up the mountains. Low-pressure systems had in fact passed over the region and likely generated the greater amounts of lift necessary to force the Pakistan aerosols to cross the mountains into Afghanistan.

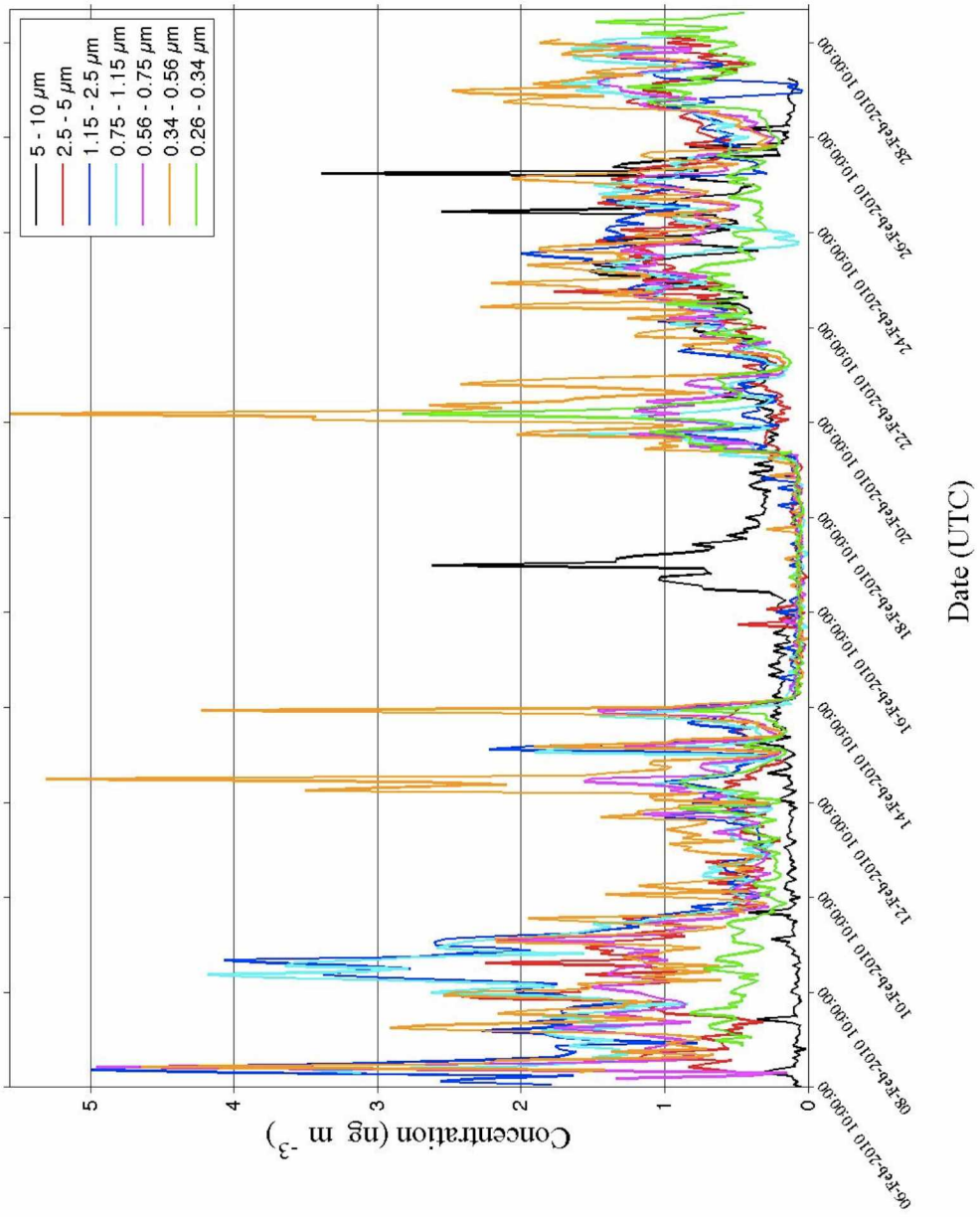

Figure 3.11. Zinc concentrations for Bagram, Afghanistan, from February 6, 2010 to February 28, 2010.

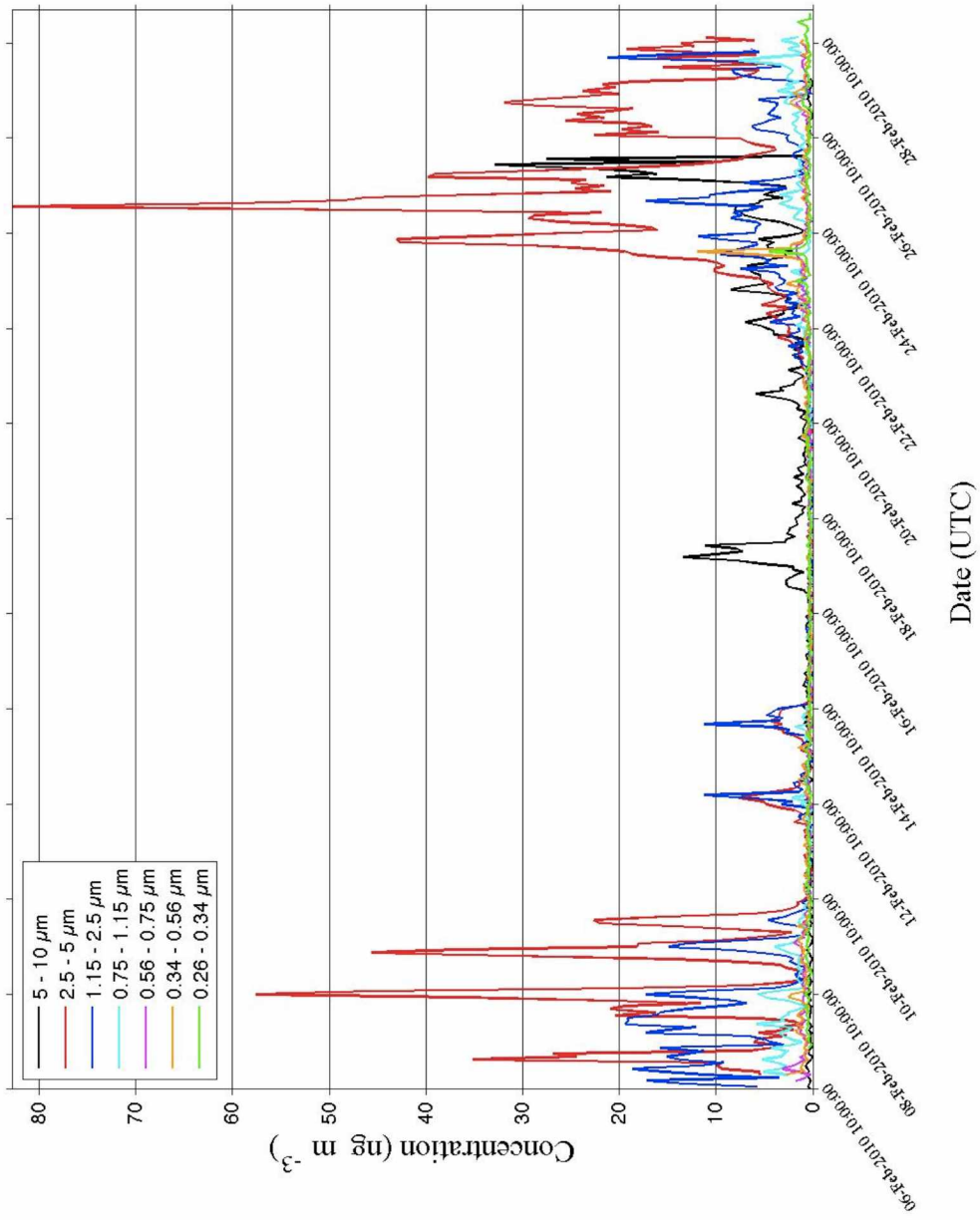

Figure 3.12. Lead concentrations for Bagram, Afghanistan, from February 6, 2010 to February 28, 2010.

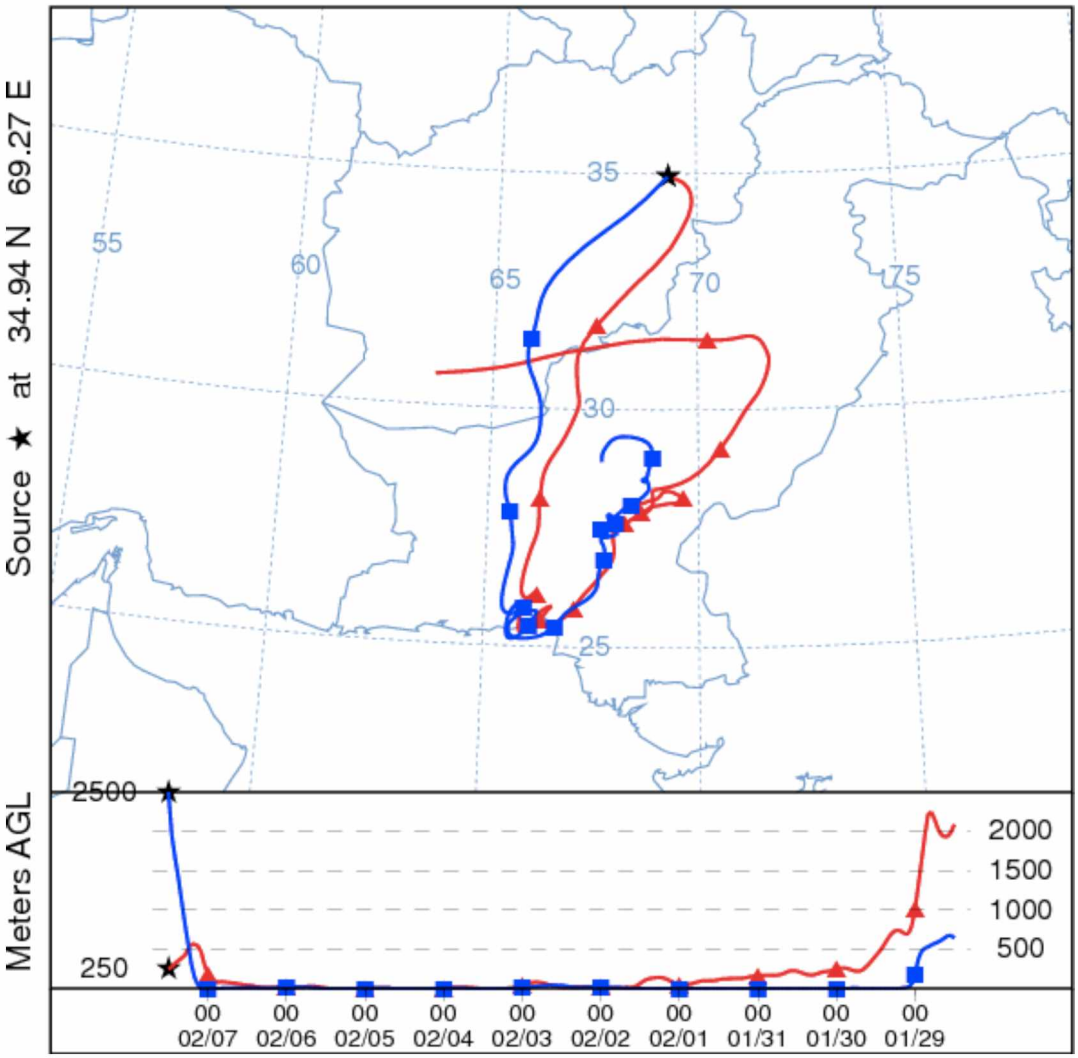

Figure 3.13. Backward trajectories for air reaching Bagram, Afghanistan, during a high lead aerosol event in February 2010.

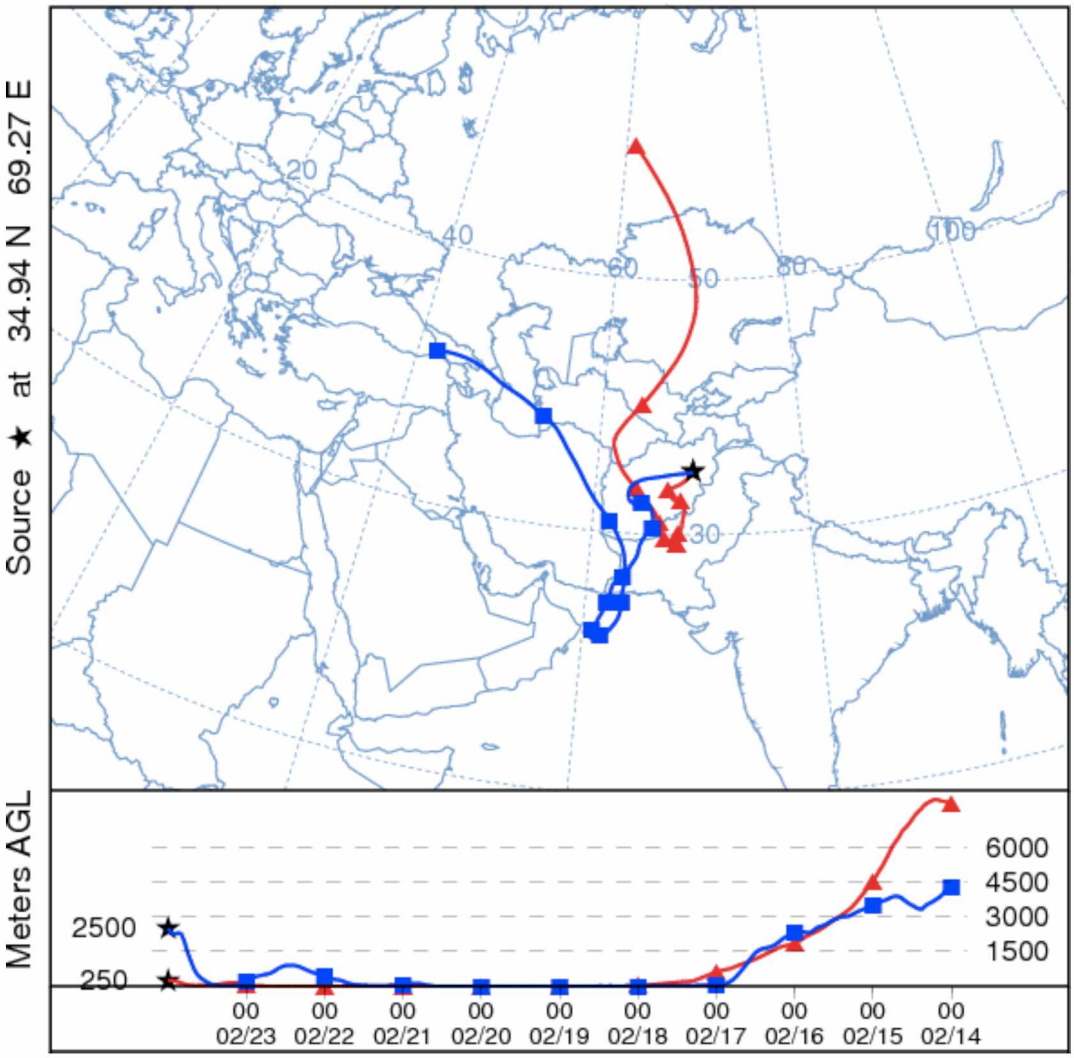

Figure 3.14. Backward trajectories for air reaching Bagram, Afghanistan, during a high lead and zinc aerosol event in February 2010.

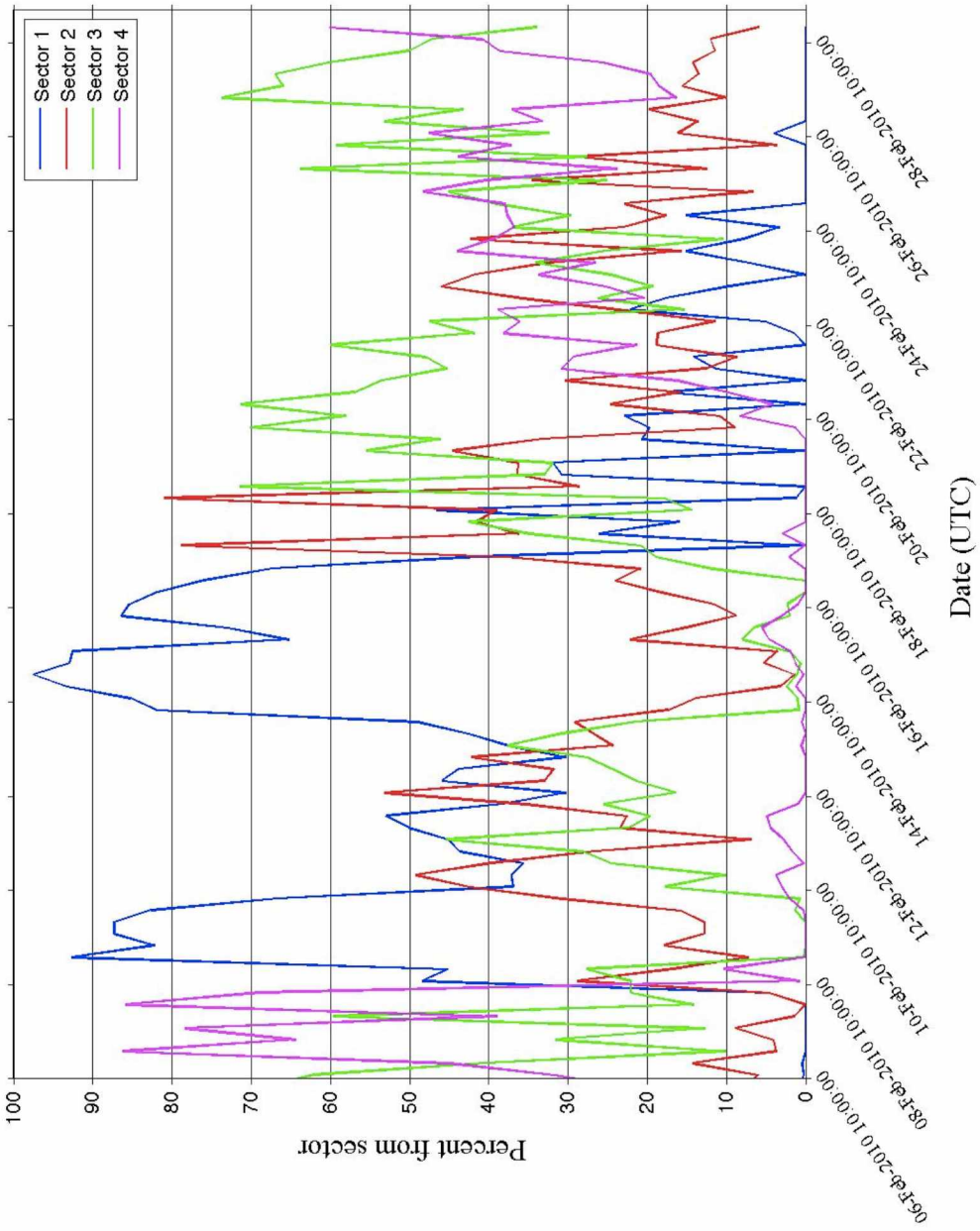

Figure 3.15. Sector analysis at Bagram, Afghanistan from February 6, 2010 to February 28, 2010. Note the days of February 6-10 and 22-28 as periods of increased contributions from sector 4 as mentioned in section 3.2.2.

Once the aerosols were injected into the ambient air in Bagram, the diurnal cycle took over and forced the aerosol-laden air in and out of Bagram each day. Further aerosol injection from Pakistan on following days caused higher daily peaks in Pb and Zn concentrations.

A unique situation arises in the latter case due to the fact that backward trajectories lead back to Pakistan (more recent) and Kazakhstan, Turkmenistan, and Uzbekistan (less recent). The spike in the submicron-sized Pb and As between February 23-24 (Figures 3.12 and 3.16) could be due to transport from any of these countries, but it is more likely from Pakistan because Smith et al. (1996) noted high ambient As levels in Pakistan. Overall this example stresses the importance of the effects that the pollution from these nations is having on Afghanistan's aerosol contaminants.

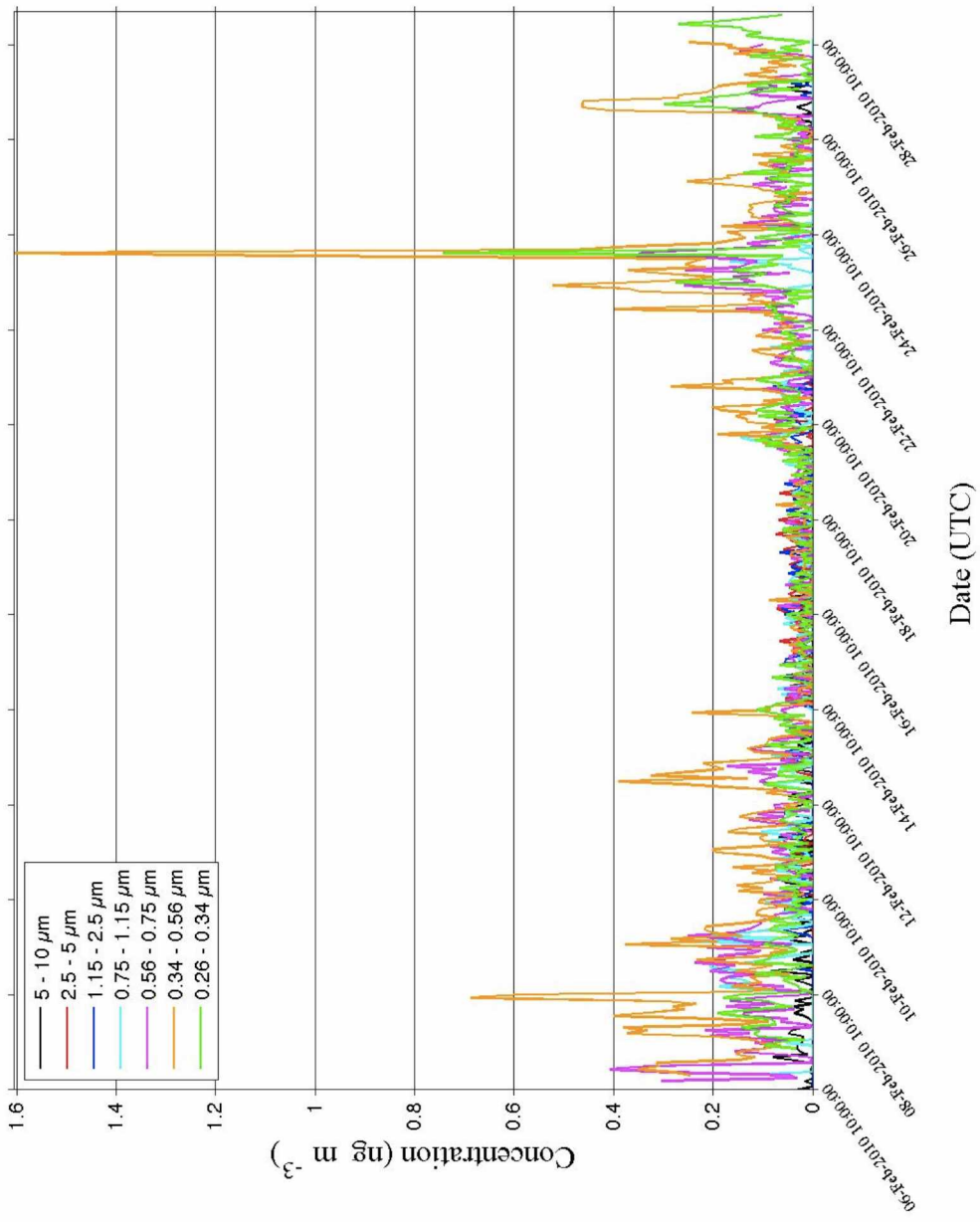

Figure 3.16. Arsenic concentrations for Bagram, Afghanistan, from February 6, 2010 to February 28, 2010.

Zinc is also found with Cu. One such case occurred in Bagram during March 23 to March 25, 2010 (Figures 3.17-3.18). A relatively strong low-pressure system passed through Kazakhstan a week prior to the air reaching Bagram, likely initiating a large flux of aerosols. Sector analysis reveals a large percentage of backward trajectory time in sector 1 (Figure 3.19). Backward trajectory analysis from Bagram for a starting position of 250 m AGL reveals that the air has history over Kazakhstan (Figure 3.20). Additionally, the backward trajectory displays history over the nearby Aral and Caspian Seas; therefore, some sea salts could be expected and actually were observed. Finally, due to the distance separating Afghanistan from Kazakhstan, the fact that larger particles are deposited more quickly than smaller particles, and the aerosols seen during this time period are primarily between 0.26 μm and 0.75 μm in aerodynamic diameter, it is reasonable to assume that these particles were transported a long distance. Altogether, these effects likely caused the increased submicron concentrations of Br, Cu, Zn, and Cl during March 23 to March 25, 2010 (Figures 3.8, 3.17, 3.18, and 3.21).

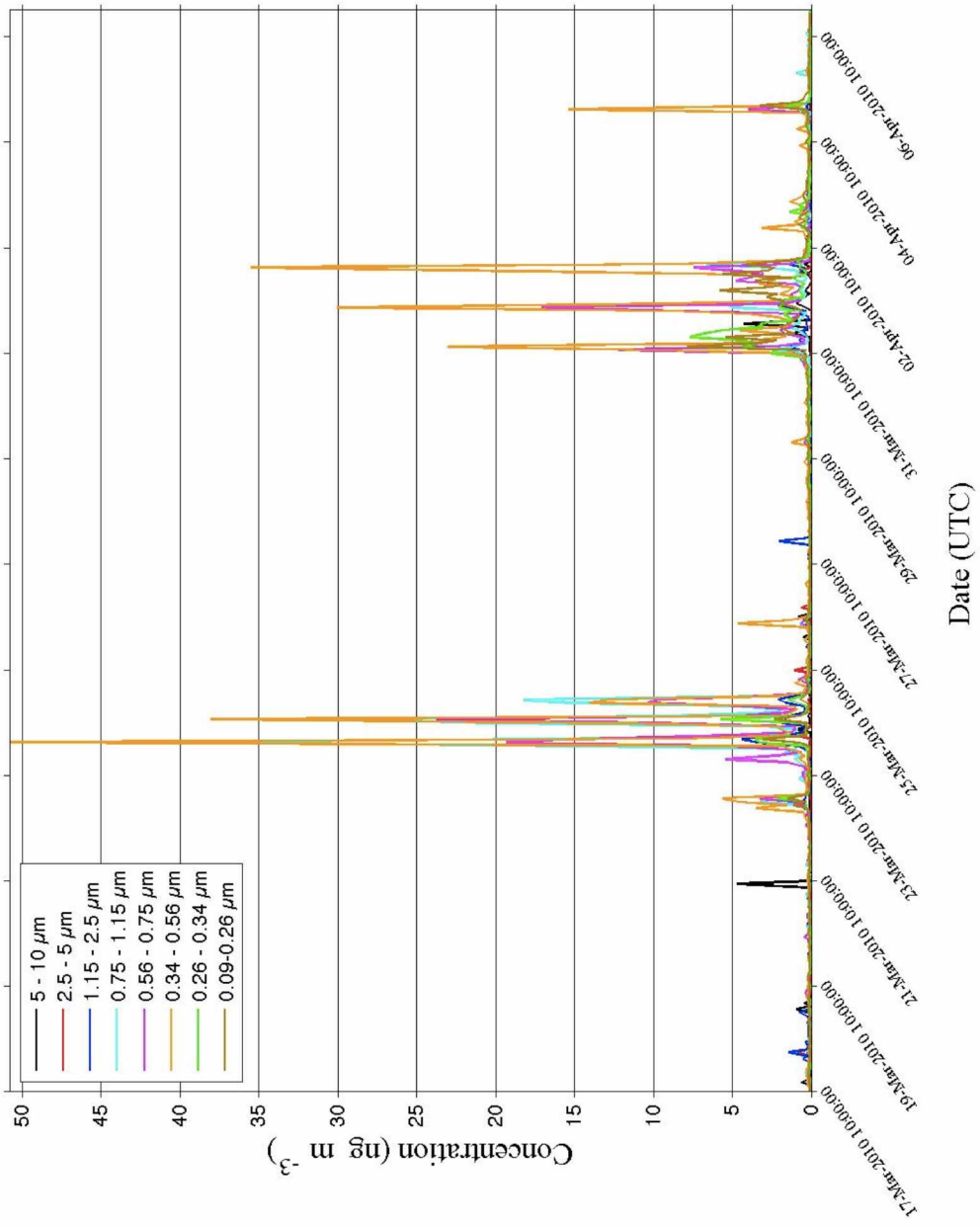

Figure 3.17. Copper concentrations for Bagram, Afghanistan, from March 17, 2010 to April 6, 2010.

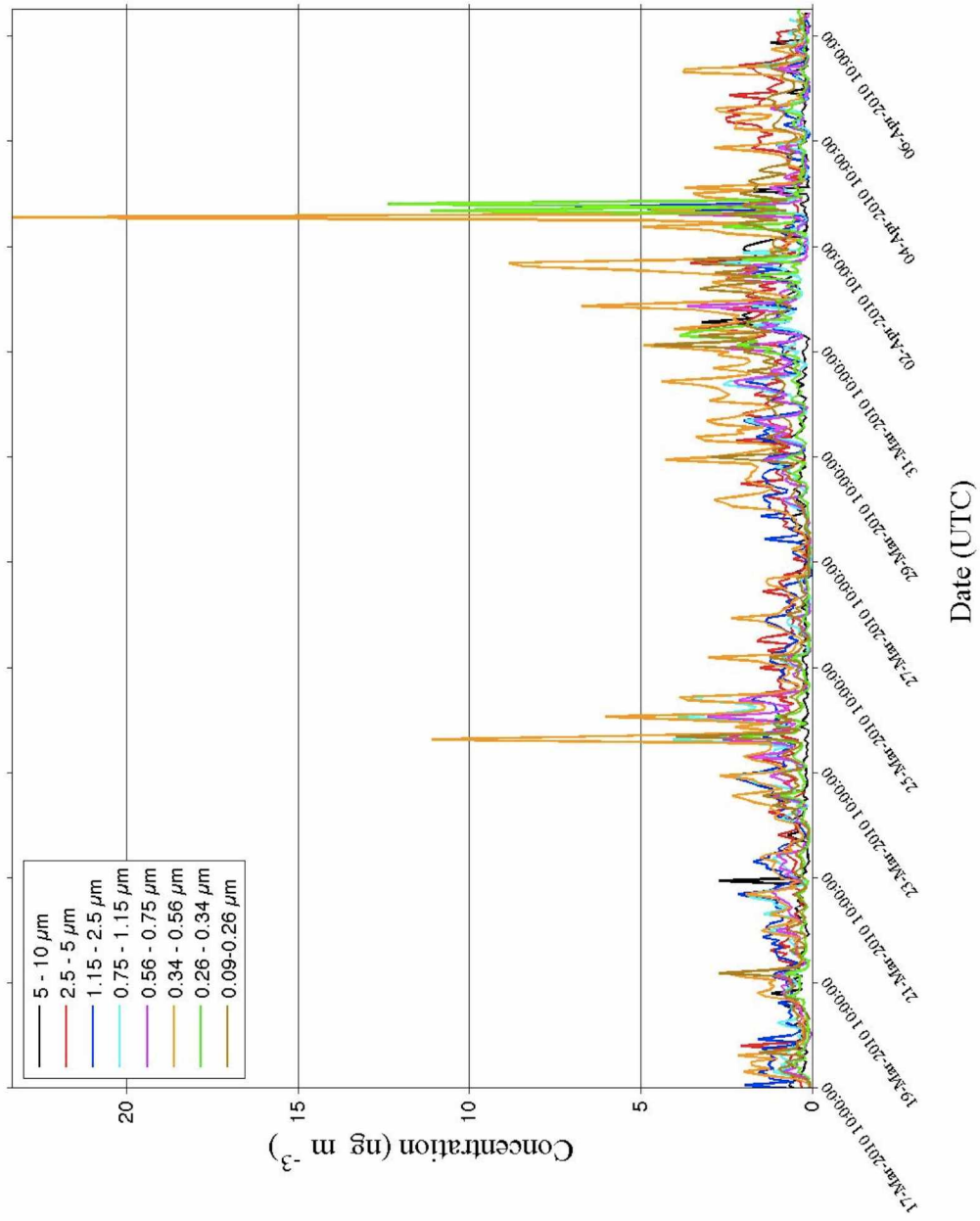

Figure 3.18. Zinc concentrations for Bagram, Afghanistan, from March 17, 2010 to April 6, 2010.

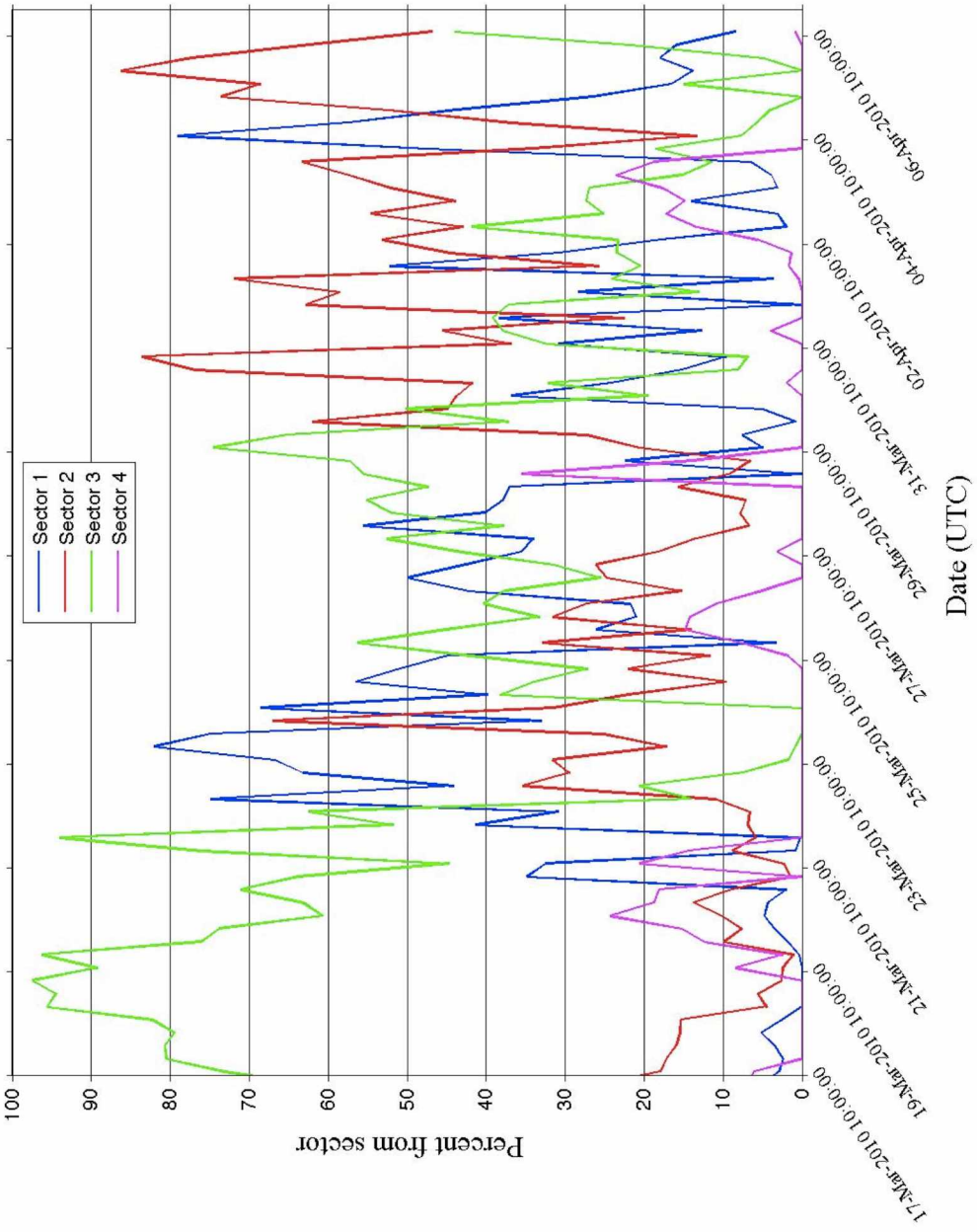

Figure 3.19. Sector analysis at Bagram, Afghanistan from March 17, 2010 to April 6, 2010. Note the sector percentages from March 23-25 and March 31 to April 2 as described in section 3.2.2.

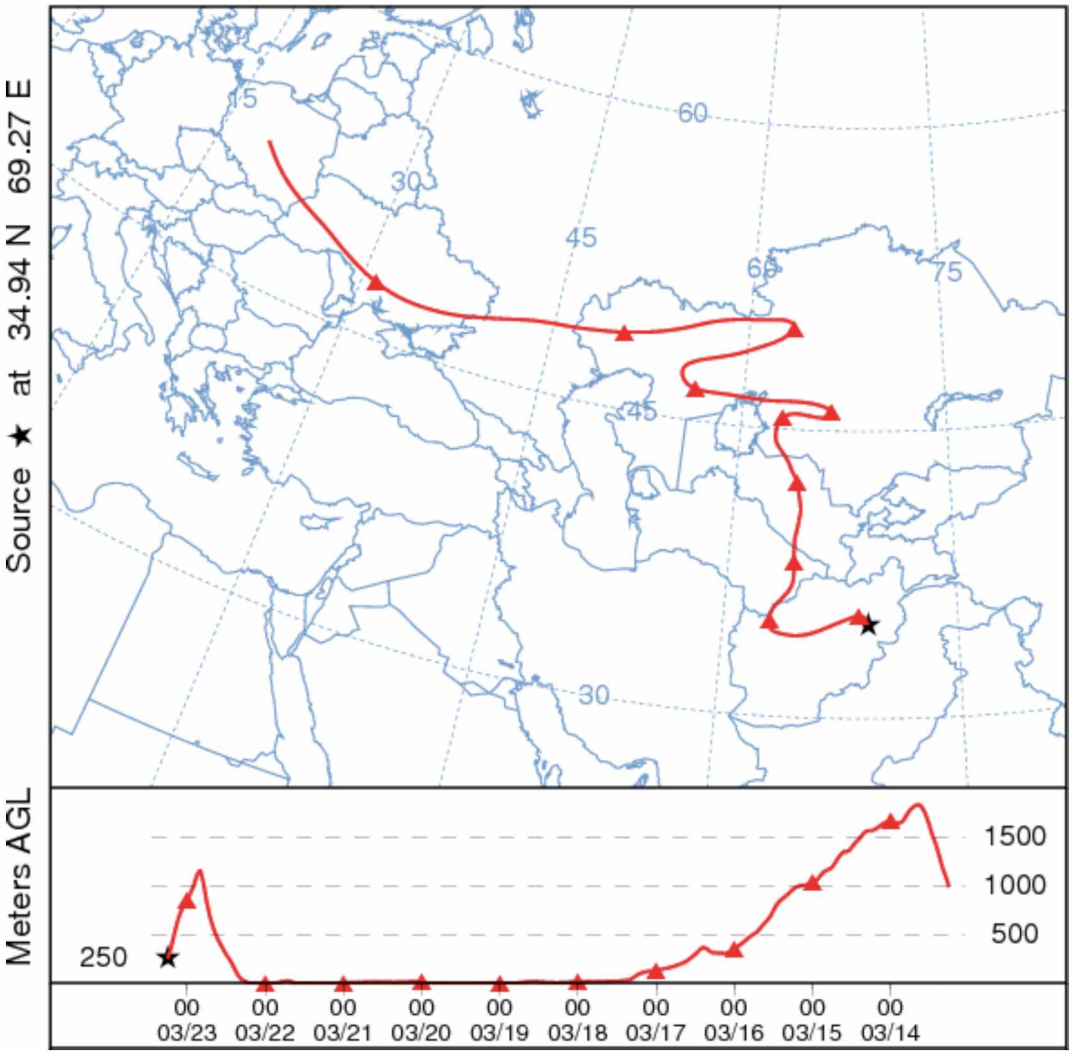

Figure 3.20. Backward trajectory for air reaching Bagram, Afghanistan, during a high zinc and copper aerosol event in March 2010.

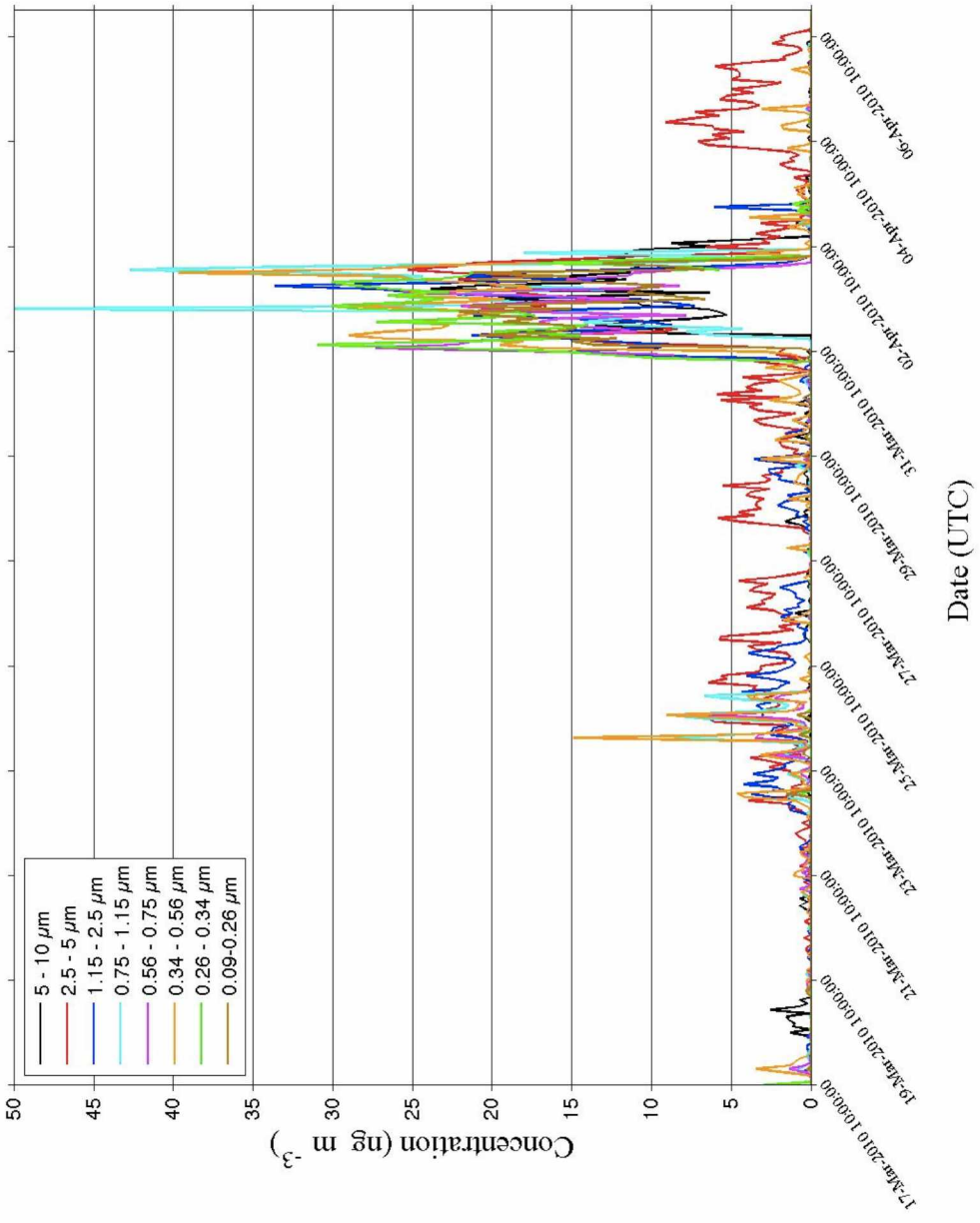

Figure 3.21. Chlorine concentrations for Bagram, Afghanistan, from March 17, 2010 to April 6, 2010.

A similar event occurred during March 31 to April 2, 2010. Copper and zinc appear to have been injected into Bagram's air and then followed a diurnal pattern (Figures 3.17-3.18). Instead of their concentration peaks decreasing in magnitude, they increased for the following days likely due to both the diurnal cycle recycling the previous day's concentrations and a further injection of aerosols from the Kazakhstan region. For this period, 250 m and 2500 m AGL starting backward trajectories not only had history over the Kazakhstan region, but additionally exhibited air history over the Mediterranean, Caspian, and Aral Seas (Figure 3.22). The prior mentioned event of March 23-25 and this event both had the same mass ratio of Zn to Cu (i.e. approximately 0.15 to 0.45; Figure 3.23), and with the backward trajectories leading back to the same area, it can be concluded that these elements are likely coming from the same source. This source could potentially be due to the mining and smelting of metals, specifically Cu and Zn.

Within the week prior to the March 31 to April 2 event, a relatively strong upper level trough (and an associated surface low-pressure system) moved across the Mediterranean Sea and initiated a larger flux of aerosols. In this case, larger amounts of sea spray aerosols. March 31 through April 2 witnessed relatively high, sustained concentrations of Cl and Br among other elements (Figures 3.8 and 3.21). Similar to previous cases, a diurnal pattern is observed in Cl and Br.

In all the cases presented, increased wind speeds at the potential source location had the opportunity to loft the observed aerosols and transport them to

Afghanistan. These events stress the importance of wind speed on aerosol lofting prior to transport.

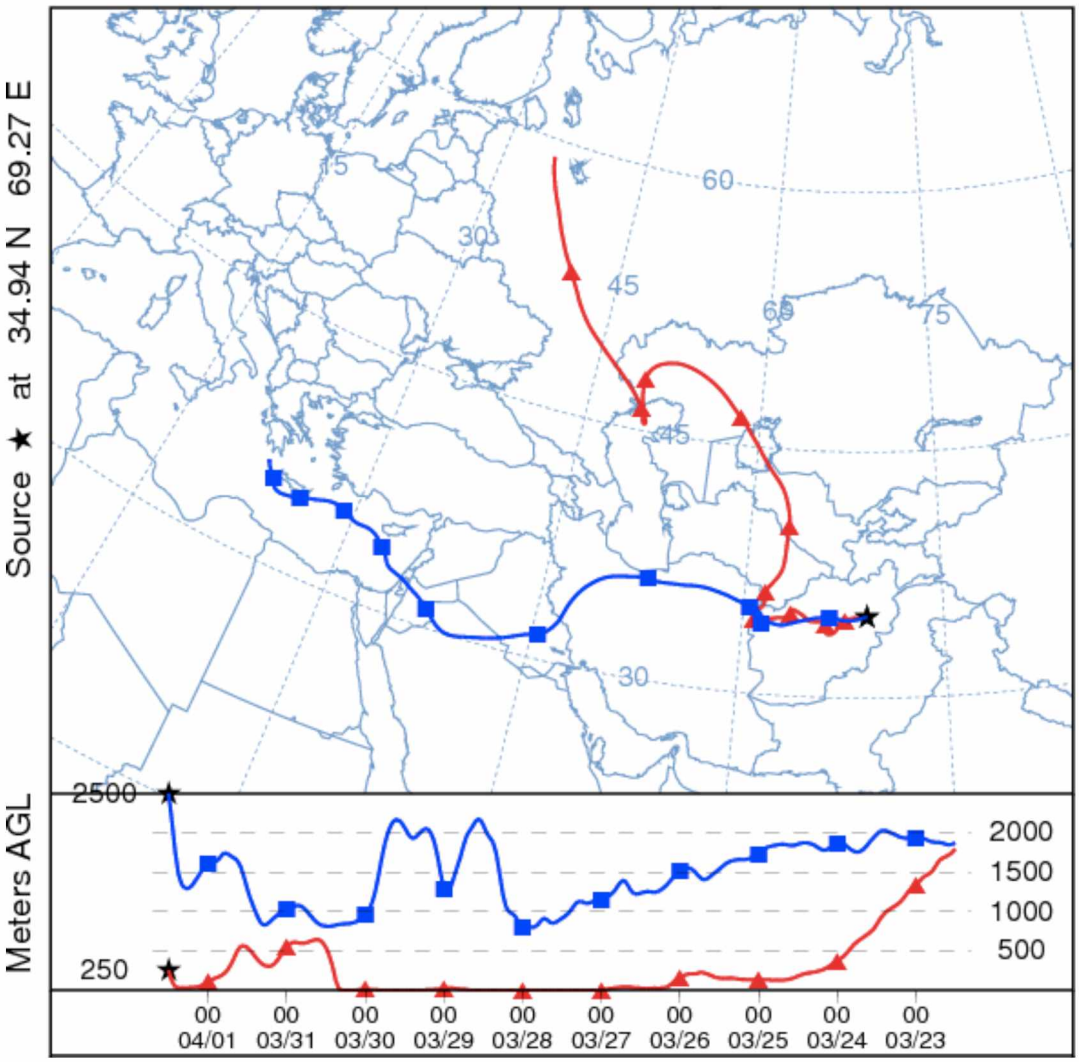

Figure 3.22. Backward trajectories for air reaching Bagram, Afghanistan, during a high lead, copper, zinc, chlorine, and bromine aerosol event in April 2010.

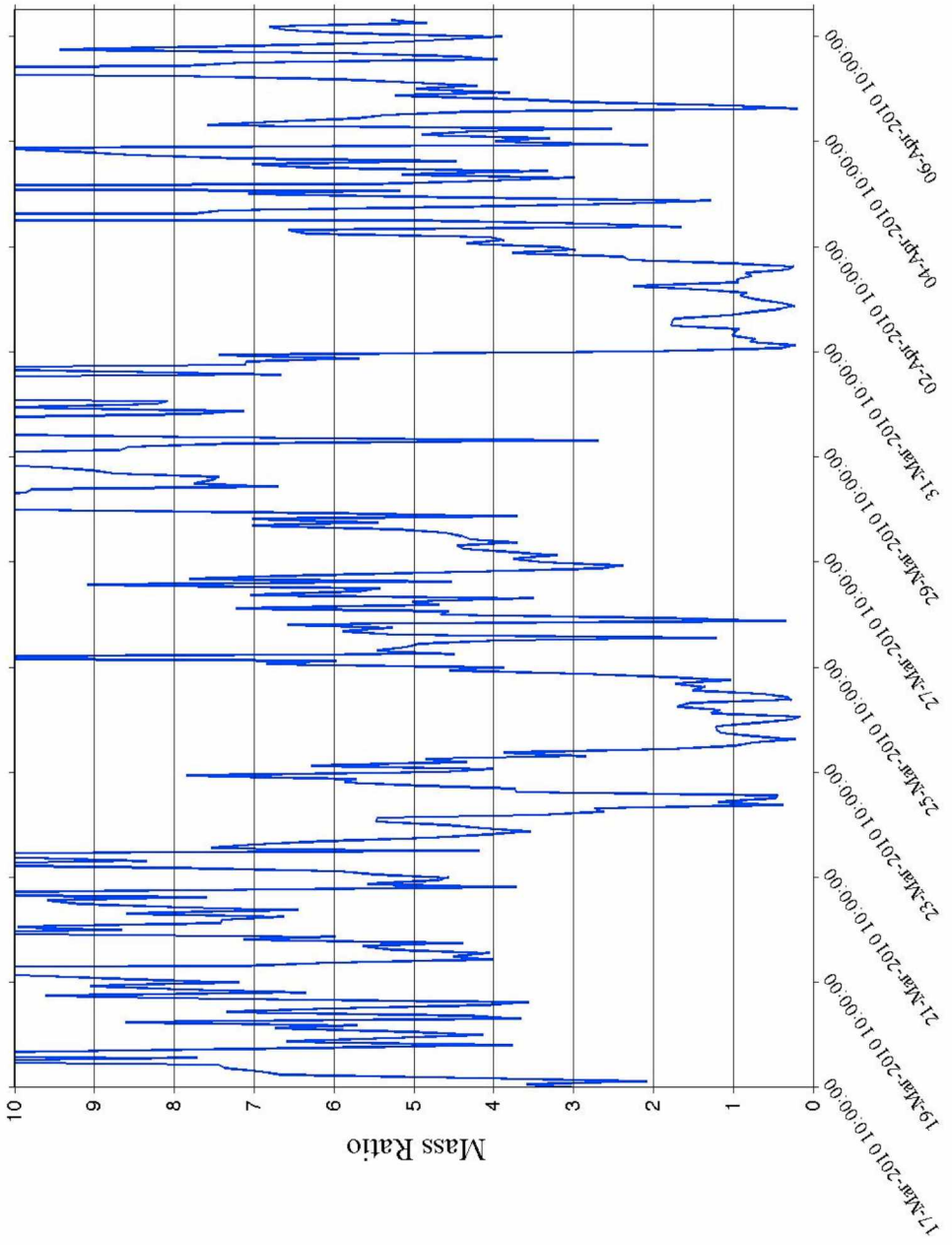

Figure 3.23. Zinc to copper elemental ratio (by mass; Zn/Cu) in the 0.34 – 0.56 µm size range for Bagram, Afghanistan, from March 17, 2010 to April 6, 2010. Note the upper boundary was cut off at a mass fraction of 10 in order to better view the low Zn/Cu mass fractions occurring between March 23-25 and March 31 to April 2.

3.3. PM_{10} and $PM_{2.5}$ concentrations and comparison to health safety standards

Similar to what was witnessed in the elemental concentration graphs, PM_{10} and $PM_{2.5}$ concentrations are reduced in the months prior to the onset of the monsoon due to decreased winds during the transition of wind direction (Figures 3.24-3.27). Once the monsoon sets up, winds will increase for the summer. Although concentration data is unavailable for the summer months, dust storm frequencies seen in Table 1.1 and testimonials from those who have been in Afghanistan reveal exceptional amounts of aerosols present in the ambient air during these months.

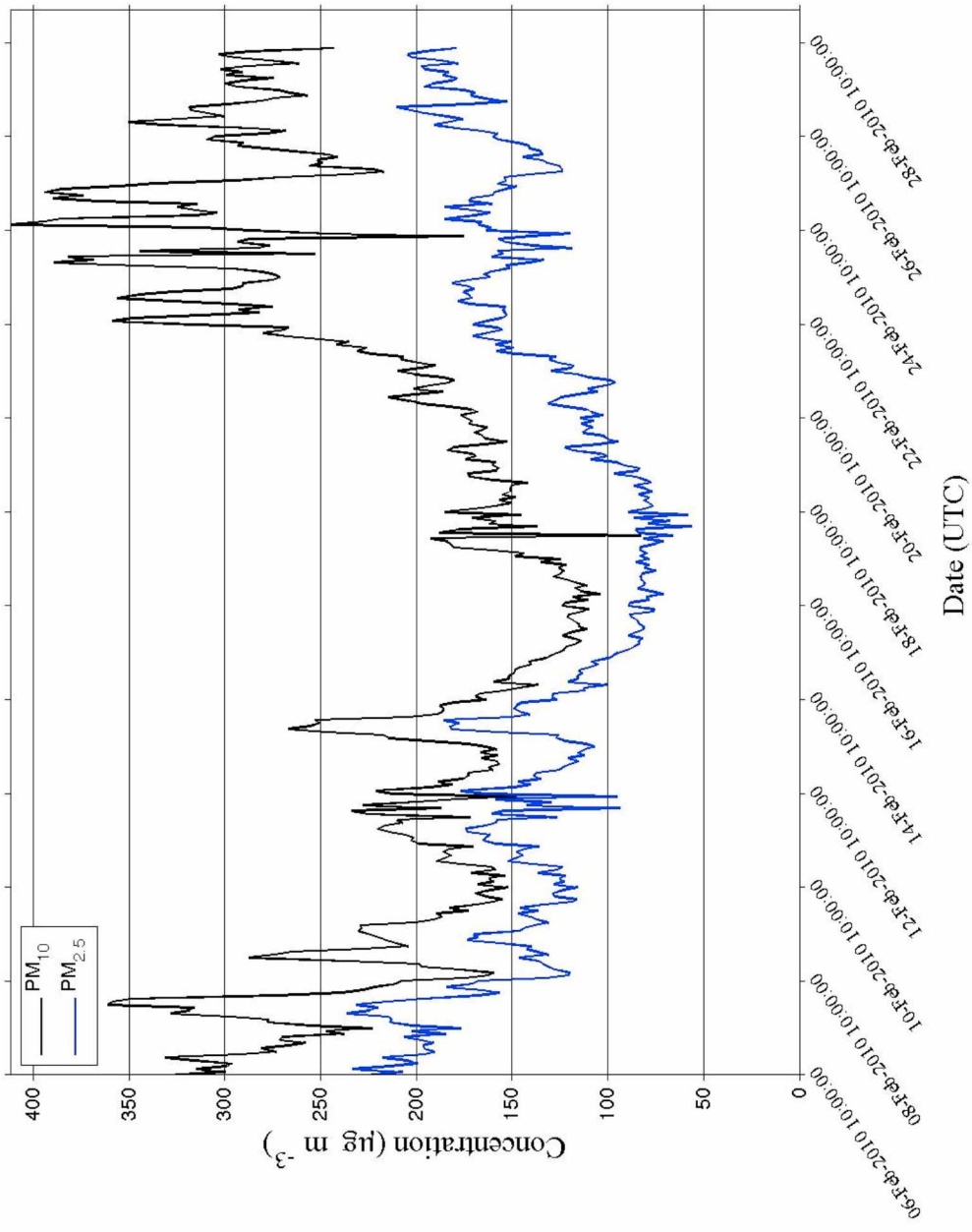

Figure 3.24. PM_{10} and $PM_{2.5}$ mass concentrations for Bagram, Afghanistan, from February 6, 2010 to February 28, 2010.

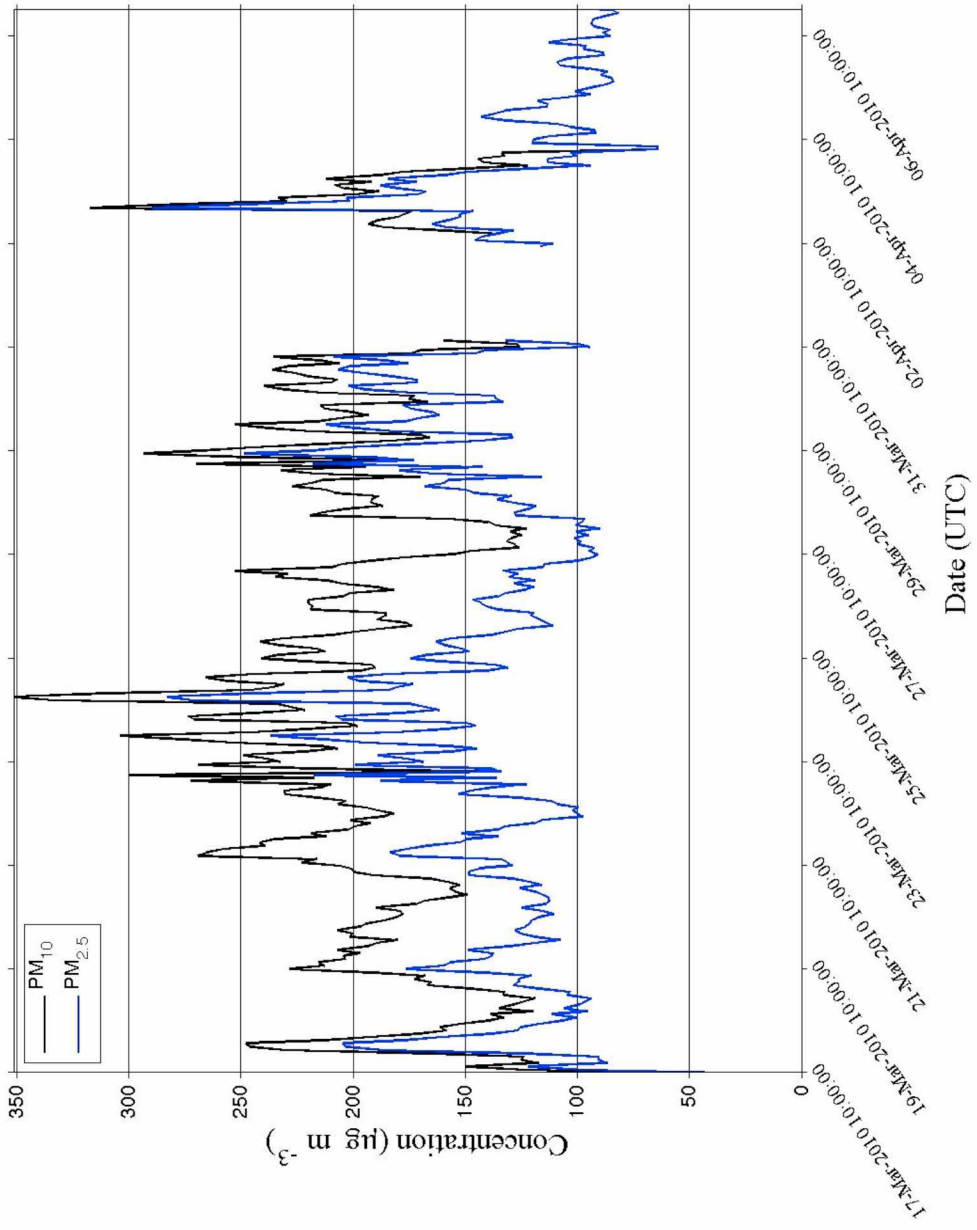

Figure 3.25. PM_{10} and $PM_{2.5}$ mass concentrations for Bagram, Afghanistan, from March 17, 2010 to April 6, 2010.

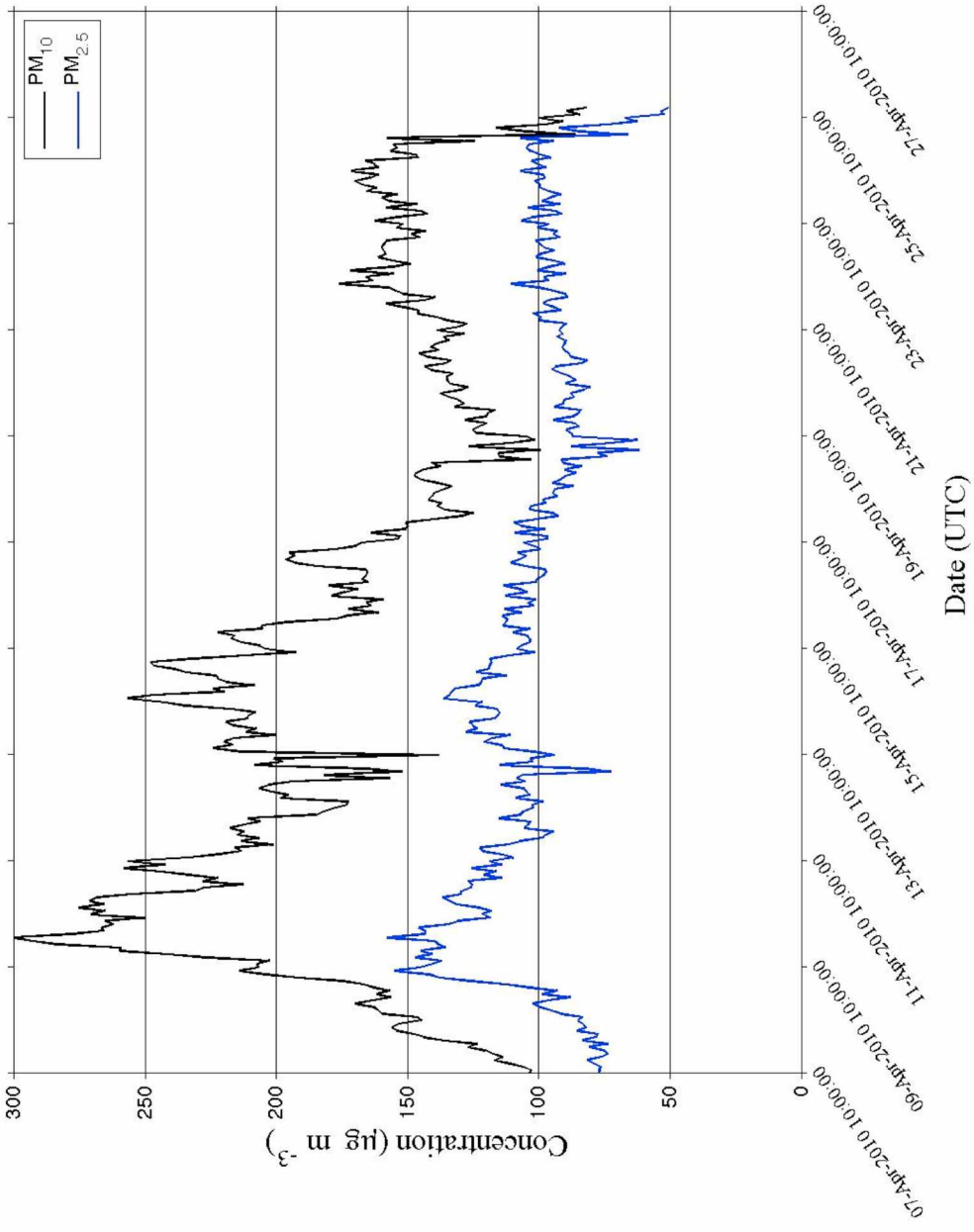

Figure 3.26. PM_{10} and $PM_{2.5}$ mass concentrations for Bagram, Afghanistan, from April 7, 2010 to April 27, 2010.

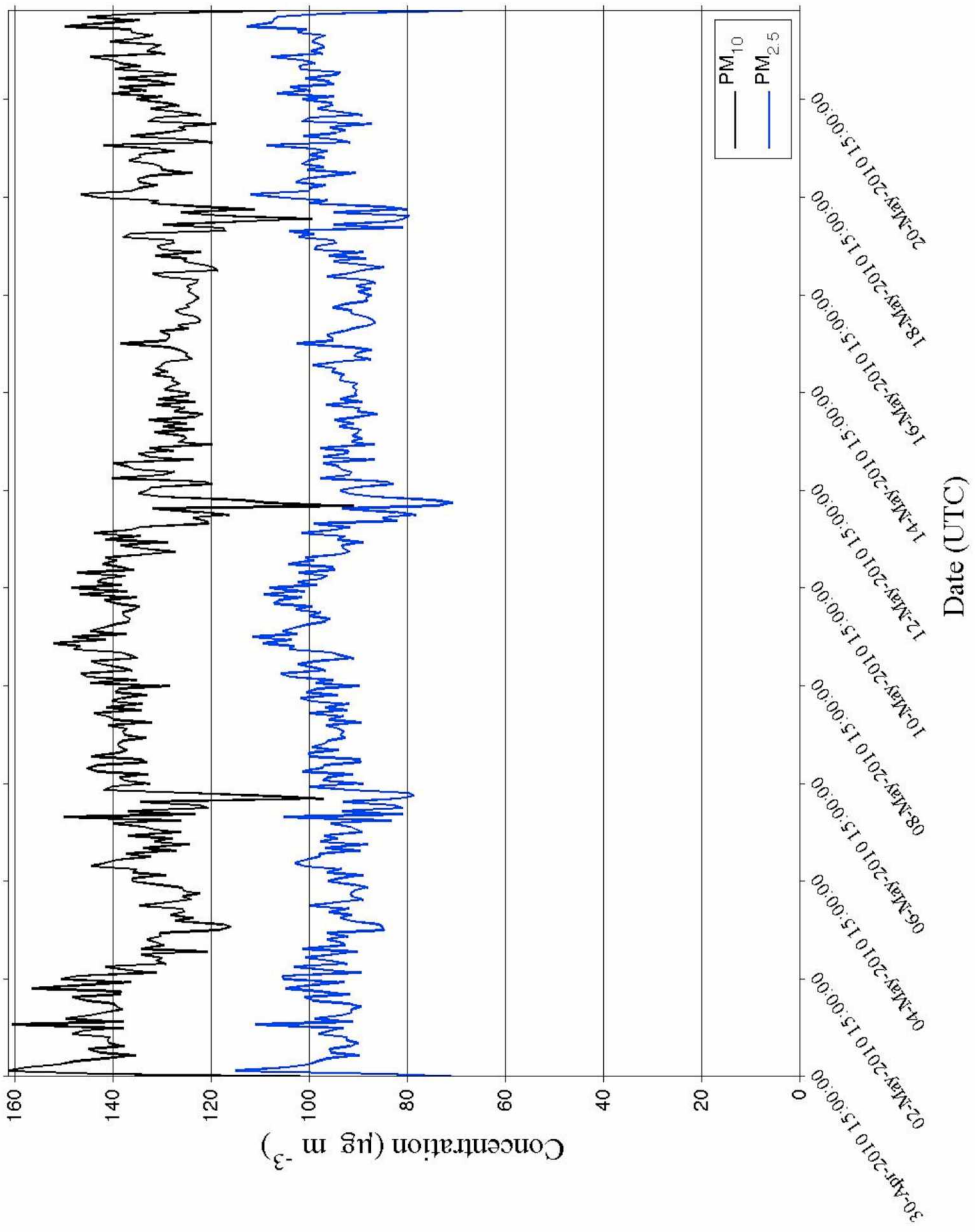

Figure 3.27. PM_{10} and $PM_{2.5}$ mass concentrations for Bagram, Afghanistan, from April 30, 2010 to May 22, 2010.

With PM_{10} concentrations often well above the NAAQS standard of 150 μg m^{-3} at all hours everyday in the measurement periods (Figures 3.24-3.27), health hazards due to PM_{10} are regular and persistent. Even worse, the $PM_{2.5}$ concentrations are consistently above health safety standards; the $PM_{2.5}$ concentrations regularly exceed 100 μg m^{-3}. This amount is nearly three times the 24-hour NAAQS safety standard. Even the lowest concentrations of $PM_{2.5}$ for these sample periods, which are present only for brief hours before increasing, are relatively high exceeding 55 μg m^{-3}. This value is over one and a half times as high as the 24-hour NAAQS standard and is roughly as high as the negligible severity 24-hour $PM_{2.5}$ air MEG. Because the $PM_{2.5}$ concentrations are high at all times for these months, and the meteorological situation during the summer favors dust lofting, it is likely that aerosol concentrations are going to increase in the summer months in Afghanistan. These facts suggest that the annual average $PM_{2.5}$ concentration will be relatively high too. Engelbrecht et al. (2008) found that the annual average $PM_{2.5}$ concentration in Bagram was 40.15 μg m^{-3}. This value is much higher than the 15 μg m^{-3} negligible severity annual $PM_{2.5}$ air MEG, but not quite as high as the 65 μg m^{-3} marginal severity annual $PM_{2.5}$ air MEG. Regardless, people in Bagram during these sample periods would have breathed months' worth of notable $PM_{2.5}$ concentrations.

To make matters worse, these values can be underestimates of the true values because during transport and handling of the samples, some of the aerosols may flake off the Mylar™. If this happens, those aerosols are not in the totals. This

loss is especially true with the larger size-fraction drums because the large number of particles sticking to the Mylar™ eventually covers the impact spot and causes the particles to stack on top of one another. If this happens, which can occur relatively frequently on the first drum stage in high aerosol environments, such as locations around the Middle East, the particles will not tend to stick as well because they are not sticking to the Mylar™ but rather to other particles. Thus, the actual aerosol mass content in the air may be even higher than recorded measurement values.

3.4. Sector analysis

The sector plots presented here for Bagram (Figures 3.15, 3.19, 3.28, and 3.29) indicate how often potential source locations change throughout each sample period. Generally speaking, sector 4 appears to have the lowest percentage of backward trajectories segments leading back to it. This behavior is likely due to the prevailing westerly wind direction at this latitude. This concept and the fact that pre-monsoon winds are predominately from the west and southwest throughout March to April leads to sectors 2 and 3 having greater percentages during these times (Figures 3.19 and 3.28). As the winds begin to shift toward the north, sector 1 appears to have a greater influence (Figure 3.29).

Simply having a higher percentage of presence within a specific sector did not directly mean that certain elemental concentrations would be elevated. For

example, during the sample period of March 17 to April 6, Cu was elevated during March 23-25 and March 31-April 2 (Figure 3.17). However, there was still a relatively large percentage of backward trajectory points in sector 1 in the days between and after these two time periods (Figure 3.19), but this did not lead to elevated Cu concentrations.

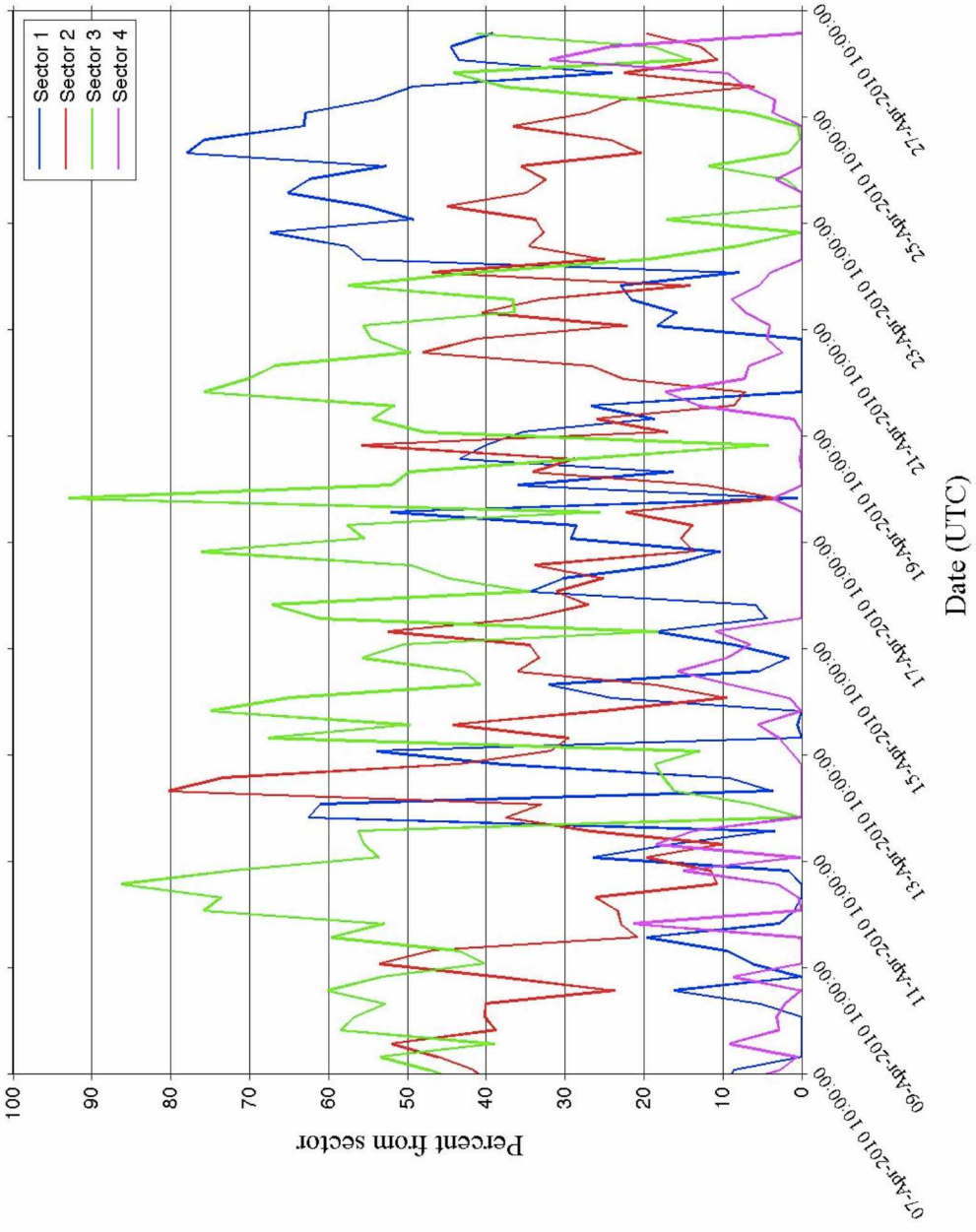

Figure 3.28. Sector analysis at Bagram, Afghanistan from April 7, 2010 to April 27, 2010.

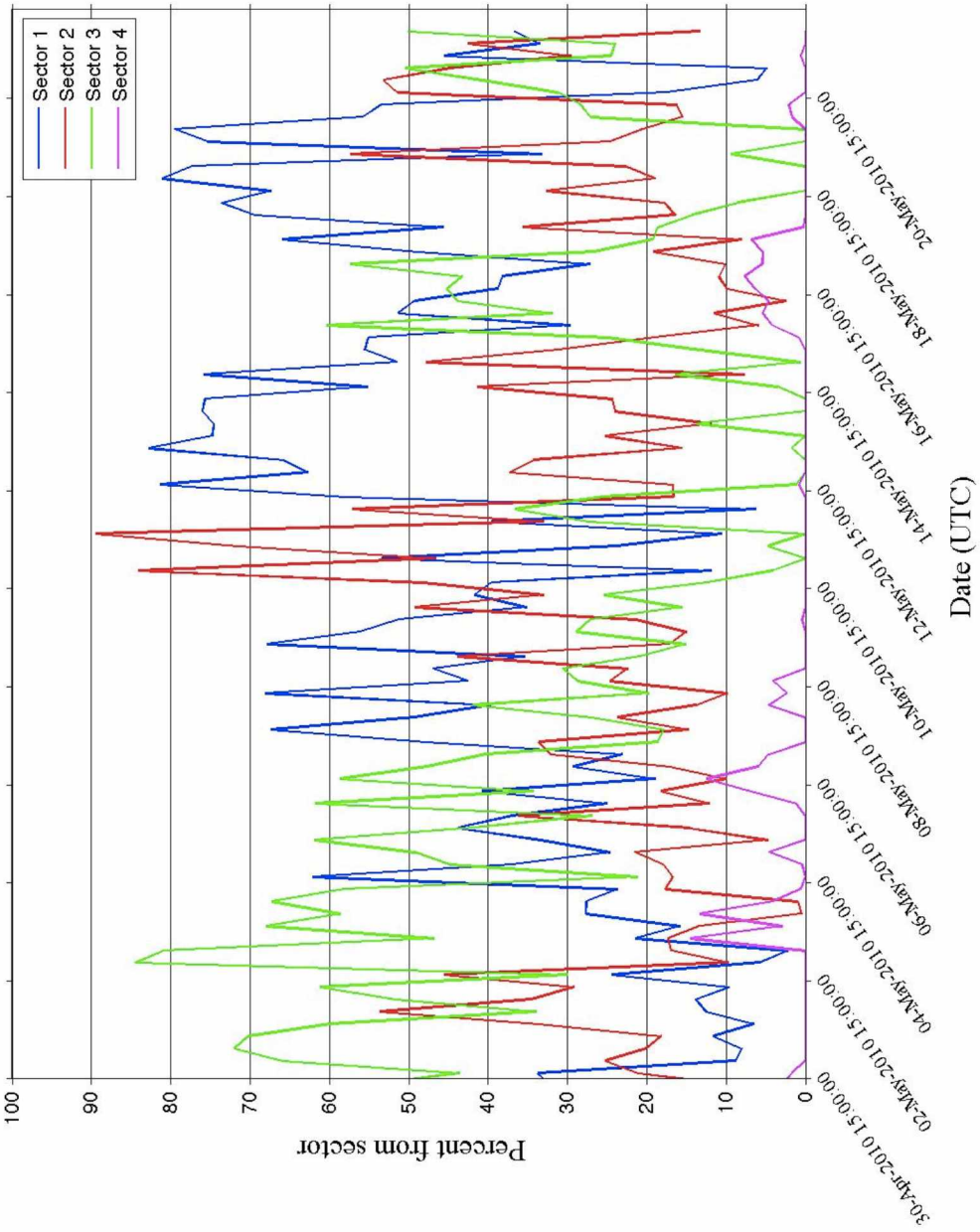

Figure 3.29. Sector analysis at Bagram, Afghanistan from April 30, 2010 to May 22, 2010.

3.5. PCA

The broken-stick model was a way to determine which principal components are significant. Based on the broken-stick model criteria, the first two components should be used for the first three sampling periods and only the first component should be used for the fourth sampling period. Therefore, only these principal components will be examined further.

The eigenvector loading values (Tables 3.1-3.4) for each element, and how they compare to other elements on the same principal component axis, were interpreted as significant sources affecting the aerosol environment in Afghanistan. In all four sampling periods (Tables 3.1-3.4), high loading values in elements such as Al, Ca, Si, Mg, Fe, and Ti, among other elements, were interpreted as dust sources in the first principal component. These sources were consistent with what was found by Engelbrecht et al. (2008) who identified geological dust as being one of the top three aerosol sources. The first principal component axis accounts for the greatest amount of the variance within the data; dust sources accounted for just over 50% of the variances among these sampling periods.

Consistent again with Engelbrecht et al. (2008) is another PCA distinguishable source involving smelting. Higher eigenvector loadings of Cu, S, and Zn, among other elements, are observed in the second principal component axes of Tables 3.1 and 3.2. These three elements are observed in the emissions from Cu and Zn smelting. It is difficult to say with high confidence whether

smelting processes are potentially causing the higher metal loadings on the second principal component or if this higher loading is due to mining practices in general. But as was mentioned earlier, there are a number of metals mined and smelted in nearby countries such as Kazakhstan and Pakistan that could be responsible for these emissions. Therefore, this source was generalized and called metal processing as it could be due to the mining, smelting, or refining processes.

Also seen in the second principal component axes of Tables 3.2 and 3.3 are higher eigenvector loadings of Cl and Br. These two elements are attributed to marine sources. There is a moisture influx seen in the northern portion of the Kabul Valley during February to April resulting in most of the precipitation (despite being relatively low total precipitation compared to most regions of the world (El Dorado Weather, 2012)) occurring during these months. Situations, such as was witnessed in Figure 3.22, occurred on several of the days of these sample periods as shown by backward trajectories leading to both the Mediterranean Sea and the countries to the north of Afghanistan. Weather systems passing through the region could be responsible for causing the simultaneous arrival of transported sea salts from the west and metals from the north. This situation is likely why Cl and Br are associated with elements such as Cu and S from metal processing. As was mentioned in section 1.4, there are large nickel deposits along the northeastern coast of the Mediterranean Sea. These deposits are likely why Ni had a larger eigenvector loading in the second principal component. Overall, the second

principal component axes accounted for approximately 13% to 18% of the variance.

Biplots were then constructed to examine how the loadings corresponded with the aerosol data from each sample period. These biplots are shown in Figures 3.30-3.33. What can be noticed is that many of the dust elements such as Al, Ca, Fe, Mg, and Si correspond to the larger size fractions while elements such as As, Br, Cl, Cu, S, Se, and Zn display loadings corresponding to the smaller size fractions. Interpretation of these plots adds evidence that dust sources, particularly local, wind-blown dust which would consist of larger particles than dust from a distant source where larger particles would have had time to settle out, is primarily causing the observed dust. It can also be interpreted for similar reasons, compounded with the fact that Afghanistan has little industry (Kuo, 2007), that distant sources are causing the eigenvector loadings of elements in the smaller size fractions.

Some elements such as sulfur are often emitted as SO_2 gas and later undergo processes in the atmosphere to form particles. This gas to particle conversion may also be true with copper in a high-temperature smelting process where it may be off-gassed into the atmosphere (Peters, 1907) and can later condense into a larger particle. This process may explain why elements such as these two saw higher loadings corresponding to the smaller size fractions in the PCA.

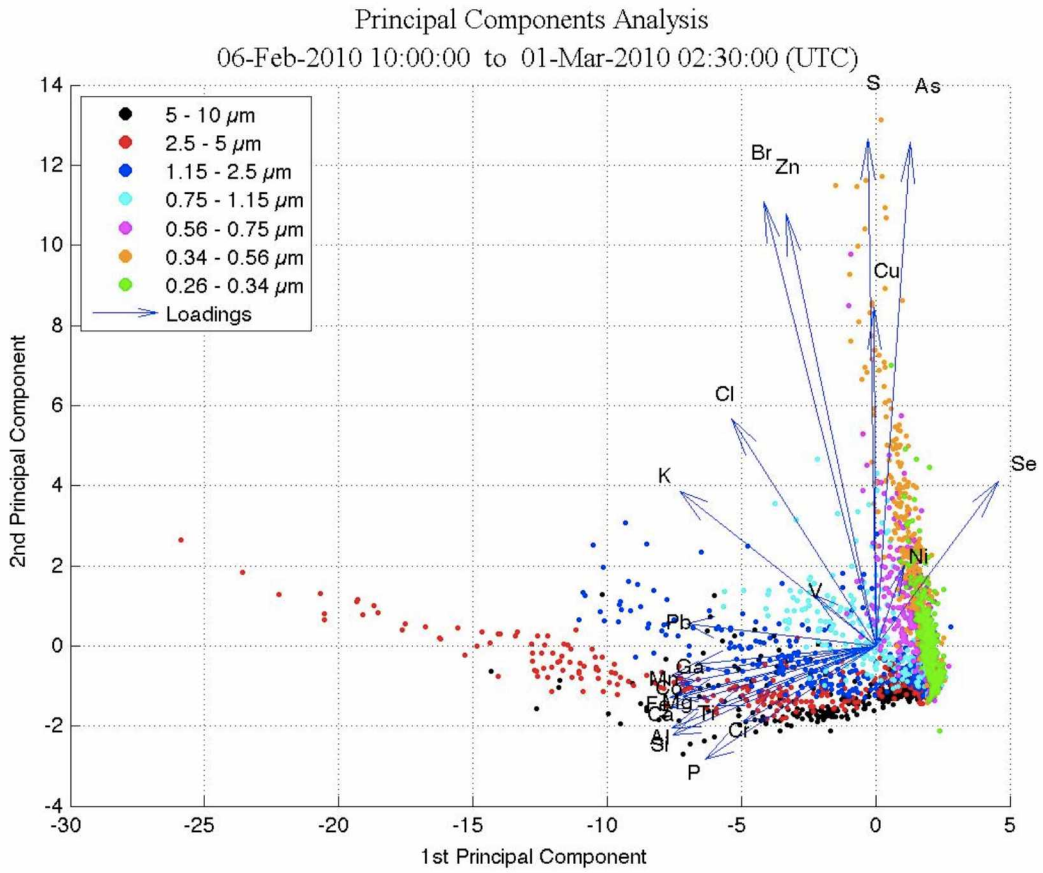

Figure 3.30. PCA biplot showing transformed aerosol data and eigenvector loadings. Eigenvector loadings have been extended 30 fold compared to values in Table 3.1 to make them more visible.

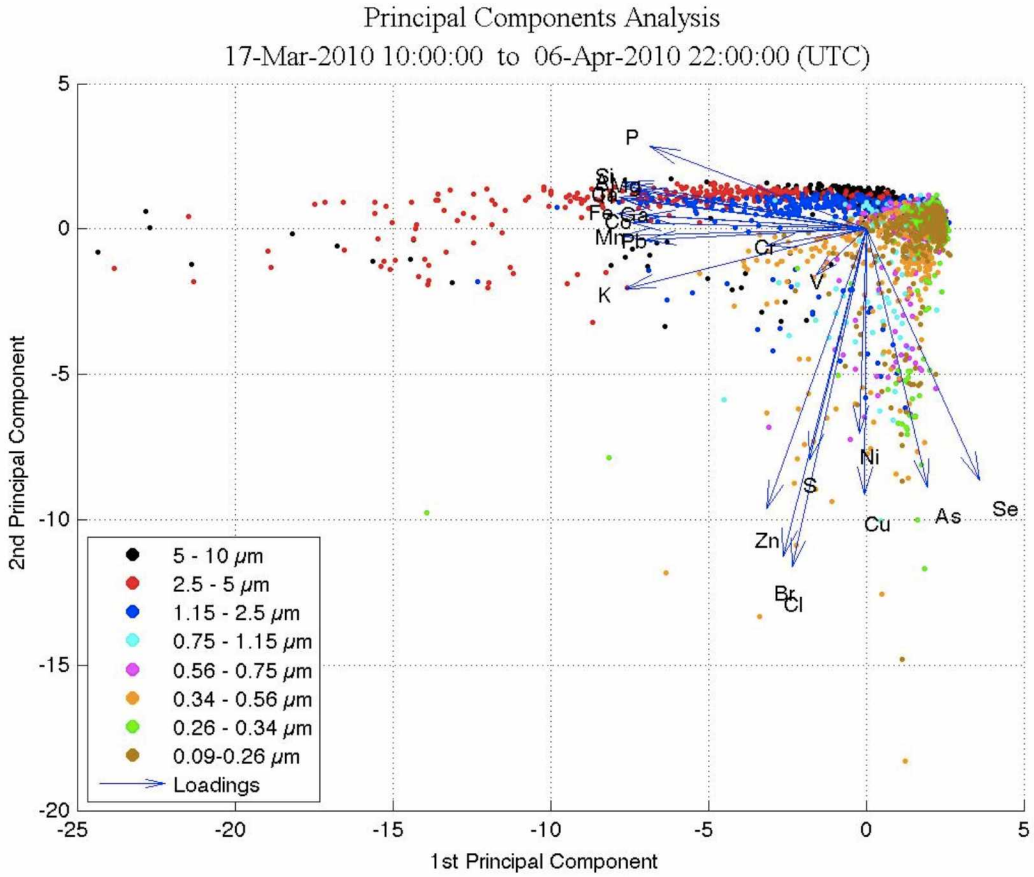

Figure 3.31. PCA biplot showing transformed aerosol data and eigenvector loadings. Eigenvector loadings have been extended 30 fold compared to values in Table 3.2 to make them more visible.

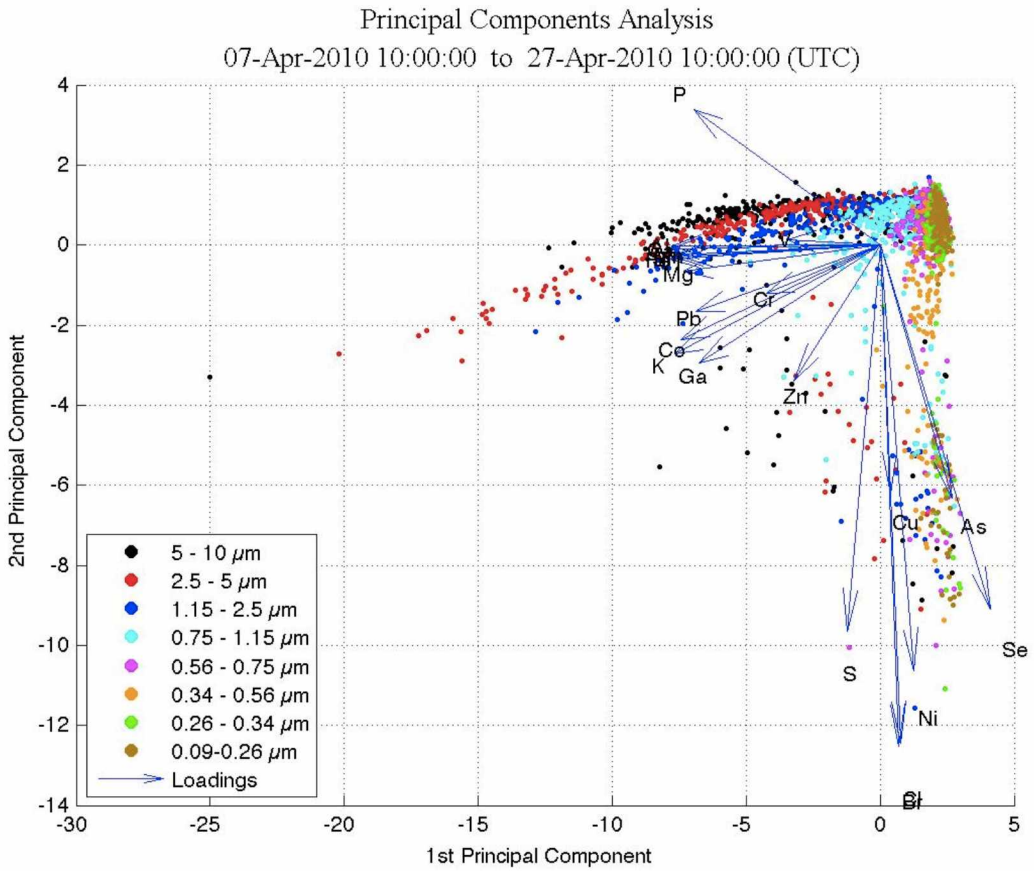

Figure 3.32. PCA biplot showing transformed aerosol data and eigenvector loadings. Eigenvector loadings have been extended 30 fold compared to values in Table 3.3 to make them more visible.

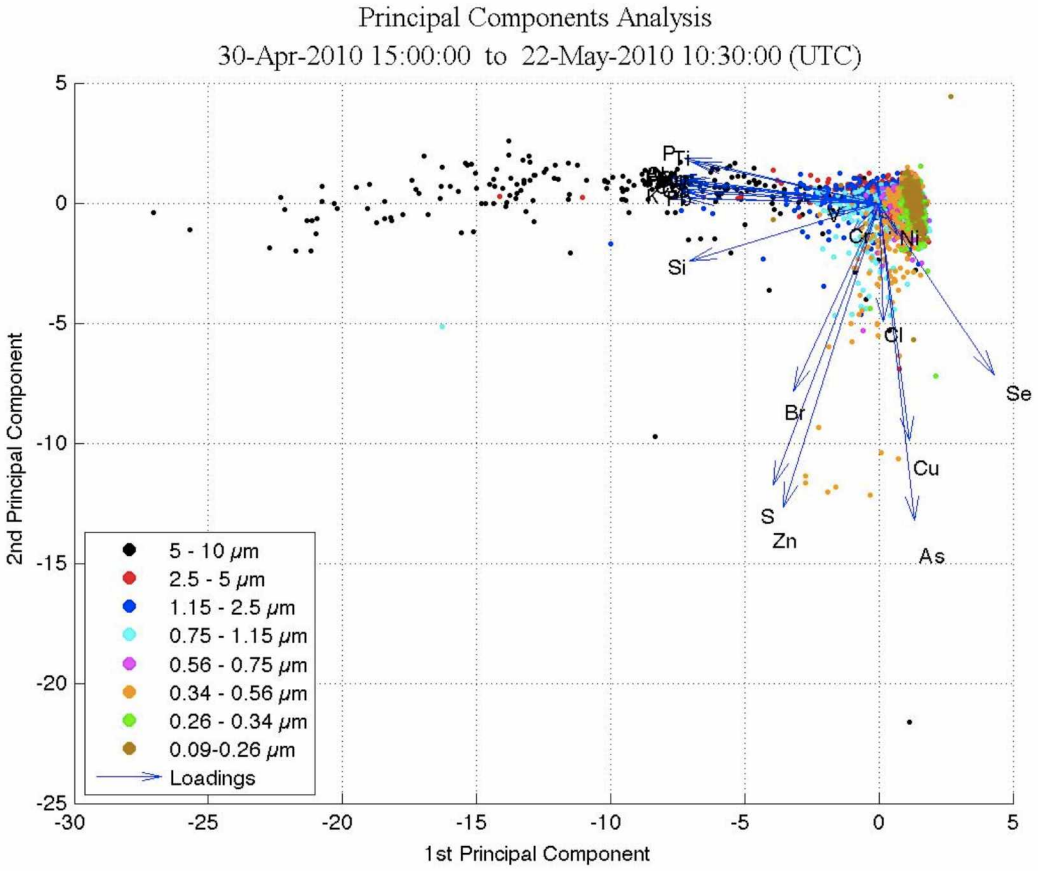

Figure 3.33. PCA biplot showing transformed aerosol data and eigenvector loadings. Eigenvector loadings have been extended 30 fold compared to values in Table 3.4 to make them more visible.

3.6. CMB model

There were a number of attempts to fit the aerosol data with a variety of source profiles including crustal material, highway road dust, lead smelters, metal mining, marine, motor vehicle exhaust, residential wood combustion, steel production, and copper production. Additionally, various time intervals were examined including some individual measurements during high concentration aerosol events and daily averages of aerosol concentrations. These resulted in poor correlations, many of which had R-squared values around 0.2 or 0.3 and mass calculations orders of magnitude higher than the measured concentration. The best results averaged aerosol concentrations over an entire sample period (approximately 3 weeks). These results are displayed in Table 3.5.

Table 3.5. CMB model results for Bagram, Afghanistan. Concentration units are in ng m^{-3}.

Sample period (2010)	R^2	Avg. measured conc.	Calculated conc.	% of total measured conc.	Source contributors	Source calculated conc.	% of total calculated conc.
02/06-02/28	0.80	3230.1	5980.3	185.1	Crustal	5868.9	98.1
					Pb smelting	2.7	0.05
					Metal mining	28.1	0.5
					Cu production	80.6	1.3
03/17-04/06	0.82	5229.8	9025.1	172.6	Crustal	8821.6	97.7
					Marine	32.3	0.4
					Cu production	129.1	1.4
					Metal mining	42.1	0.5
04/07-04/27	0.84	2847.1	4811.6	169.0	Crustal	4711.6	97.9
					Marine	41.0	0.9
					Cu production	49.6	1.0
					Metal mining	9.4	0.2
04/30-5/22	0.86	765.9	1181.1	154.2	Crustal	1153.1	97.6
					Pb smelting	19.4	1.6
					Metal mining	8.6	0.7

The CMB model had relatively decent correlations (see Table 3.5) after averaging over the entire sampling period. There are several likely reasons why the CMB model outputs were poorer than desired. A majority of the available source profiles were for PM_{10} when source profiles for $PM_{2.5}$ may have provided more accuracy. Further variations within each source profile, such as if the actual source profile had higher or lower weightings of elements than what was used, would cause greater errors in the calculation of the mass concentration. Finally, not all sources were taken into account. Since the interpretation of PCA is qualitative, and some sources can be embedded in a principal component if similar elements are present in the sources, some sources could not be determined by PCA. There are several dust sources affecting Afghanistan including from the north, from far in the west, and local. Dust sources separated by vast distances are going to have some variations in their source profiles. Because many of these dust source profiles are non-existent in the literature, a generic crustal source profile was used. This generalization caused errors in the model as it tried to correlate the elements to the generic crustal source profile rather than numerous individual dust source profiles.

The total concentrations were overestimated by a factor of about 1.5 to 2 as seen in Table 3.5. It is very likely that the model's attempt at fitting crustal elements to their measured concentrations caused these high concentrations and the high percentage of the mass contained within the crustal source.

A total of five sources were used including crustal, marine, lead smelting, copper production, and metal mining. Table 3.5 shows the percentage from each

source based on the calculated total concentration and source contribution concentration. From these results, it can be seen that crustal sources accounted for roughly 98% of the total calculated concentration for all sample periods. Each of the other sources accounted for approximately 0.1 to 1.5% of the masses. These values are based on the measured elemental concentrations only. If elemental and organic carbon, oxygen from oxides, and other unaccounted species were taken into consideration, these values should be much different.

Overall the results from the CMB model are limited and lack in encompassing the full scenario. Yet to some degree, they help confirm the sources found through PCA because using the sources found through PCA gave somewhat reasonable results.

4. Conclusions

The aerosol data collected in Bagram, Afghanistan, demonstrate several key aspects concerning aerosols and health concerns in Afghanistan. First, it illustrates the importance of the wind upon the concentrations and compositions of the observed aerosols. The Indian monsoon essentially dictates the overall wind patterns throughout the year from a more northerly flow pattern in Afghanistan during the monsoon season to a more westerly/southwesterly flow pattern during the post- and pre-monsoon seasons. These flow patterns have dramatic effects on the overall amount of aerosols and dust storms present in the surrounding region. Synoptic-scale low-pressure weather systems associated with stronger wind speeds were present at each potential source location likely inducing the lofting of aerosol particles. These systems led to the transport of aerosols to Afghanistan. Once injected into the ambient air, diurnal patterns had the tendency to recycle aerosols in subsequent days.

It has been shown that aerosols deriving from Pakistan, Kazakhstan, Uzbekistan, and Turkmenistan have a large influence on Afghanistan's aerosols, especially the heavy metals. Other countries and geographical features such as Iran, the Mediterranean Sea, and the Caspian Sea were also seen to have contributed to Afghanistan's aerosol environment.

Dust was found to have the largest impact on the variance of the data using PCA and was the largest contributor to the aerosol loadings in Afghanistan based

on the CMB model. The CMB model used to determine source contributions lacked in many aspects so the model's results are not definitive, but do suggest potential aerosol sources. Other notable aerosol sources identified by PCA were oceans/seas, smelters, mining, and copper production.

Health hazards due to airborne particulate matter are present in Afghanistan. PM concentrations were found to be well above NAAQS and WHO safety standards for the general population, especially $PM_{2.5}$ whose concentrations during the sample periods regularly exceeded about three times the 24-hour NAAQS standard and about six times the annual NAAQS standard. The PM_{10} and $PM_{2.5}$ 24-hour concentrations found here both fall into the U.S. military's negligible severity MEG category.

Although concentration data was unavailable during a majority of the year, it should be noted from the information provided throughout this thesis that notable aerosol concentrations are expected throughout the summer months. Therefore, despite Engelbrecht et al. (2008) showing that the annual average $PM_{2.5}$ concentration in Bagram was below the annual $PM_{2.5}$ marginal severity MEG, $PM_{2.5}$ concentrations are a health hazard because for several consecutive months they are elevated near or well above the annual $PM_{2.5}$ marginal severity MEG.

5. Future work

There are several ways in which this study could be improved upon in the future.

1) Add in positive matrix factorization (PMF; Paatero, 1997) as an analysis technique. PMF is a powerful statistical technique that would compliment the PCA done within this thesis. PMF differs from PCA in that data points are weighted based on analytical uncertainties and factor loading scores are non-negative reducing the ambiguity caused by PCA eigenvector loadings. Furthermore, PMF expresses factor loadings in mass units and provides uncertainty values for these factor loadings allowing easier inputs into quantitative procedures such as a CMB model.

2) Set up a DRUM sampler in Iran, Pakistan, Kazakhstan, Uzbekistan, and/or Turkmenistan. This would give better insight into the quantity of pollution transporting from these countries, confirm those that are contributing more than others and track the evolution of the aerosols as they transport.

3) Attain a more complete set and better source profiles as inputs for the CMB model. Source profiles, especially the variations in dust source profiles among Asian dust sources, are limited. Soil samples gathered by Engelbrecht et al. (2008) showed that soils varied among locations in the Middle East and even extensively within individual countries.

References

Afifi, A., Clark, V.A., May, S., Computer-Aided Multivariate Analysis (Fourth Edition). Chapman and Hall/CRC, New York, New York, 2004.

Allen, M.B., Armstrong, H.A., Reconciling the Intertropical Convergence Zone, Himalayan/Tibetan tectonics, and the onset of the Asian monsoon system. *Journal of Asian Earth Sciences*, In Press, 2011.

Amouroux, D., Donard, O.F.X., Maritime emissions of selenium to the atmosphere in Eastern Mediterranean Seas. *Geophysical Research Letters*, **23**(14), 1777-1780, 1996.

Amouroux, D., Liss, P.S., Tessier, E., Hamren-Larsson, M., Donard, O.F.X., Role of oceans as biogenic sources of selenium. *Earth and Planetary Science Letters*, **189**, 277-283, 2001.

Arimoto, R., Kim, Y.J., Quinn, P.K., Bates, T.S., Anderson, T.L., Gong, S., Uno, I., Chin, M., Huebert, B.J., Clarke, A.D., Shinozuka, Y., Weber, R.J., Anderson, J.R., Guazzotti, S.A., Sullivan, R.C., Sodeman, D.A., Prather, K.A., Sokolik, I.N., Characterization of Asian Dust during ACE-Asia. *Global and Planetary Change,* **52**, 23-56, 2006.

Aryal, R.K., Lee, B.K., Karki, R., Gurung, A., Baral, B., Byeon, S.H., Dynamics of $PM_{2.5}$ concentrations in Kathmandu Valley, Nepal. *Journal of Hazardous Materials*, **168**, 732-738, 2009.

Ball, W.P., Dickerson, R.R., Doddridge, B.G., Stehr, J.W., Miller, T.L., Savoie, D.L., Carsey, T.P., Bulk and size-segregated aerosol composition observed during INDOEX 1999: Overview of meteorology and continental impacts. *Journal of Geophysical Research*, **108** (D10), 8001, doi:10.1029/2002JD002467, 2003.

Cahill, C.F., Asian aerosol transport to Alaska during ACE-Asia. *Journal of Geophysical Research*, **108** (D23), 8664, doi:10.1029/2002JD003271, 2003.

Cahill, C.F., Cahill, T.A., Perry, K.D., The size- and time-resolved composition of aerosols from a sub-Arctic boreal forest prescribed burn. *Atmospheric Environment*, **42**, 7553-7559, 2008.

Cahill, T.A., Goodart, C., Nelson, J.W., Eldred, R.A., Nasstrom, J.S., Feeney, P.J., Design and evaluation of the DRUM aerosol impactor. In: Ariman, T., Veziroglu, T. (Eds.), Proceedings of the International Symposium on Particulate and Multiphase Processes, vol. 2. Hemisphere Publishing Corporation, 319-325, 1985.

Cahill, T.A., Wakabayashi, P., Compositional analysis of size-segregated aerosol samples. In: Newman. L. (Ed.), Measurement Challenges in Atmospheric Chemistry. American Chemical Society, 211-228, 1993.

Cahill, T.A., Cliff, S.S., Perry, K.D., Jimenez-Cruz, M.P., McHugo, S.A., Size and time resolved anthropogenic components of aerosols via synchrotron X-ray fluorescence: Application to Asian aerosol transport, Eos Trans. AGU, **80**(46), Fall Meeting Supplemental, Abstract A12C-09, 1999.

Chan, T.W., Mozurkewich, M., Application of absolute principal component analysis to size distribution data: identification of particle origins. *Atmospheric Chemistry and Physics*, 7, 887-897, 2007.

Chen, F.H., Chen, J.H., Holmes, J., Boomer, I., Austin, P., Gates, J.B., Wang, N.L., Brooks, S.J., Zhang, J.W., Moisture changes of the last millennium in arid central Asia: a review, synthesis and comparison with monsoon region. *Quaternary Science Reviews*, **29**, 1055-1068, 2010a.

Chen, X., Qu, W., Han, S., Eleonora, S., Yang, N., Chen, Z., Zeng, F., Du, A., Wang, Z., Re-Os geochronology of Cu and W-Mo deposits in the Balkhas metallogenic belt, Kazakhstan and it geological significance. *Geoscience Frontiers*, **1**, 115-124, 2010b.

Cianfrani, C.M., Hession, W.C., Rizzo, D.M., Watershed imperviousness impacts on stream channel condition in southeastern Pennsylvania. *Journal of the American Water Resource Association*, August 2006.

Clearing-House for the Partnership for Clean Fuels and Vehicles, cited 2011: Global Strategy for Phase-out of Leaded Gasoline of the Partnership for Clean Fuels and Vehicles. [Available online at http://www.unep.org/transport/pcfv/PDF/PCFVLeadStrategy-Mar08.pdf].

Colbeck, I., Nasir, Z.A., Ali, Z., The state of ambient air quality in Pakistan—a review. *Environmental Science and Pollution Research*, **17**, 49-63, doi:10.1007/s11356-009-0217-2, 2010.

Coulter, C.T., Scalco, J.V., Chemical Mass Balance Software: EPA-CMB8.2. Proceedings of A&WMA's 98th Conference & Exhibition; Minneapolis, MN, June 21-24, 2005.

Cunde, X., Shichang, K., Dahe, Q., Tandong, Y., Jiawen, R., Transport of atmospheric impurities over the Qinghai-Xizang (Tibetan) Plateau as shown by snow chemistry. *Journal of Asian Earth Sciences*, **20**, 231-239, 2002.

Dahl, C., Kuralbayeva, K., Energy and the environmental in Kazakhstan. *Energy Policy*, **29**, 429-440, 2001.

Draxler, R.R. and Rolph, G.D., HYSPLIT (HYbrid Single-Particle Lagrangian Integrated Trajectory) Model access via NOAA ARL READY Website (http://ready.arl.noaa.gov/HYSPLIT.php). NOAA Air Resource Laboratory, Silver Spring, MD, 2003.

Dumka, U.C., Moorthy, K.K., Kumar, R., Hegde, P., Sagar, R., Pant, P., Singh, N., Babu, S.S., Characteristics of aerosol black carbon mass concentrations over a high altitude location in the Central Himalayas from multi-year measurements. *Atmospheric Research*, **96**, 510-521, 2010.

El Dorado Weather, cited 2011: Kabul, Afghansitan Annual Yearly Climate Averages. [Available online at http://www.eldoradocountyweather.com/climate/afghanistan/Kabul.html].

El Dorado Weather, cited 2012: Countries of the World City Temperature and Rainfall Statistics. [Available online at http://www.eldoradocountyweather.com/climate/world-country-climate-listing.html]

Emsley, J., Nature's Building Blocks: An A-Z Guide to the Elements. Oxford University Press, 2002.

Engconsult Ltd., "Draft KAQM Strategy Report". TA No. 4415-AFG Kabul Air Quality Management, 2007.

Engelbrecht, J.P., McDonald, E.V., Gillies, J.A., Jayanty, R.K.M., Casuccio, G., Gertler, A.W., Department of Defense Enhanced Particulate Matter Surveillance Program (EPMSP), Final Report. Desert Research Institute, February, 2008.

EPA, Lead Poisoning and Your Children. EPA 747-K-00-003, 2000.

EPA, EPA-CMB8.2 User's Manual. Report No. EPA-452/R-04-011. U.S. Environmental Protection Agency, Research Triangle Park, NC; December, 2004.

EPA, cited 2011a: Final Revisions to the National Ambient Air Quality Standards for Particle Pollution (Particulate Matter). [Available online at http://www.epa.gov/particles/pdfs/20060921_factsheet.pdf].

EPA, cited 2011b: National Ambient Air Quality Standards (NAAQS). [Available online at http://www.epa.gov/air/criteria.html].

EPA, cited 2011c: SPECIATE Data Browser. [Available online at http://cfpub.epa.gov/si/speciate/ehpa_speciate_browse.cfm].

Faiz, Y., Tufail, M., Tayyeb Javed, M., Chaudhry, M.M., Naila-Siddique, Road dust pollution of Cd, Cu, Ni, Pb and Zn along Islamabad Expressway, Pakistan. *Microchemical Journal*, **92**, 186-192, 2009.

Farmer, A.A., Farmer, A.M., Concentrations of cadmium, lead and zinc in livestock feed and organs around a metal production centre in eastern Kazakhstan. *The Science of the Total Environment*, **257**, 53-60, 2000.

Gajananda, K., Kuniyal, J.C., Momin, G.A., Rao, P.S.P., Safai, P.D., Tiwari, S., Ali, K., Trend of atmospheric aerosols over the north western Himalayan region, India. *Atmospheric Environment*, **39**, 4817-4825, 2005.

Garcia-Veigas, J., Rosell, L., Zak, I., Playa, E., Ayora, C., Starinsky, A., Evidence of potash salt in the Pliocene Sedom Lagoon (Dead Sea Rift, Israel). *Chemical Geology*, **265**, 499-511, 2009.

Ghauri, B.M., Mirza, M.I., Richter, R., Dutkiewicz, V.A., Rusheed, A., Khan, A.R., Husain, L., Composition of aerosols and cloud water at a remote mountain site (2.8 kms) in Pakistan. *Chemosphere - Global Change Science*, **3**, 51-63, 2001.

Goudie, A.S., Middleton, N.J., Dust storms in south-west Asia. *Geographica,* **Supplementum**, 73-83, 2000.

Haggett, P. (Ed.), Encyclopedia of World Geography, Vol. 8. Andromeda Oxford Ltd, 2002.

Hall, J.V., Assessing health effects of air pollution. *Atmospheric Environment*, **30**, 743-746, 1996.

Han, Y., Fang, X., Kang, S., Wang, H., Kang, F., Shifts of dust source regions over central Asia and Tibetan Plateau: Connections with the Arctic oscillation and the westerly jet. *Atmospheric Environment*, **42**, 2358-2368, 2008.

Iino, N., Kinoshita, K., Tupper, A.C., Yano, T., Detection of Asian dust aerosols using meteorological satellite data and suspended particulate matter concentrations. *Atmospheric Environment*, **38**, 6999-7008, 2004.

Jaffe, D., McKendry, I., Anderson, T., Price, H., Six 'new' episodes of trans-Pacific transport of air pollutants. *Atmospheric Environment,* **37**, 391-404, 2003.

Jaklevic, J.M., Gatti, R.C., Goulding, F.S., Loo, B.W., Beta gauge instrumentation for the measurement of aerosol mass. EPA report number: EPA-600/7-80-081. May 1980.

Jolliffe, I.T., Principal Component Analysis, second edition. Springer, New York: Verlag New York, Inc., 2002.

Kandler, K., Benker, N., Bundke, U., Cuevas, E., Ebert, M., Knippertz, P., Rodríguez, S., Schütz, L., Weinbruch, S., Chemical composition and complex refractive index of Saharan Mineral Dust at Izaña, Tenerife (Spain) derived by electron microscopy. *Atmospheric Environment*, **41**, 8058-8074, 2007.

Kennedy, I.M., The health effects of combustion-generated aerosols. *Proceedings of the Combustion Institution*, **31**, 2757-2770, 2007.

Kim, D., Stockwell, W.R., An online coupled meteorological and air quality modeling study of the effect of complex terrain on the regional transport and transformation of air pollutants over the Western United States. *Atmospheric Environment*, **42**, 4006-4021, 2008.

Kuo, C.S., The Mineral Industry of Afghanistan. *2006 Minerals Yearbook*, U.S. Geological Survey, September, 2007.

Labban, R., Veranth, J.M., Chow, J.C., Engelbrecht, J.P., Watson, J.G., Size and Geographical Variation in PM1, PM2.5, and PM10: Source Profiles from Soils in the Western United States. *Water, Air, and Soil Pollution*, **157**, 13-31, 2004.

Lawson, D.R., Impaction surface coatings intercomparison and measurements with cascade impactors. *Atmospheric Environment*, **14**, 195-199, 1980.

Lella, L.A.D., Loppi, S., Protano, G., Riccobono, F., Toxic trace elements and organic compounds in the ambient air of Kabul, Afghanistan. *Atmospheric Environment*, **40**, 225-237, 2006.

Liu, Y., Geng, Z., Hou, S., Spatial and seasonal variations of major ions in Himalayan snow and ice: A source consideration. *Journal of Asian Earth Sciences*, **37**, 195-205, 2010.

Lundgren, D.A., An aerosol sampler for determination of particle concentration as a function of size and time. *Journal of the Air Pollution Control Association*, **17**, 225, 1967.

Mac Arthur, R.H., On the relative abundance of bird species. *Proceedings of the National Academy of Science*, **43**, 293-295, 1957.

Mukai, H., Machida, T., Tanaka, A., Vera, Y.P., Uematsu, M., Lead isotope ratios in the urban air of eastern and central Russia. *Atmospheric Environment*, **35**, 2783-2793, 2001.

Nabi Bidhendi, G.R., Halek, F., Aerosol Size Segregated of Tehran's Atmosphere in Iran. *International Journal of Environmental Research*, **1**(1), 58-65, 2007.

NCDC, cited 2012: Online Climate Data Director. [Available online at http://www.ncdc.noaa.gov/oa/climate/climatedata.html].

NOAA CPC, cited 2011: Asian-Australian Monsoons. [Available online at http://www.cpc.ncep.noaa.gov/products/Global_Monsoons/Asian_Monsoons/Asian_Monsoons.shtml].

NY DOH, cited 2012: Lead Exposure in Adults: A Guide for Health Care Providers. [Available online at http://www.health.ny.gov/publications/2584].

Orgill, M.M., Sehmel, G.A., Frequency and diurnal variation of dust storms in the contiguous U.S.A. *Atmospheric Environment*, **10**, 813-825, 1976.

Orlovsky, L., Orlovsky, N., Durdyev, A., Dust storms in Turkmenistan. *Journal of Arid Environments*, **60**, 83-97, 2005.

Paatero, P., Least squares formulation of robust non-negative factor analysis. *Chemometrics and Intelligent Laboratory Systems*, **37**, 23-35, 1997.

Pearson, K., On Lines and Planes of Closest Fit to Systems of Points in Space. *Philosophical Magazine*, **2**(6), 559-572, 1901.

Peters, E.D., The principals of copper smelting. New York: Hill Publishing Company, 1907.

Pio, C.A., Nunes, T.V., Borrego, C.S., Assessment of air pollution sources in an industrial atmosphere using principal component and multilinear regression analysis. *Science of the Total Environment*, **80**, 279-292, 1989.

Polichetti, G., Cocco, S., Spinali, A., Trimarco, V., Nunziata, A., Effects of particulate matter (PM_{10}, $PM_{2.5}$ and PM_1) on the cardiovascular system. *Toxicology*, **261**, 1-8, 2009.

Prospero, J.M., Ginoux, P., Torres, O., Nicholson, S.E., Gill, T.E., Environmental characterization of global sources of atmospheric soil dust identified with the Nimbus 7 total ozone mapping spectrometer (TOMS) absorbing aerosol product. *Reviews of Geophysics*, **40** (1), 1002, doi:10.1029/2000RG000095, 2002.

Raabe, O.G., Braaten, D.A., Axelbaum, R.L., Teague, S.V., Cahill, T.A., Calibration studies of the DRUM aerosol impactor. *Journal of Atmospheric Science*, **19**(2), 183-195, 1988.

Rolph, G.D., 2003. Real-time Environmental Applications and Display sYstem (READY) website (http://ready.arl.noaa.gov/index.php). NOAA Air Resources Laboratory, Silver Spring, MD.

Saide, P.E., Carmichael, G.R., Spak, S.N., Gallardo, L., Osses, A.E., Mena-Carrasco, M.A., Pagowski, M., Forecasting urban PM10 and PM2.5 pollution episodes in very stable nocturnal conditions and complex terrain using WRF-Chem CO tracer model. *Atmospheric Environment*, **45**, 2769-2780, 2011.

Samet, J.M., Zeger, S.L., Dominici, S., Curriero, F., Coursac, I., Dockery, D.W., Schwartz, J., Zanobetti, A., The National Morbidity, Mortality, and Air Pollution Study Part II: Morbidity and Mortality from Air Pollution in the Uninted States. Health Effects Institute, Research Report Number 94 Part II, 2000.

Schneidemesser, E., Stone, E.A., Quraishi, T.A., Shafer, M.M., Schauer, J.J., Toxic metals in the atmosphere in Lahore, Pakistan. *Science of the Total Environment*, **408**, 1640-1648, 2010.

Schott, F.A., McCreary Jr., J.P., The monsoon circulation of the Indian Ocean. *Progress in Oceanography*, **51**, 1-123, 2001.

Shahgedanova, M., Burt, T.P., New data on air pollution in the former Soviet Union. *Global Environmental Change*, **4**(3), 201-227, 1994.

Shaw, P.J.A., Multivariant Statistics for the Environmental Sciences. United Kingdom: John Wiley & Sons Ltd, 2003.

Shrestha. A.B., Wake, C.P., Dibb, J.E., Mayewski, P.A., Whitlow, S.I., Carmichael, G.R., Ferm, M., Seasonal variations in aerosol concentrations and compositions in the Nepal Himalaya. *Atmospheric Environment*, **34**, 3349-3363, 2000.

Singer, A., Zobeck, T., Poberezsky, L., Argaman, E., The PM_{10} and $PM_{2.5}$ dust generation potential of soils/sediments in Southern Aral Sea Basin, Uzbekistan. *Journal of Arid Environments*, **54**, 705-728, 2003.

Smeyers-Verbeke, J., Den Hartog, J.C., Dekker, W.H., Coomans, D., Buydens, L., Massart, D.L., The use of principal components analysis for the investigation of an organic air pollutants data set. *Atmospheric Environment*, **18**(11), 2471-2478, 1984.

Smith, D.J.T., Harrison, R.M., Luhana, L., Pio, C.A., Castro, L.M., Tariq, M.N., Hayat, S., Quraishi, T., Concentrations of particulate airborne polycyclic aromatic hydrocarbons and metals collected in Lahore, Pakistan. *Atmospheric Environment*, **23**, 4031-4040, 1996.

Smolik, J., Zdimal, V., Schwarz, J., Lazaridis, M., Havránek, V., Eleftheriadis, K., Mihalopoulos, N., Bryant, C., Colbeck, I., Size resolved mass concentration and elemental composition of atmospheric aerosols over the eastern Mediterranean area. *Atmospheric Chemistry and Physics Discussions*, **3**, 2547-2573, 2003.

Strang, G., Introduction to Linear Algebra, 3rd edition. Wellesley-Cambridge Press, 2003.

Tanaka, T.Y., Kurosaki, Y., Chiba, M., Matsumura, T., Nagai, T., Yamazaki, A., Uchiyama, A., Tsunematsu, N., Kai, K., Possible transcontinental dust transport from North Africa and the Middle East to East Asia. *Atmospheric Environment*, **39**, 3901-3909, 2005.

Tanner, R.L., Bairai, S.T., Olszyna, K.J., Valente, M.L., Valente, R.J., Diurnal patterns in $PM_{2.5}$ mass and composition at a background, complex terrain site. *Atmospheric Environment*, **39**, 3865-3875, 2005.

Thurston, G.D., Spengler, J.D., A quantitative assessment of source contributions to inhalable particulate matter pollution in metropolitan Boston. *Atmospheric Environment*, **19**(1), 9-25, 1985.

Tindale, N.W., Pease, P.P., Aerosols over the Arabian Sea: Atmospheric transport pathways and concentrations of dust and sea salt. *Deep-Sea Research II*, **46**, 1577-1595, 1999.

USAPHC, cited 2010: Technical Guide 230, Environmental Health Risk Assessment and Chemical Exposure Guidelines for Deployed Military Personnel. [Available online at http://phc.amedd.army.mil/PHC%20Resource%20Library/TG230.pdf].

USGS, cited 2012a: USGS projects in Afghanistan. [Available online at http://afghanistan.cr.usgs.gov/afghan_geo.php].

USGS, cited 2012b: Minerals Information: Asia and the Pacific. [Available online at http://minerals.usgs.gov/minerals/pubs/country/asia.html].

USGS, cited 2012c: Minerals Information: Europe and Central Eurasia. [Available online at http://minerals.usgs.gov/minerals/pubs/country/europe.html].

USGS, cited 2012d: Minerals Information: Africa and the Middle East. [Available online at http://minerals.usgs.gov/minerals/pubs/country/africa.html].

Vekemans, B., Jensens, K., Vincze, L., Adams, F., Van Espen, P., Analysis of X-ray spectra by iterative least squares (AXIL): new developments. *X-Ray Spectrometry*, **23** (11), 278-285, 1994.

Viana, M., Querol, X., Alastuey, A., Gil, J.I., Menéndez, M., Identification of PM sources by principal component analysis (PCA) coupled with wind direction data. *Chemosphere*, **65**, 2411-2418, 2006.

Vondou, D.A., Nzeukou, A., Mkankam Kamga, F., Diurnal cycl of convective activity over the West of Central Africa based on Meteosat images. *International Journal of Applied Earth Observation Geoinformation*. **12S**, S58-S62, 2010.

Wang, Y., Liu, X., Herzschuh, U., Asynchronous evolution of the Indian and East Asian Summer Monsoon indicated by Holocene moisture patterns in monsoonal central Asia. *Earth-Science Reviews*, **103**, 135-153, 2010.

WHO, cited 2011: WHO Air quality guidelines for particulate matter, ozone, nitrogen dioxide, and sulfur dioxide. [Available online at http://whqlibdoc.who.int/hq/2006/WHO_SDE_PHE_OEH_06.02_eng.pdf].

Wu, G., Xu, B., Yao, T., Zhang, C., Gao, S., Heavy metals in aerosol samples from the Eastern Pamirs collected 2004-2006. *Atmospheric Research*, **93**, 784-792, 2009.

Zavialov, P.O., Ni, A.A., 2010. Chemistry of the Large Aral Sea. In: Kostianoy, A.G., Kosarev, A.N. (Eds.), *The Aral Sea Environment*, Handbook of Environmental Chemistry (2010) 7, pp 219-233, doi:10.1007/698_2009_3.